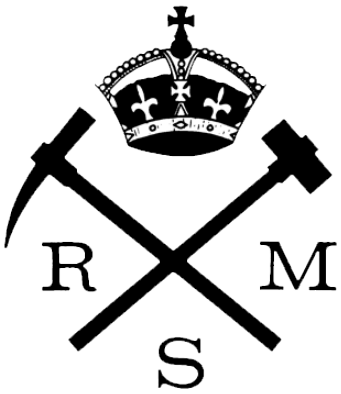
Pore Scale Insights into the Impacts of Wetting State, Pore Structure and Sandstone Mineralogy on Low Salinity Water Flooding

Edward P Andrews

2022

A doctoral thesis submitted in fulfillment of the requirements for the degree of Doctor of Philosophy of Imperial College London



Imperial College London

Department of Earth Science and Engineering

The work submitted is substantially the result of my own work except where explicitly indicated in the text. The report may be freely copied and distributed provided the source is explicitly acknowledged

Declaration of Originality

I declare that this thesis, written under the supervision of Dr Samuel Krevor and Professor Ann Muggeridge in the Department of Earth Science & Engineering at Imperial College London, is my own work. Any material that is not my own has been properly acknowledged. This thesis has not been previously submitted in whole or in part for a degree or any other qualification at this University or any other institution.

Edward Andrews

2022

Funding Acknowledgments

We gratefully acknowledge the EPSRC and BP Exploration for providing funding [EPSRC CASE voucher 18000038] for this project

Copyright Declaration

The copyright of this thesis rests with the author. Unless otherwise indicated, its contents are licensed under a Creative Commons Attribution-Non Commercial 4.0 International Licence (CC BY-NC).

Under this licence, you may copy and redistribute the material in any medium or format. You may also create and distribute modified versions of the work. This is on the condition that: you credit the author and do not use it, or any derivative works, for a commercial purpose.

When reusing or sharing this work, ensure you make the licence terms clear to others by naming the licence and linking to the licence text. Where a work has been adapted, you should indicate that the work has been changed and describe those changes.

Please seek permission from the copyright holder for uses of this work that are not included in this licence or permitted under UK Copyright Law.

Edward Andrews

2022

List of publications

Andrews, E., Muggeridge, A., Garfi, G., Jones, A. and Krevor, S., 2021. Pore-Scale X-ray Imaging of Wetting Alteration and Oil Redistribution during Low-Salinity Flooding of Berea Sandstone. Energy & Fuels, 35(2), pp.1197-1207.

Alhosani, A., Lin, Q., Scanziani, A., **Andrews, E.**, Zhang, K., Bijeljic, B. and Blunt, M.J., 2021. Pore-scale characterization of carbon dioxide storage at immiscible and near-miscible conditions in altered-wettability reservoir rocks. International Journal of Greenhouse Gas Control, 105, p.103232.

Conference Proceedings

- AGU Fall Meeting, December 2019, San Francisco, USA - poster presentation
- Interpore, September 2020, online - oral presentation
- AGU Fall Meeting, December 2020, online - poster presentation
- EAGE Improved Oil Recovery Symposium, April 2021, online - oral presentation
- SPE Improved Oil Recovery, April 2022, online - invited speaker
- EGU, May 2022, online - oral presentation

Acknowledgements

A PhD is not a solo endeavour. Without a caring, supportive, and inspiring network of colleagues, friends and family, I would not have been able to complete this thesis. Here, I will attempt to do justice to all those that have helped me along the way.

Firstly, I am extremely grateful to my supervisors Sam, Ann and Alistair. I have learnt a lot from my supervisors, and I admire them all greatly as scientists and mentors. Even in the depths of the pandemic, their support made me feel part of a team and never isolated in my research. This speaks to their complete commitment to the wellbeing of their students – for this, above all else, I am extremely grateful.

I could not have asked for a better primary supervisor than Sam. His guidance and sound advice throughout the project have made me feel secure, trusted and motivated. I am grateful to Ann for her brilliant scientific insights and support. I am certain that without our many impromptu coffee chats (often, a vent about lab woes), I would have struggled far more throughout the PhD. I feel very lucky that Alistair joined as a co-supervisor in the second year of my project. I am grateful for his insightful feedback and careful advice which have improved my research immensely.

I wish to thank Bilal and Ian, my industry collaborators within BP. I am extremely grateful for their countless important insights which helped to plan the direction of my research and motivated me to push forward.

I would like to thank every member of Sam's research group for their unique insights, useful discussions and, above all, their inspiring research. Being around such a talented group of scientists has always motivated me to push on with my own research. I'd particularly like to thank Catherine and Gaetano who took me under their wings when I first started my PhD. They not only became treasured colleagues, but great friends, and I will always be grateful for their comradery, support and advice.

I'd like to thank everyone that helped me in the lab over the years. I'd particularly like to thank Ed, Vincenzo, Lewis, Gaetano and Catherine. The lab can be a daunting place to a

new PhD student. My colleagues supported me so that I never felt isolated or overwhelmed. Ultimately, this led to the successful experiments which form the backbone of this thesis.

I wish to thank my family for their unending support. Their strength to stay positive through the ups and downs that life has thrown at them has always inspired me. Thank you for sparking and fostering my love of the natural world. Without the countless zoo trips and Attenborough box-sets I would not have had the ambition to become a scientist.

Finally, I am extremely grateful to my partner, Laura. From the moment I started the PhD, she has been there every step of the way. Supporting me through the stress of lab set-backs and research dead-ends, she has given me the strength to push forward.

Nomenclature

Symbol	Description
AFM	Atomic Force Microscopy
COBR	Crude Oil Brine Rock
CCS	Carbon Capture and Storage
EOR	Enhanced Oil Recovery
HSB	High Salinity Brine
HSWF	High Salinity Water flooding
LSB	Low Salinity Brine
LSWAG	Low Salinity Water Alternating Gas Injection
LSWF	Low Salinity Water Flooding
PV	Pore Volumes
A_{ij}	Measured surface area per unit of pore volume shared by fluid i with solid j
a_{ij}	Fraction of the total surface area of solid j coated by fluid i
β	Roughness factor
I	Intensity of X-ray source
K	Permeability
κ	Mean fluid-fluid interfacial curvature
κ_d	Deficit curvature of a ganglion
ϕ	Porosity
$\mu(s)$	The linear attenuation coefficient along the ray path of X-ray beam s
N_c	Number of contact loops that a ganglion shares with a solid surface
S_w	Water saturation
S_o	Oil saturation
σ	Interfacial tension
θ_t	Thermodynamic contact angle
θ_{macro}	Macroscopic contact angle

List of Figures

2.1 Frequency of a) tertiary recovery factors b) incremental secondary recovery factors, compiled from publications. From *Wang and Fu* (2018). 8

2.2 Results of a residual oil saturation prediction model. From *Aladasani et al.* (2014). 10

2.3 Overview of sandstone LSWF EOR mechanisms. From *Wang and Fu* (2018). . . 14

2.4 Diagram summarising the different approaches to low salinity waterflooding research across scales. From *Bartels et al.* (2019). 15

2.5 A two-dimensional view of pore-scale fluid occupancy and manual oil-brine contact angle measurements in a Berea sample. From *Khishvand et al.* (2017). . . . 18

2.6 Volume rendering of oil blobs after spontaneous imbibition of high salinity brine and low salinity brine in a Berea sandstone sample. From *Shabaninejad et al.* (2018). 18

2.7 Size distributions of brine-filled pore elements at the end of high salinity waterflooding (HSWF) and low salinity water flooding (LSWF) of oil-wet carbonate sample. From *Qin et al.* (2019). 20

2.8 Mineral specific oil-coated area fractions computed in one water-wet Berea sample and one Berea sample of altered wetting state. From *Garfi et al.* (2020a). . . 26

2.9 Oil droplets displaced from clay surface after exposure to low salinity brine. From *Cense et al.* (2011). 30

3.1 X-ray micro-CT images of the three lithologies used in this work: a) Berea sandstone; b) Bunter sandstone; c) Castlegate sandstone. 36

3.2 Plot of pore radius distributions as a fraction of total pore volume for each sample 37

3.3 An overview of the experimental workflow for all samples 40

3.4 Schematic diagram of experimental apparatus for unsteady state flow experiment. Adapted from *Lin et al.* (2018) 41

3.5 Schematic diagram of a typical laboratory micro-CT setup. From *Wildenschild and Sheppard* (2013). 46

3.6 A brief overview of the image analysis workflow. 50

3.7 Maximum inscribed balls extracted from a subvolume of the Castlegate sample, overlaid on a volume rendering of the subvolume. 53

4.1 Profile water saturation, S_w, averaged perpendicular to the flooding direction across the entire region of interest for the unaltered and altered Berea samples . 57

4.2 S_w values after 12PV of high salinity flooding (HSWF 12PV), 4PV of low salinity flooding (LSWF 4PV), and 20PV of low salinity flooding (LSWF 20PV) for the unaltered and altered Berea samples. As discussed in chapter 4.2.3 we calculate a standard error of 0.00125 for the saturation measurements in this work. . . . 58

4.3 Oil-coated area fractions computed for both the unaltered sample and the altered samples after each flow step 60

4.4 The size distribution for all brine saturated pores in the unaltered sample and the altered samples after each flow step 62

4.5 The size distribution for all pores where saturation changed from oil to brine or brine to oil between during low salinity water flooding in the unaltered and altered Berea samples 63

4.6 A volume rendering of a) Oil displaced during twenty pore volumes of low salinity water flooding (LSWF 20PV) in the altered sample. Only 20% of this displaced oil is produced, the rest is redistributed and retrapped within the core, as shown in b). 65

4.7 The size distribution for all brine saturated pores in 4 sub volumes within the altered Berea sample. 68

4.8 S_w values after 12PV of high salinity flooding (HSWF 12PV), 4PV of low salinity flooding (LSWF 4PV), and 20PV of low salinity flooding (LSWF 20PV) in subvolumes a,b,c, and d. As discussed in Chapter 4.2.3, we estimate a standard error of 0.00125 for the saturation measurements. 69

4.9 A brine snap-off event in the altered sample where oil connected across multiple pores is broken up. The configuration of oil (red) and brine (blue) in a subvolume after a) high salinity water flooding b) 20 PV of low salinity water flooding. The rock is transparent in each case. 70

4.10 A brine snap-off event in the altered Berea sandstone sample 71

5.1 S_w values after 12PV of high salinity flooding (HSWF 12PV), 4PV of low salinity flooding (LSWF 4PV), and 20PV of low salinity flooding (LSWF 20PV) for the Berea, Bunter and Castlegate samples. As discussed in Chapter 4.2.3, we estimate a standard error of 0.00125 for the saturation measurements. 76

5.2 Profile of water saturation averaged perpendicular to the flooding direction across the region of interests of the Berea, Bunter and Castlegate sandstone samples after each flowstep. 78

5.3 Oil-coated area fractions calculated in the Berea, Bunter and Castlegate sandstone samples after each flowstep. 79

5.4 The size distribution for all brine saturated pores in the Berea, Bunter and Castlegate sandstone samples after each flowstep. 81

5.5 The size distribution for all pores where saturation changed from oil to brine or brine to oil during low salinity flooding in the Berea, Bunter and Castlegate sandstone samples. 84

5.6 Volume rendering of largest pores accounting for 60% of pore volume in the Berea, Bunter and Castlegate sandstone samples. 88

5.7 Volume rendering of the three largest brine blobs after high salinity water flooding and low salinity water flooding in the Berea, Bunter and Castlegate sandstone samples. 90

5.8 Volume rendering of the largest pores in the Bunter sandstone, presented with saturation profile and volume rendering largest three brine blobs after high and low salinity waterflooding. 91

5.9 Volume rendering of largest pores in Bunter sandstone presented alongside the size distribution for all pores where saturation changed from oil to brine or brine to oil during low salinity waterflooding. 92

6.1 A slice of the X-ray micro-CT image of the Berea, Castlegate Bunter samples, presented above corresponding segmented images showing clay distribution. . . . 97

6.2 The fraction of clay-rich ($>$ 50%clay coverage) pores in different radii bins for the Berea, Bunter and Castlegate samples. 98

6.3 Mineral specific Oil-coated area fractions calculated in the Berea, Bunter and Castlegate sandstone samples after high and low salinity water flooding. 99

6.4 The total brine saturation (S_w) in pore radius bins for clay-poor and clay-rich pores in the Berea, Bunter and Castlegate sandstone samples after high and low salinity water flooding. 102

6.5 The size distribution for all brine saturated clay-poor pores and clay-rich pores in the Berea, Bunter and Castlegate sandstone samples after high and low salinity water flooding. 104

6.6 The size distribution for all clay-poor pores and clay-rich pores where saturation changed from oil to brine or brine to oil during low salinity waterflooding in the Berea, Bunter and Castlegate samples. 105

6.7 Bar chart showing the contribution of clay-rich and clay-poor pores to additional recovery during low salinity flooding in the Berea, Bunter and castlegate samples. 107

6.8 Direct observations of mineralogy and fluid distribution within a subvolume of the Berea sample. 110

6.9 Direct observations of mineralogy and fluid distribution within a subvolume of the Bunter sample. 111

6.10 Direct observations of mineralogy and fluid distribution within a subvolume of the Castlegate sample. 112

List of Tables

3.1 A summary of rock properties for the Berea, Castlegate, and Bunter samples used in this work 36

3.2 The brine recipes for both the high and low salinity brines used in the study . . 38

4.1 Average water saturation in the region of interest for the unaltered and altered Berea samples after all flow steps 56

4.2 Water saturation values for 4 subvolumes in the altered Berea sandstone sample after each flow step 67

5.1 Average water saturation in the region of interests of he Berea, Bunter and Castlegate sandstone samples after each flowstep. 76

5.2 The fraction of the oil in place after high salinity water flooding that is mobilised during 20 PV of low salinity water flooding in the Berea, Bunter and Castlegate samples, and the fraction of this mobilised oil that is produced. 86

5.3 Absolute permeability values calculated across all pores, and the network of largest pores in the Berea, Bunter and Castlegate samples. As discussed previously the 'largest pores' are those that comprise 60% of the pore volume 87

6.1 Oil saturation values for clay-poor, clay-rich and very clay-rich pores in the Berea, Bunter and Castlegate samples. 108

Abstract

Low salinity waterflooding is a promising enhanced oil recovery technique that has been observed to increase recovery by up to 14% in experiments over a range of scales. However, results vary dramatically and there is currently no way of predicting which systems will respond well to low salinity waterflooding. This is partly due to an absence of mechanistic explanations linking fluid-solid interactions at the microscopic scale to oil recovery at core and field scales. Pore scale observations of low salinity flooding are crucial to bridging this gap in understanding and improving predictive capabilities. In this work, we utilise X-ray micro-CT imaging and advances in image analysis techniques to make comprehensive pore scale observations of low salinity waterflooding experiments across four sandstone samples of varied pore structures.

We first analyse the impact of initial wetting state on recovery during low salinity flooding by comparing observations in two Berea sandstone cores of different initial wetting states. The wetting state of one core is altered with exposure to crude oil. The second core is not altered so that it is initially water-wet. We characterise the wetting state of both samples using imagery of fluid-solid fractional wetting and pore occupancy analysis. In the unaltered rock, oil saturation, fractional mineral surface area covered by oil and size distribution of oil filled pores remain constant between high salinity flooding and subsequent low salinity floods. In contrast, in the altered sample, we observe a shift in the mineral surface area covered by oil after low salinity flooding towards decreasing coverage, consistent with a change to a less oil-wetting state. This change is also reflected in the observed variation in fluid pore occupancy. The wetting alteration results in the redistribution of 22% of oil within the rock, but an additional recovery of just three percentage points. We hypothesise that the success of low salinity water flooding depends on both a wetting alteration and a pore structure which facilitates the production of mobilised oil.

We investigate the impact of pore structure on recovery during low salinity flooding by comparing the pore scale observations in the aforementioned altered Berea sandstone sample with observations in altered Bunter sandstone and Castlegate sandstone samples. This comprises the first systematic comparison of the pore scale response to low salinity flooding across multiple

sandstone samples. We observe fluid saturations and characterise the wetting state of samples using imagery of fluid-solid fractional wetting and pore occupancy analysis. In the Berea sample, we observed an additional oil production of 3 percentage points during low salinity water flooding, with large volumes of oil displaced from small pores but also re-trapping of mobilised oil in large pores. In the Bunter sandstone, we observe four percentage points of additional recovery with significant displacement of oil from small pores and no significant retrapping of oil in large pores. In the Castlegate sample, we observed just 1 percentage point of additional recovery and relatively small volumes of oil mobilisation. We observe a significant wettability alteration towards more water-wet conditions in the Berea and Bunter sandstones, but no significant alteration in the Castlegate sample. We show evidence that the pore structure, specifically the connectivity of the largest pores in each sample, affected recovery. This work gives the first pore scale insights into the role of pore geometry and topology on the mobilisation and retrapping of oil during low salinity waterflooding.

We assess the role of mineralogy on low salinity response. The presence of clay minerals is generally accepted to be a necessary condition for favourable response to low salinity flooding in sandstones. However, there have been no in situ pore scale observations of oil detachment from clay minerals during low salinity water flooding. Furthermore, there is a growing body of evidence that suggests that significant oil detachment can occur on quartz and feldspar mineral surfaces during low salinity flooding. We further analyse the dataset described above to make the first pore scale in situ observations of clay behaviour during low salinity flooding in oil-wetting sandstone samples. We find that clay minerals are initially significantly more oil-wetting than other mineral groups in all samples. We observe significant wettability alteration for clay minerals and non-clay minerals in both the Berea and Bunter samples. No significant wettability alteration is observed in either mineral group in the Castlegate sample. We observe pore occupancy changes consistent with wettability alteration towards more water-wetting conditions in clay-poor pores in all samples. In all samples, clay-poor pores contribute significantly more to total oil production during low salinity waterflooding than clay-rich pores. Clay-rich pores are found to account for only 15%, 5% and 3% of total additional recovery in the Berea, Bunter, and Castlegate samples respectively. We see no evidence that clays dominate the response to

low salinity flooding in any of the samples. This work adds to the growing body of evidence that questions the presence of clays as a necessary condition for a favourable response to low salinity flooding in sandstones.

This work gives unique insights into low salinity water flooding through a more systematic and controlled set of pore-network scale observations and analyses. We have shown that initial wetting state strongly controls behaviour during low salinity waterflooding, with more oil mobilisation and production associated with more oil-wetting initial conditions. Pore structure is also shown to impact oil mobilisation, with well connected large pores associated with lower volumes of mobilised oil during low salinity flooding. Lastly, we show that clay-poor pores contribute more to additional recovery during low salinity flooding than clay-rich pores.

Contents

1 Introduction **2**

1.1 Scientific Background and Motivation 2

1.2 Research Objectives 4

1.3 Thesis Outline 5

2 Literature Review **7**

2.1 Low Salinity Flooding - Disparities in Experimental Results 7

2.2 Necessary Conditions and Predictive Capabilities 8

2.3 Underlying Mechanisms 11

2.3.1 Double Layer Expansion 11

2.3.2 Multiple Ion Exchange 12

2.3.3 Fines Migration 12

2.3.4 Other Mechanisms 13

2.3.5 Summary of Mechanisms 13

2.4 Wettability Alteration - Observations Across Scales 13

2.5 Pore Scale Observations 16

2.5.1 Sandstones 16

2.5.2 Carbonates 19

2.6 Areas for Further Research 20

2.6.1 Wettability - Initial Wetting State and Wettability Characterisation . . . 21

2.6.2 Pore structure 27

2.6.3 Mineralogy 28

2.7 Summary 32

3 Materials and Methods **34**

3.1 Rock Sample and Fluid Properties 34

3.1.1 Lithologies and Rock Properties 34

3.1.2 Fluid Properties 38

3.2 Experimental Workflow 39

3.2.1 Tertiary Low Salinity Water Flooding of Water-Wet Berea Sandstone . . 40

3.2.2 Tertiary Low Salinity Water Flooding of Altered-Wettability Berea Sandstone 42

3.2.3 Tertiary Low Salinity Water Flooding of Altered-Wettability Castlegate Sandstone 43

3.2.4 Tertiary Low Salinity Water Flooding of Altered-Wettability Bunter Sandstone 43

3.2.5 Summary of Experiments 44

3.3 X-ray micro-CT Imaging: Acquisition and Processing 45

3.3.1 Fundamentals of X-ray Micro-CT Imaging 45

3.3.2 X-ray Micro-CT Acquisition 47

3.3.3 Image Analysis Workflow 47

3.3.4 Estimating Saturation Distribution 49

3.3.5 Surface Area Coverage 51

3.3.6 Pore Fluid Occupancy 52

4 The Impact of Wetting State on Low Salinity Water flooding 55

4.1 Overview and Objectives 55

4.2 Results 56

4.2.1 Saturation Distribution 56

4.2.2 Surface Area Fractional Coverage 59

4.2.3 Pore and Throat Occupancy 61

4.2.4 Displacement Processes in The Pores 67

4.3 Conclusions 72

5 The Impact of Pore Structure on Low Salinity Water flooding 74

5.1 Objectives 74

5.2 Pore Scale Observations 75

5.2.1 Saturation Distribution 75

5.2.2 Surface Area Fractional Coverage 77

5.2.3 Global Pore Occupancy 80

5.2.4 Fluid Mobilisation and Redistribution 83

5.2.5 Linking Observations to Pore Geometry and Topology 86

5.3 Conclusions 93

Conclusions 93

6 The Impact of Sandstone Mineralogy on Low Salinity Water flooding 95

6.1 Objectives 95

6.2 Pore Scale Observations 96

6.2.1 Clay distribution 96

6.2.2 Mineral-Specific Surface Area Fractional Coverage 96

6.2.3 Pore Occupancy 101

6.2.4 Clays as a Screening Criterion 109

6.3 Conclusions 115

7 Conclusions and Future Outlook 117

7.1 Conclusions 117

7.2 Future Work 122

7.2.1 Pore Structure - Sensitivity Analysis 122

7.2.2 Clay Availability 123

7.2.3 Synchrotron Imaging 123

7.2.4 Low Salinity Water Alternating Gas Injection 124

Bibliography 125

Chapter 1

Introduction

1.1 Scientific Background and Motivation

Fifteen percent of global energy-related greenhouse gas emissions come from the production of oil and gas resources. Increasing the efficiency of oil production has been cited as a key way to minimise the carbon intensity of these core operations (*IEA*, 2015a). Enhanced Oil Recovery (EOR) techniques are thought to be an important suite of technologies for increasing this efficiency. Techniques including polymer flooding, miscible gas injection, chemical flooding, water alternating gas injection, and surfactant flooding, have long been developed and deployed to increase recovery factors from mature reservoirs above the typical range of 20% to 40% (*Lake et al.*, 2014; *Muggeridge et al.*, 2014).

Another and particularly promising, EOR technique is low salinity water flooding. In low salinity waterflooding, oil recovery is improved through the reduction or modification of the ionic content of injected brines (*Bartels et al.*, 2019; *Jackson et al.*, 2016a; *Loahardjo et al.*, 2007; *Mahani et al.*, 2015a,b). The technique has been shown to have the potential to improve oil recovery by up to 14% in laboratory experiments across scales and in field scale pilot projects (*Abdulla et al.*, 2013; *Lager et al.*, 2008a,b; *Lake et al.*, 2014; *Ligthelm et al.*, 2009; *Rivet et al.*, 2010; *Seccombe et al.*, 2010; *Tang and Morrow*, 2002; *Vledder et al.*, 2010; *Yousef et al.*, 2010, 2011). Due largely to its simplicity, it can also be combined with other EOR techniques, with

promising results. For example, it is thought to be able to increase both oil recovery and CO_2 storage capacity during water alternating gas (WAG) injection (*AlQuraishi et al.*, 2017; *Dang et al.*, 2016; *Naderi and Simjoo*, 2019; *Teklu et al.*, 2017), and has the potential to significantly improve the efficiency of polymer flooding projects (*Unsal et al.*, 2018; *Vermolen et al.*, 2014; *Zhao et al.*, 2021). However, commercial deployment of the technology is inhibited by a lack of reliable reservoir characterisation criteria capable of predicting which systems will respond favourably to the technique.

The uncertainty surrounding low salinity response is partly due to a poor understanding of how microscopic chemical and displacement processes within individual pores of rocks relate to oil production at the larger scales of core flood tests and reservoirs (*Bartels et al.*, 2019). Most experimental observations of low salinity flooding can be split into two length scales, the first focused on the sub-pore scale (*Alotaibi et al.*, 2011; *Basu and Sharma*, 1996; *Berg et al.*, 2010; *Buckley et al.*, 1997; *Sheng*, 2014), and the second on the core-scale, where samples typically range from a few to tens of centimetres (see summary by *Jackson et al.* (2016a)). There are few observations of low salinity water flooding across the scale of networks of pores - typically millimetres in rocks with permeability of order 10^{-14}m^2. At this scale the impact on oil distribution may be heterogeneous due to, e.g., mineralogy and stagnant regions of high salinity brine, and oil may be observed to release and be trapped again (*Aziz et al.*, 2019; *Sohrabi et al.*, 2017). As a result of this lack of pore scale observations, there are gaps in mechanistic explanations linking chemical processes at the microscopic scale to oil redistribution and recovery at core and field scales.

Recently, X-ray micro-CT imaging has been used to bridge this gap in length scales, with observations at micron resolution across millimetre scale domains (*Bartels et al.*, 2019). Observations have been made of the preferential release of oil from clays (*Shabaninejad et al.*, 2015), the dynamics of fluid pore occupancy changes at the pore-network scale (using fast-synchrotron X-ray micro-CT imaging (*Bartels et al.*, 2017a)), potential osmosis events (*Sandengen et al.*, 2016), and the expansion of water layers during low salinity water flooding (*Chen et al.*, 2020). However, more analysis is needed to link sub-pore scale processes to fluid distribution and oil production over core and field scales. In particular, a deeper understanding of the role of wetting

state, pore structure, and mineralogy is required to take a step closer to building a predictive model capable of identifying systems that are responsive to low salinity water flooding.

1.2 Research Objectives

There is currently a poor understanding of how wettability alteration at the microscopic scale impacts oil redistribution and recovery at core and field scales (*Bartels et al.*, 2019). A lack of pore scale observations of low salinity water flooding has been identified as a leading factor behind this shortcoming. In this work, we make use of advances in X-ray micro-CT imaging and image analysis techniques to observe pore scale behaviour during low salinity flooding of various sandstone samples. We specifically focus on the role of wetting state, pore structure and mineralogy in the response to low salinity water flooding.

Wettability is known to be a leading control on displacement mechanisms and fluid distribution during flow in porous media, and is therefore extremely important to consider in the context of low salinity waterflooding experiments. However, thus far there has been no consistency in the initial wetting state of sandstone samples used for pore scale observations of low salinity water flooding. Experiments have been carried out using sandstones with initial wetting states ranging from oil-wet (*Bartels et al.*, 2017a; *Khishvand et al.*, 2017) to weakly water-wet (*Chen et al.*, 2020; *Shabaninejad et al.*, 2018), with little consideration of how this will impact results. In this work, we aim to carry out the first systematic comparison of pore scale response to low salinity water flooding in samples of different initial wetting states, comparing observations in an oil-wet and water-wet Berea sample. Furthermore, in low salinity waterflooding studies, pore scale observations of wetting state have been limited to automatic and manual geometric contact angle measurements. This is a noisy measure of wetting state that is reliant on the accurate identification of the three phase contact line and is, therefore, very sensitive to segmentation workflow. More robust measures of wetting state have been developed but are yet to be implemented to observe wetting state during low salinity flooding in sandstones. We aim to make use of a combination of pore occupancy and fluid coated area fraction analysis

(developed by *Garfi et al.* (2020a)) to make robust measurements of wetting state in the two Berea samples.

Pore structure is known to have a strong control on displacement mechanisms, flow regimes and fluid distribution (*An et al.*, 2016; *Blunt*, 2017; *Holtzman*, 2016; *Shams et al.*, 2021; *Singh et al.*, 2019, 2022; *Tanino and Blunt*, 2012; *Xu et al.*, 2014). However, very little research has addressed the impact of pore structure on the efficacy of low salinity waterflooding. This is partly due to the fact that pore scale observations of low salinity flooding in sandstones have been limited to Berea sandstone. To better understand the effect of pore structure, observations are required over a range of samples with a diverse range of pore geometry and topologies. In this work we aim to make pore scale observations of low salinity water flooding in Berea, Bunter and Castlegate sandstone samples which have varied pore structure.

There is general agreement that clays are necessary for favourable recovery during low salinity water flooding in sandstones. This view is based largely on core scale experiments (*Loahardjo et al.*, 2007, 2010; *Morrow et al.*, 2011, 1998; *Tang and Morrow*, 2002; *Zhang and Morrow*, 2006; *Zhang et al.*, 2007), and sub-pore scale observations of oil detachment from clays on artificial surfaces within flow cells (*Berg et al.*, 2010; *Cense et al.*, 2011; *Mahani et al.*, 2015b; *Nasralla et al.*, 2013). Despite the long held belief that clays are crucial for low salinity flooding there have not yet been any in-situ pore scale observations of oil detachment from clay. In this work we aim to make use of recent advances in mineral specific wettability characterisation to observe the behaviour of clays at the pore scale during low salinity water flooding.

1.3 Thesis Outline

Chapter 2: Literature Review and Outlook reviews the scientific background of low salinity waterflooding research. The chapter discusses observations across scales and explores the relative lack of pore scale observations. Recent advances in X-ray micro-CT technology and their importance in the context of low salinity flooding research are investigated. Lastly, the chapter highlights three areas of research that could significantly improve our understanding of

low salinity waterflooding.

Chapter 3: Materials and Methods presents the rock lithologies, and the composition and properties of fluids used in this work. Experimental workflows and image analysis techniques for each experiment used in this work are also described.

Chapter 4: The Impact of Wetting Sate on Low Salinity Water Flooding investigates the impact of initial wetting state on the response to low salinity water flooding. Results from tertiary low salinity flooding experiments using two separate Berea sandstone rock samples having different wetting states are presented.

Chapter 5: The Impact of Pore Structure on Low Salinity Water flooding presents the first systematic comparison of low salinity waterflooding in Berea, Bunter and Castlegate sandstone samples using pore scale imaging. The chapter identifies the leading role of pore structure on recovery during low salinity waterflooding, paving the way for a more complete set of screening criteria and better predictive capabilities.

Chapter 6: The Impact of Sandstone Mineralogy on Low Salinity Water flooding investigates the role of mineralogy on the low salinity response. We quantify the role of clays in the response to low salinity water flooding across the sandstone samples introduced in Chapter 5. This represents the first pore scale in situ observations of clay behaviour during low salinity flooding in oil-wet samples.

Chapter 7: Conclusions and outlook summarises the research and its potential applications, as well as suggests next steps and areas for development.

Chapter 2

Literature Review

2.1 Low Salinity Flooding - Disparities in Experimental Results

Waterflooding, where brine is pumped into a reservoir, has been widely used to improve oil recovery for almost a century (*Bass Jr et al.*, 1956; *Dykstra and Parsons*, 1950; *Uren and Fahmy*, 1927). Naturally, great interest in the optimisation of the process followed its initial use. The impact of injected brine's composition became an area of focus by the late 1950s (*Martin et al.*, 1959). Despite this, it was not until the 1990s, when Morrow and co-workers released several landmark papers (*Jadhunandan et al.*, 1995; *Morrow et al.*, 1998; *Tang and Morrow*, 2002; *Tang et al.*, 1997; *Tang and Morrow*, 1999), that low salinity water flooding became an area of interest.

A range of studies have since shown that low salinity flooding can increase oil recovery from centimetre scale laboratory cylindrical rock (core) samples and in the field where displacements occur over several hundred metres to kilometres (*Lager et al.*, 2008a,b; *Ligthelm et al.*, 2009; *Rivet et al.*, 2010; *Tang and Morrow*, 2002; *Vledder et al.*, 2010; *Yousef et al.*, 2010, 2011). Recovery is typically improved by 5-14% of the oil initially in place in systems responsive to low salinity flooding. However, many other works have shown little or no incremental oil recovery

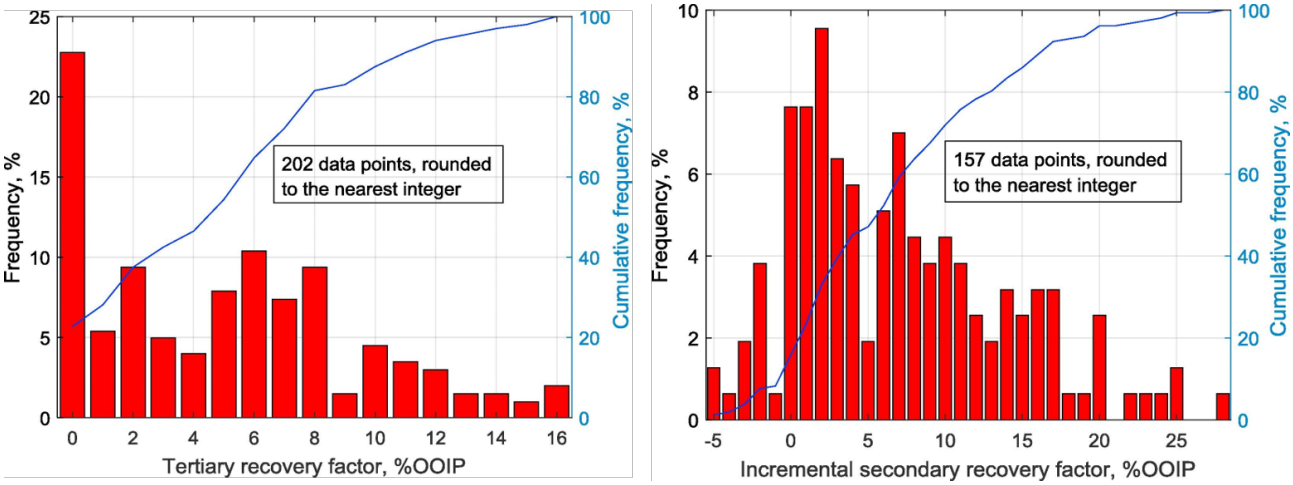


Figure 2.1: Frequency of a) tertiary recovery factors b) incremental secondary recovery factors, compiled from publications. From *Wang and Fu* (2018).

during low salinity water flooding (*Cissokho et al.*, 2010a; *Nasralla et al.*, 2014; *RezaeiDoust et al.*, 2010; *Shaker Shiran et al.*, 2012; *Soraya et al.*, 2009). These disparities in experimental results (best summarised by Fig 2.1 from *Wang and Fu* (2018)) have sparked a continuing drive to build a predictive model capable of identifying systems that will respond favourably to low salinity water flooding. However, this is yet to be achieved and so there remains significant uncertainty around how a given crude oil-brine-rock (COBR) system will respond to low salinity water flooding.

2.2 Necessary Conditions and Predictive Capabilities

The push to build predictive models capable of identifying COBR systems that are responsive to low salinity flooding has led to the development of a widely accepted list of necessary conditions for low salinity flooding to significantly improve oil recovery in sandstones (*Jackson et al.*, 2016a; *Morrow et al.*, 2011; *Tang and Morrow*, 1999):

1. The presence of formation water
2. An exposure to oil containing polar components
3. The presence of multivalent ions in the connate water

4. A significant clay fraction

This list of necessary conditions appears to be a significant step forward in predicting which COBR systems will respond favourably to low salinity water flooding. However, there have been many recorded cases where these conditions were met but no additional production was observed. This suggests that the above is not an exhaustive list of necessary conditions (*Jackson et al.*, 2016a). There is, therefore, currently no way of predicting responses to low salinity water flooding in a given COBR system. Developing predictive capabilities remains the single most important pursuit in low salinity water flooding research. A robust workflow to accurately predict the response of COBR systems based upon simple properties and measures of the system would be valuable; that way, low salinity flooding could be used in a targeted manner to offer efficient, reliable enhanced recovery in suitable reservoirs. To this end, there have been a number of studies that have compared results from a large number of core flooding experiments in an attempt to isolate parameters and build an exhaustive list of necessary conditions for additional recovery during low salinity waterflooding.

Suijkerbuijk et al. (2012) carried out a series of spontaneous imbibition experiments on Berea sandstone and reservoir rock samples. The group found that initial wettability, controlled partly by the concentration of divalent cations in formation water, had a significant influence on the response to low salinity waterflooding. The highest oil production during low salinity flooding was observed when the formation water was high in divalent cations and initial wetting state was more oil-wetting. However, no exhaustive list of necessary conditions was found.

Aladasani et al. (2014) analysed results from 411 low salinity core flooding experiments in the literature. They used a multivariate statistical analysis to link properties of COBR systems to recovery values. A number of parameters were analysed including divalent cation content, salinity, permeability, porosity, ionic strength, interfacial tension, mineralogy (specifically clay content), initial water saturation, ageing time, total acid number, and total base number. The group found a weak correlation of 65% between predicted residual oil saturations and experimental observations (Fig 2.2), but no clear favourable rock and fluid properties were identified.

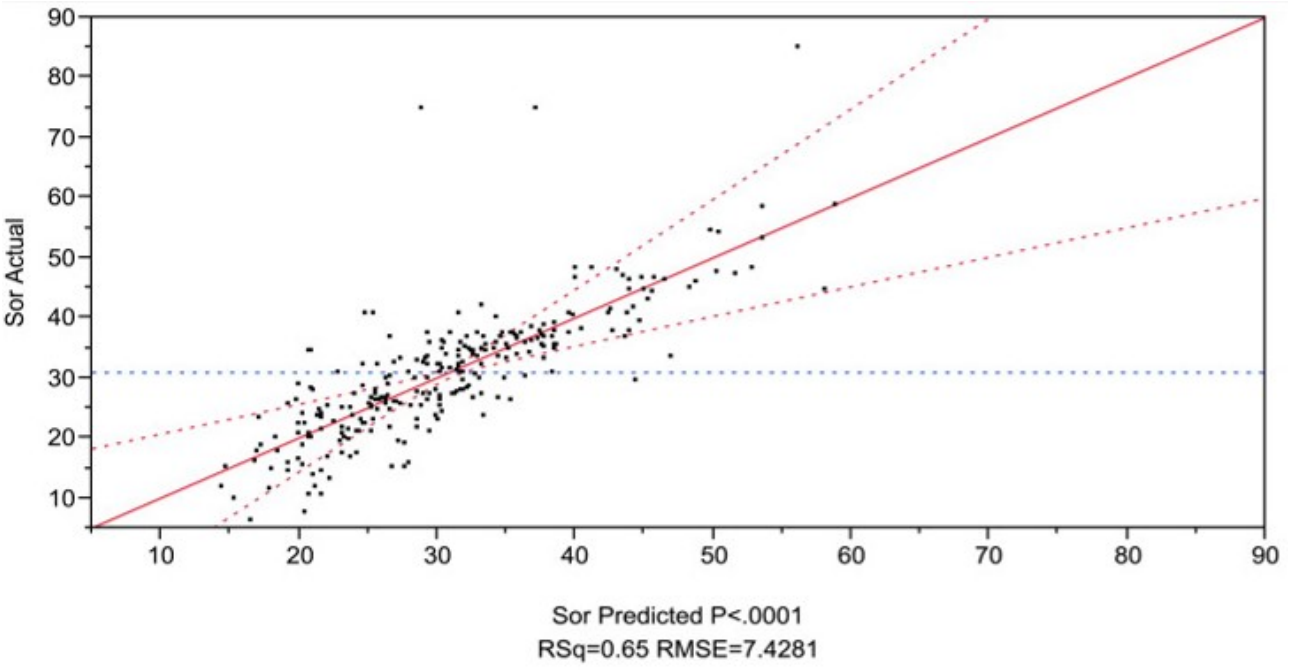


Figure 2.2: Results of a residual oil saturation prediction model from *Aladasani et al.* (2014). Results were computed by multivariate statistics on sandstones. A weak correlation of 65% between predicted S_{or} values and experimental results. Results are presented for 411 separate experiments (each represented by a black dot). The red line represents the regression curve.

Wang and Fu (2018) extracted data from 202 tertiary low salinity core flooding experiments in the literature. They assessed the impact of various initial experimental conditions on low salinity recovery, and found that no single condition was necessary or sufficient for incremental oil recovery. Combinations of initial conditions showed better correlation with extent of incremental oil recovery, but no single combination was found to be sufficient for a favourable low salinity response.

As is explained in detail in *Bartels et al.* (2019), works which focus on inferring necessary conditions for favourable low salinity response from core scale experimental results are solving an inverse problem. This inversion is typically based on limited data such as pressure drops and injection and production fluid volumes and chemistry. Crucially, this approach is unable to uncover the physical processes that occur within the core. There may, therefore, be significant changes in fluid distribution and surface properties that are not recorded. As a result, the method is typically robust when explaining favourable responses to low salinity flooding, but is often unable to explain the absence of a response. This shortcoming has driven a growing

body of work which focuses on identifying the underlying mechanisms of low salinity flooding.

2.3 Underlying Mechanisms

Another approach to the development of predictive models is the pursuit of knowledge around the underlying mechanisms of low salinity flooding. The hope is that understanding the exact mechanisms by which recovery is improved, a comprehensive list of necessary conditions can be developed. Here I will briefly describe some of the most widely studied and accepted underlying mechanisms of low salinity waterflooding. This is to give the reader an idea for the scope of research and a brief understanding of sub-pore scale surface interactions. However, this is not intended to be an exhaustive summary of the literature. For a comprehensive summary, see one of *Jackson et al.* (2016a); *Katende and Sagala* (2019).

2.3.1 Double Layer Expansion

Ligthelm et al. (2009) suggested that low salinity brine causes an expansion of the electrical double layer at mineral-brine interfaces. This expansion is thought to lead to increased electrostatic repulsion between mineral surfaces and adsorbed polar oil components, causing polar oil components to desorb leaving more water-wetting mineral surfaces (*Jackson et al.*, 2016a; *Ligthelm et al.*, 2009). There have been a significant number of publications that support this hypothesis (*Hassenkam et al.*, 2011; *Nasralla et al.*, 2014; *Tang and Morrow*, 1999; *Xie et al.*, 2016). However, the theory is inconsistent with many mineral-surface-scale adhesion tests, which suggest that, at a fixed pH, adhesion of oil increases with a decrease in salinity (*Buckley and Morrow*, 1990; *Drummond and Israelachvili*, 2004; *Lebedeva and Fogden*, 2010). Furthermore, a recent molecular study carried out by *Mehana et al.* (2020) cast doubt on the mechanism, concluding that during low salinity flooding, little change in the thickness of the electrical double layer occurs.

2.3.2 Multiple Ion Exchange

Lager et al. (2008b) suggested that multiple ion exchange occurs between low salinity brine and clay minerals during low salinity flooding. The theory states that multivalent ions (most likely Ca^{2+} and Mg^{2+}) adsorb onto clay surfaces in exchange for polar oil compounds. This releases oil initially adsorbed onto clay minerals, making the surfaces more water-wet. The theory is consistent with a number of studies in the context of low salinity waterflooding (*Alagic and Skauge*, 2010; *Lager et al.*, 2008a,b; *Tang and Morrow*, 1999). In a modelling study, *Wilmott et al.* (2019) concluded that multiple ion exchange is probably a dominant mechanism during low salinity flooding, but will vary depending on oil and clay chemistry. *Chen et al.* (2018) argued that multiple ion exchange in the presence of basal-charged clays prompts an increase in pH - which in itself is often cited as an underlying mechanism.

2.3.3 Fines Migration

Another suggested mechanism for low salinity recovery is fines migration, where the presence of low salinity brine causes the swelling of clays and the detachment of fines from mineral surfaces (*Bernard*, 1967; *Tang and Morrow*, 1999). *Zeinijahromi et al.* (2015) were able to history match production data from the Zichebashskoe reservoir by assuming a fines migration regime. In addition there have been a number of core scale experiments consistent with fines migration as a production mechanism during low salinity water flooding, where a pressure drop and the production of fines were associated with additional recovery (*Agbalaka et al.*, 2009; *Bernard*, 1967; *Loahardjo et al.*, 2007; *Soraya et al.*, 2009; *Tang and Morrow*, 1999). However, a number of experimental results have shown additional production without significant fines migration (*Cissokho et al.*, 2010b; *Lager et al.*, 2008a,b; *RezaeiDoust et al.*, 2011). Moreover, fines migration is often associated with a decrease in production due to reduced permeability and formation damage (*Bennion et al.*, 1998; *Blume et al.*, 2002; *Prempeh et al.*, 2020).

2.3.4 Other Mechanisms

A number of more poorly understood and more sparsely researched mechanisms have also been proposed. These mechanisms include osmosis (*Sandengen et al.*, 2016), and increasing oil-brine interface viscoelasticity (*Kar et al.*, 2022; *Mahmoudvand et al.*, 2021). It is believed that more viscoelastic oil-brine interfaces makes snap-off less favourable, so that the oil phase is more continuous and therefore can be more easily produced (*Chavez-Miyauchi et al.*, 2016; *Morin et al.*, 2016). However, more work is needed to fully understand how and if such mechanisms improve recovery during low salinity waterflooding.

2.3.5 Summary of Mechanisms

There is still great debate as to the exact underlying mechanisms of low salinity flooding. However, there is a common theme among all of the most widely accepted mechanisms: they result in a wettability alteration towards more water-wet conditions. As such, a wettability alteration can be thought of as the pore scale manifestation of one or a combination of the underlying mechanisms described above. This concept is summarised nicely in figure 2.3 from *Wang and Fu* (2018). In turn, a wettability alteration towards more water-wetting conditions is thought to be the primary driver for improved recovery during low salinity waterflooding (*Bartels et al.*, 2019; *Jackson et al.*, 2016a; *Sheng*, 2014). This point was emphasised by *Wang and Fu* (2018), who observed that a wettability alteration towards more water wetting conditions was strongly correlated with incremental oil production when comparing the results of 202 tertiary low salinity waterflooding experimental results from the literature.

2.4 Wettability Alteration - Observations Across Scales

A wettability alteration during low salinity waterflooding has been observed in a range of experiments, with the bulk of work focusing on the sub pore scale. Most commonly, wettability alteration is quantified by zeta potential measurements (*Alhuraishawy et al.*, 2018; *Alotaibi*

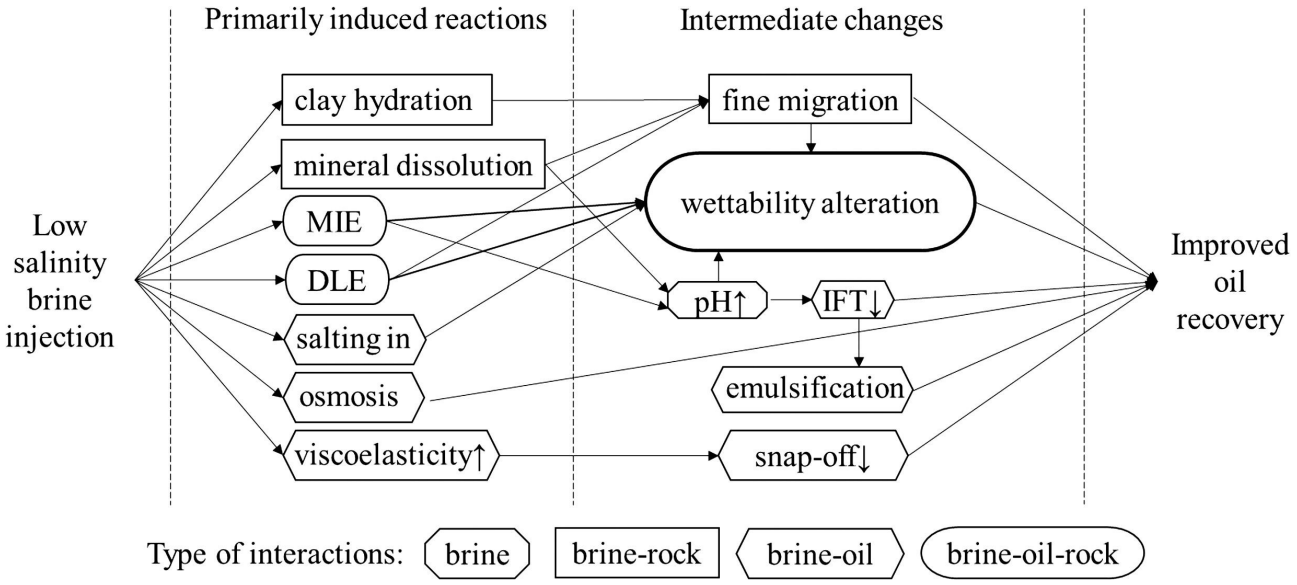


Figure 2.3: Overview of sandstone LSWF EOR mechanisms. From *Wang and Fu* (2018).

et al., 2011; *Basu and Sharma*, 1996; *Jackson et al.*, 2016b), contact angle measurements on flat surfaces (*Alotaibi et al.*, 2011; *Berg et al.*, 2010; *Buckley et al.*, 1997; *Fogden*, 2011; *Lebedeva and Fogden*, 2010; *Mahani et al.*, 2015b; *Nasralla et al.*, 2014; *Yang et al.*, 1999), or adhesion measurements using Atomic Force Microscopy (*Basu and Sharma*, 1999; *Drummond and Israelachvili*, 2004; *Hassenkam et al.*, 2011, 2012; *Hilner et al.*, 2015; *Yesufu-Rufai et al.*, 2020).

Wettability alteration has also been observed on the core scale (10s of centimetres) with wetting state typically characterised using spontaneous imbibition (SI) experiments (*Chen et al.*, 2010; *Sohrabi et al.*, 2017; *Suijkerbuijk et al.*, 2012; *Wickramathilaka et al.*, 2010), and over field scale with *Vledder et al.* (2010) identifying a change in wettability over a field scale during low salinity water flooding, inferred from a shift in relative permeabilities.

Whilst there is general agreement that wettability alteration is the primary driver for improved recovery during low salinity waterflooding, exactly how these changes in wetting state lead to the redistribution and production of oil remains poorly understood. A wettability alteration by no means inherently results in additional recovery. To fully understand how low salinity flooding enhances recovery, a full mechanistic explanation linking wettability alteration at the microscopic scale to oil redistribution and recovery at core and field scales is needed (*Bartels et al.*, 2019). Features such as pore structure, mineralogy and stagnant regions of high salinity

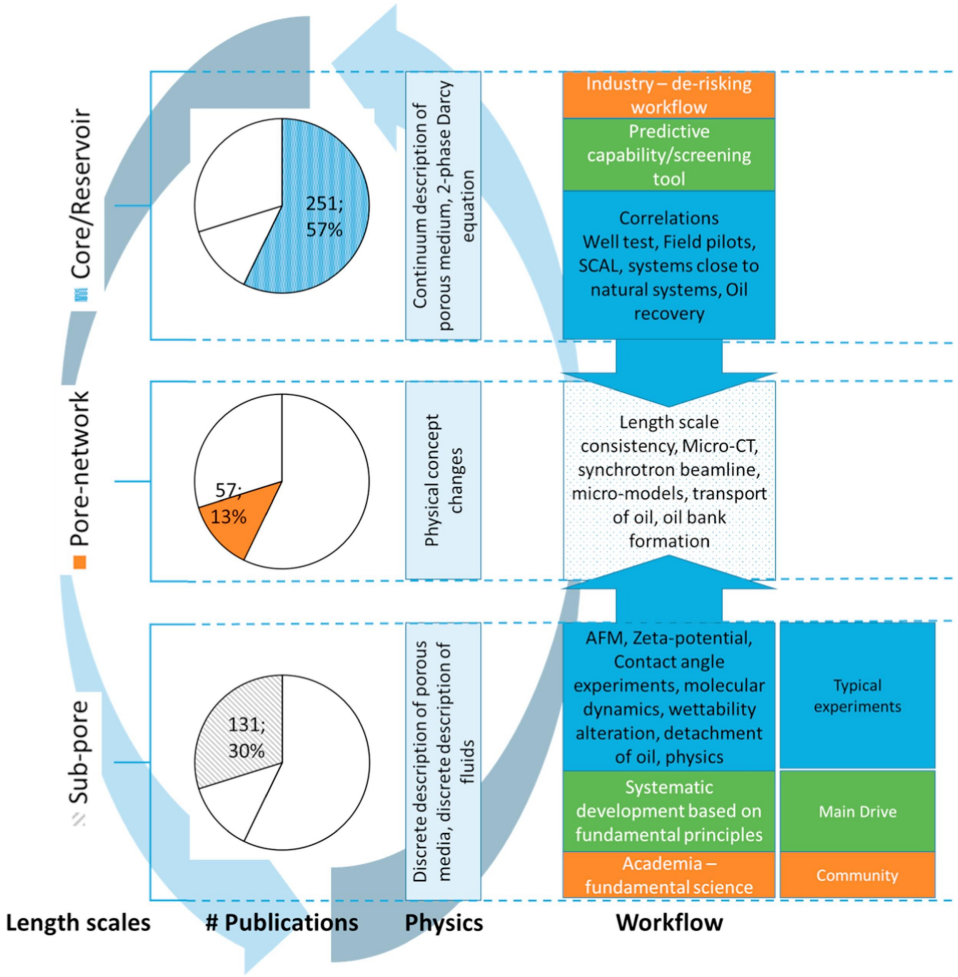


Figure 2.4: From *Bartels et al.* (2019). Diagram summarising the different approaches to low salinity waterflooding research across scales. The pie charts show the number of publications in each length scale (as of 2018). There is a relative lack of pore-network observations compared to sub-pore (mostly driven by academic research) and core/reservoir scale (mostly driven by industrial research).

brine all impact local oil distribution, leading to heterogeneous impacts across pore-network scales (*Aziz et al.*, 2018, 2019; *Sohrabi et al.*, 2017). It appears that a wettability alteration during low salinity waterflooding is necessary but not sufficient for favourable recovery to occur.

The lack of a mechanistic explanation linking wettability alteration at the microscopic scale to oil recovery at core and field scales in largely due to a relative lack of observations over pore and pore-network scales - typically millimetres in rocks with permeability of order 10^{-14}m^2. This gap in length scales is summarised in figure 2.4, and described at length by *Bartels et al.* (2019). Most experimental observations of low salinity waterflooding are either on the sub-pore scale (sub-micron resolution across sub-millimetre domains) or the core-scale (where samples

typically ranging from a few to tens of centimetres). Sub-pore scale observations are typically made using micromodels and flow cells as well as Atomic Force Microscopy (AFM) observations. Core scale observations typically consist of pressure drops and injection and production fluid volumes and chemistry during experiments using samples typically range from a few to tens of centimetres (see summary by (*Jackson et al.*, 2016a)). Pore scale observations are vital to better understand how underlying mechanisms translate to oil production over core and reservoir scales. In recent years, X-ray Micro-CT imaging has been employed to help fill this gap in understanding.

2.5 Pore Scale Observations

Finally, I will discuss the current state of the art with regards to pore scale observations of low salinity water flooding. In doing so, I will identify gaps in understanding and suggest approaches to develop insights into production mechanisms during low salinity waterflooding, paving the way for better predictive capabilities.

In recent years, X-ray micro-CT imaging has had a tremendous impact on the field of multiphase flow in porous media. The technology has been utilised for in situ wettability characterisation, for direct observations of fluid distributions and observations of phenomena such as Haines Jumps, roof snap off, and intermittency (*AlRatrout et al.*, 2017, 2018; *Berg et al.*, 2013; *Blunt et al.*, 2021; *Bultreys et al.*, 2018; *Spurin et al.*, 2019, 2021; *Sun et al.*, 2021). There is great potential for the technology to revolutionise our understanding of low salinity water flooding at the pore scale.

2.5.1 Sandstones

Already, X-ray micro-CT imaging has provided important insights into the pore scale response to low salinity flooding. In particular, pore scale observations have given valuable insights into wettability alteration during low salinity waterflooding, and the effect this can have on fluid

distributions. Below, I will highlight the major pore scale observations of low salinity flooding in sandstones.

Khishvand et al. (2017) were the first group to make pore scale observation of in situ wettability alteration during low salinity water flooding. The group used X-ray micro-CT technology to image a limited number of in situ contact angles before and after both low salinity and high salinity secondary waterfloods of miniature Berea cores (Fig. 2.5). No change in contact angles was observed during high salinity waterflooding, whereas a change from 115°to 89° was observed after low salinity water flooding. The group also observed a decrease in the average pore diameter of water-filled pore elements during low salinity waterflooding, indicative of a wettability alteration towards more water-wet conditions. This was found to correspond to approximately a 33% increase in recovery compared to high salinity water flooding, as water displaced oil from previously inaccessible smaller pores.

Bartels et al. (2017a) also observed pore occupancy changes during low salinity waterflooding, but using synchrotron-based fast X-ray tomography, so that changes in oil distribution on the order of seconds could be observed. The group observed changes in oil/brine distribution in the larger pores for a Ketton carbonate sample and smaller pores in a Berea sandstone sample. These mixed results may have been due to an absence of multivalent cations in both the high salinity and low salinity brines. The only salt present was potassium iodide (200 g/L for high salinity, and 27 g/L for low salinity), meaning an absence of multivalent cations in both brines, hence ruling out any significant multiple ion exchange, and, potentially, any low salinity effect.

Shabaninejad et al. (2018) used X-ray micro-CT technology to image Berea micro-cores before and after spontaneous imbibition of low salinity brine. Connectivity of residual oil, interfacial area and mean interfacial curvature were all measured. Decreased connectivity of residual oil (due to increased blob retreat and snap off events); a decrease in oil/brine interfacial curvature and increase in brine/grain interfacial area; and a small change in mean oil/brine interfacial curvature from negative to positive, were all observed after spontaneous imbibition of low salinity brine. Each of these observations are consistent with a shift towards more water wet conditions. Direct observations of brine snap-off events, consistent with water-wetting

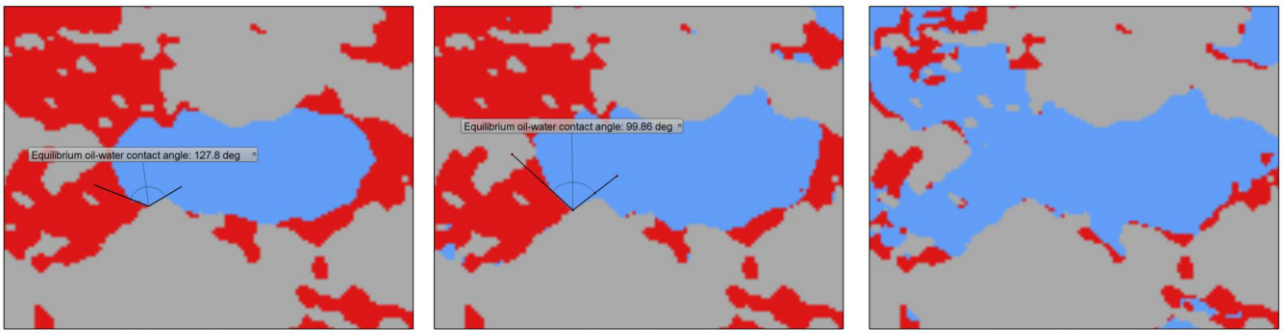


Figure 2.5: A two-dimensional view of pore-scale fluid occupancy and manual oil (red) - brine (blue) contact angle measurements in a Berea sample of altered wettability after a) 0.5 Pore volumes of low salinity waterflooding b) 5 Pore volumes of low salinity waterflooding and c) 10 Pore volumes of low salinity waterflooding. Image sizes: 0.21 × 0.16 mm. From *Khishvand et al.* (2017).

conditions, during low salinity water flooding were also presented (shown in Figure 2.6).

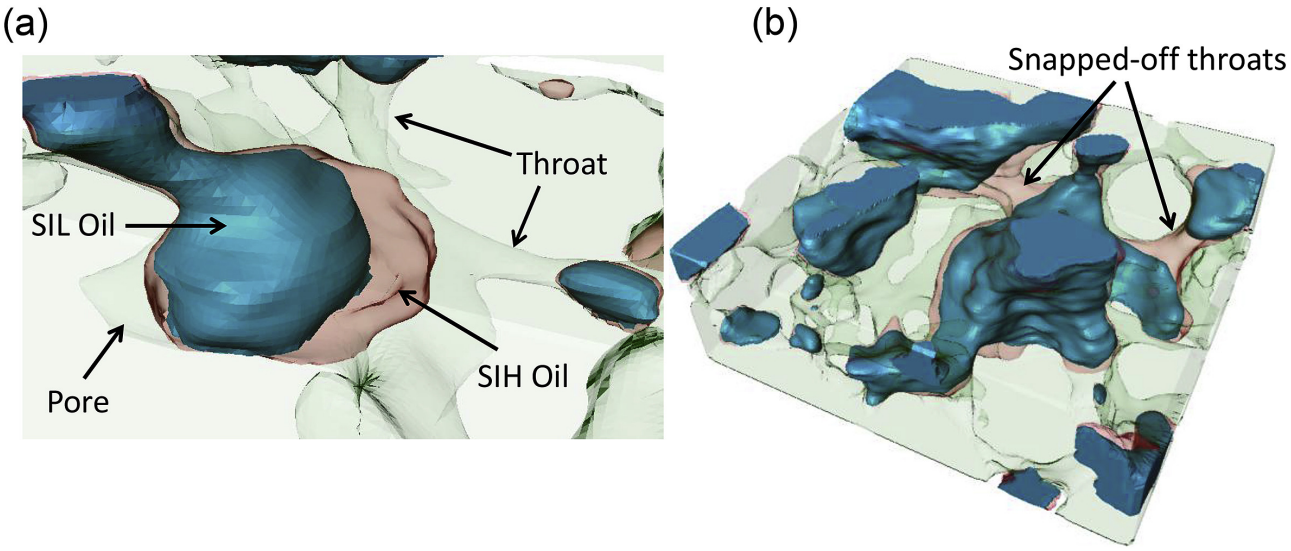


Figure 2.6: Iso-surfaces of oil blobs after spontaneous imbibition of high salinity brine (brown) and spontaneous imbibition of low salinity brine (green), showing (a) close-up of an oil ganglion in a single pore (0.26 × 0.16 × 0.10 mm), and (b) changes in oil distribution, including snap-off events, over a larger subvolume (0.50 × 0.46 × 0.16 mm). From *Shabaninejad et al.* (2018).

Chen et al. (2020) observed increases in water film thickness during tertiary low salinity water flooding of a Berea sandstone core. This was linked to a wettability alteration towards more water-wet conditions which was argued to be the primary mechanism for the five percentage point additional recovery that was observed during low salinity flooding. More recently, *Chen et al.* (2021) analysed secondary and tertiary low salinity flooding of oil-wet Berea sandstone samples. The group used automatic contact angle measurements to observe a shift to more

water wetting conditions during both secondary and tertiary low salinity flooding. The group observed significantly higher recovery during secondary low salinity waterflooding, than during tertiary low salinity waterflooding. This difference was attributed to differences in fluid morphology before low salinity flooding. Oil and water distributions after tertiary low salinity water flooding were observed to inherit the distribution after the secondary high salinity waterflooding. This finding implies that the generation of preferential flow pathways during secondary high salinity influenced the flow of low salinity brine and thus limited oil displacement.

2.5.2 Carbonates

Pore scale observations of low salinity waterflooding have also been made in carbonate samples. The underlying mechanisms of low salinity flooding in carbonates are thought to be distinct from those in sandstones. Therefore, observations are not directly applicable to sandstones (which are the focus of this literature review). However, insights into pore scale behaviour can be useful because in both lithologies production is thought to be associated with a wettability alteration towards more water-wetting conditions. *Qin et al.* (2019) presented the most thorough pore scale observations of low salinity water flooding in carbonates to that point. The group used manual contact angle measurements to show a wettability alteration towards more water wetting conditions, with results closely matching the aforementioned findings of *Khishvand et al.* (2017) who carried out similar analysis for a Berea sandstone sample. The group also showed significant changes in pore occupancy during low salinity water flooding, with an increase in brine saturation in small and medium pores, consistent with a shift to more water wetting conditions (Fig 2.7) and again consistent with the findings of *Khishvand et al.* (2017). Since then, *Selem et al.* (2021) published an even more comprehensive pore scale study of low salinity flooding in carbonates. The group implemented thermodynamic contact angle calculation, interfacial curvature measurements, automatic contact angle measurements and pore occupancy analysis to investigate pore scale response to secondary low salinity waterflooding in an oil-wet carbonate sample. Each measure showed a shift to more water-wetting conditions during secondary low salinity waterflooding. Such a comprehensive pore scale investigation has

not yet been carried out using sandstone samples.

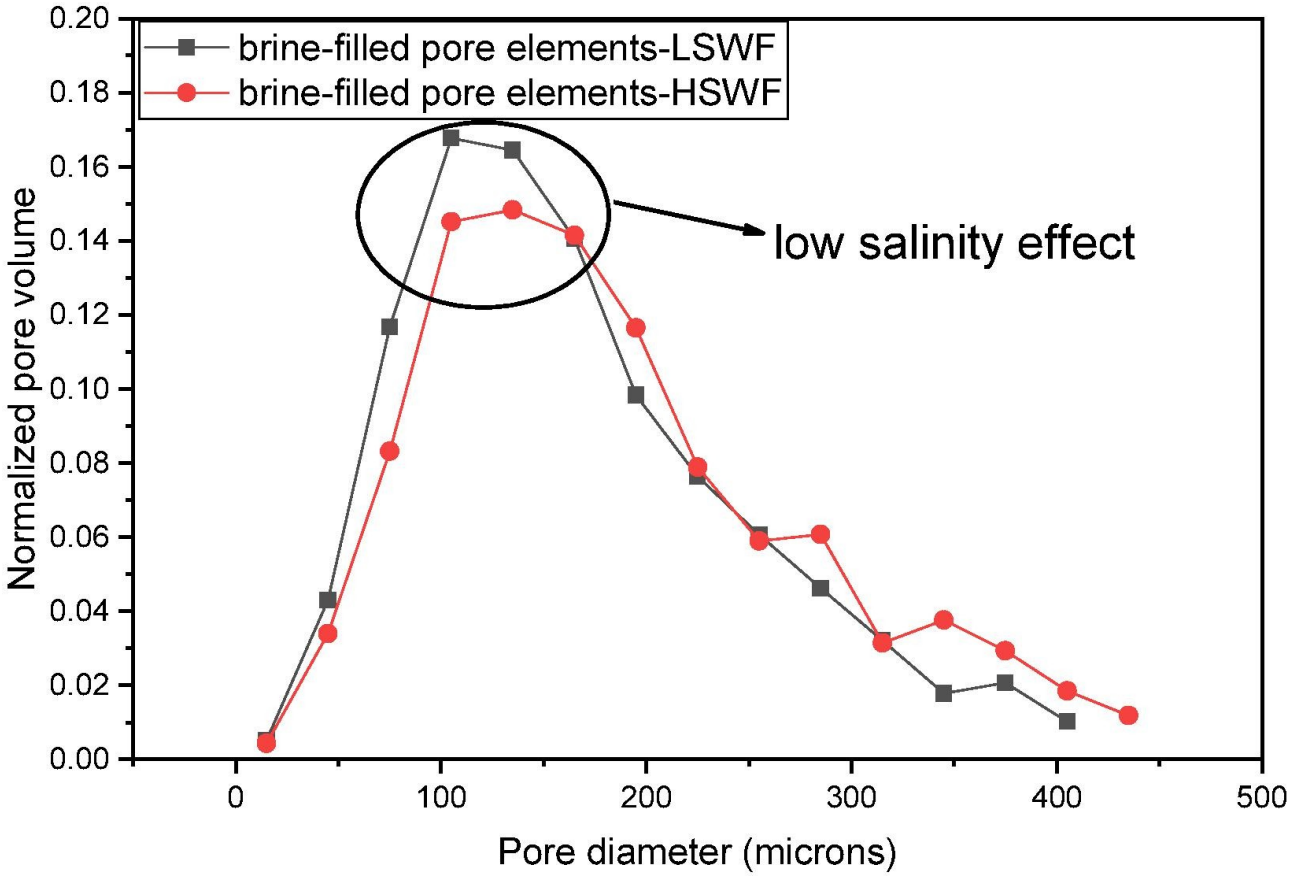


Figure 2.7: From *Qin et al.* (2019). Size distributions of brine-filled pore elements at the end of high salinity waterflooding (HSWF) and low salinity water flooding (LSWF) of oil-wet carbonate sample. There is a significant increase in brine saturation in small and medium sized pores during LSWF, indicative of a shift to more water-wetting conditions.

2.6 Areas for Further Research

So far in this section, we have discussed recent advancements in pore scale observations of low salinity waterflooding, and the valuable insights that these have provided. However, more detailed pore scale observations are needed to further our understanding of production mechanisms during low salinity waterflooding, and potentially provide further screening criteria to take a step closer to obtaining predictive capabilities. In this section, I will outline three areas where X-ray micro-CT imaging can be used to advance knowledge and pave the way to building predictive models of low salinity flooding in sandstones.

2.6.1 Wettability - Initial Wetting State and Wettability Characterisation

Initial Wetting State

It has been known for decades that wetting state has a vital control on fluid distribution, displacement mechanisms and recovery during waterflooding (*Blunt*, 2017; *Donaldson et al.*, 1969). This body of work has been carried out with a number of techniques including corefloods (*Akbarabadi and Piri*, 2013; *El-Maghraby and Blunt*, 2012; *Krevor et al.*, 2011), micromodel experiments (*Hu et al.*, 2017; *Wang et al.*, 2016) and pore network modelling (*Blunt et al.*, 1997; *Bultreys et al.*, 2015, 2016a; *Spiteri et al.*, 2008). As mentioned previously, *Suijkerbuijk et al.* (2012) found that initial wettability had a significant influence on the response to low salinity flooding in experiments over multiple experiments on Berea and reservoir samples. However, the controls of initial wetting state on the pore scale response to low salinity waterflooding is poorly understood.

As described above, *Shabaninejad et al.* (2018) used micro-CT technology to observe fluid distribution, interfacial area and mean interfacial curvature before and after spontaneous imbibition of low salinity brine in micro-cores. Observations were consistent with a small shift towards more water wet conditions. However, the experiments were carried out on initially weakly water-wet samples. This is unrealistic when compared to reservoir conditions, which are typically mixed or oil-wet (*Blunt*, 2017). Similarly, *Chen et al.* (2020) observed a shift to more water-wetting conditions, inferred from an increase in water film thickness, during low salinity waterflooding of Berea sandstone, however, the study was carried out in a sample that did not undergo an ageing process and was observed to be weakly water-wet. Therefore, similarly to the study by *Shabaninejad et al.* (2018) described above, the relevance of these observations is questionable as the sample did not reflect realistic wetting conditions of reservoir systems (*Blunt*, 2017). This is in contrast to results presented by *Bartels et al.* (2017a); *Khishvand et al.* (2017), where the wetting state of the Berea micro-cores used were altered by exposure to crude oil prior to flow experiments, making them more oil-wetting. The varied initial wetting states

among the limited number of pore scale low salinity flooding experiments makes comparing results challenging. A systematic comparison of low salinity waterflooding in similar samples with identical experimental conditions but different wetting states is required to better understand the control of initial wetting states on the pore scale response to low salinity flooding.

Wettability Characterisation

As described in the previous section, *Khishvand et al.* (2017) were the first group to explicitly observe an in situ wettability alteration during low salinity water flooding at the pore scale. The study used X-ray micro-CT technology to image a limited number of in situ contact angles before and after both low salinity and high salinity secondary waterfloods of miniature cores. Whilst these results are compelling, there is increasing evidence to suggest that contact angle measurements are a noisy measure of wetting state. Firstly, X-ray micro-CT resolution is not sufficient to resolve exact contact points, pore geometries, and surface roughness, all of which are known to have a strong control on effective contact angle (*Rabbani et al.*, 2018; *Raeini et al.*, 2014; *Schmatz et al.*, 2015). Secondly, since contact angles are measured from three phase contact lines, measurements are highly sensitive to both segmentation and smoothing of raw images. Lastly, measured angles do not represent advancing contact angles, rather effective values at rest on rough surfaces, which generally leads to artificially low angles (*Lin et al.*, 2018). It is therefore insufficient to infer wettability from contact angle measurements alone. More robust measures of wetting state should be utilised.

Advanced Measures of Wettability Characterisation

In recent years there have been a number of breakthroughs in measuring wetting state from pore scale images. A number of methods have been developed which are more robust and less sensitive to image analysis workflows than traditional geometric contact angle measurements. However, these have yet to be implemented to observe the pore scale response of to low salinity waterflooding in sandstones. Below I will briefly describe each method, with a particular focus on surface coated area coverage. This is not intended to be an exhaustive review of each

method, but rather a brief introduction. For a more thorough review of state of the art of pore scale wetting state characterisation, see *Garfi* (2021).

Thermodynamic contact angle

Blunt et al. (2019) have recently proposed a framework to estimate the contact angle characteristic of a displacement. To do this, they combine a generalised Young equation with an energy balance between the states before and after the displacement. The thermodynamic contact angle θ_t can be approximated from:

$$\Delta a_{1s} cos\theta_t = \kappa\phi\Delta S_1 + \Delta a_{12} \tag{2.1}$$

Where Δa_{1s} and Δa_{12} are the changes in fluid-solid and fluid-fluid interfacial areas per unit of porous medium control volume. ΔS_1 is the change in saturation of phase 1, ϕ is the medium porosity and κ is the mean fluid-fluid interfacial curvature.

A major advantage of this approach is that advances in X-ray micro-CT imaging mean that all the terms in the expression, apart from θ_t, can be measured directly. The method is superior to geometrically measured contact angles for a number of reasons. Firstly, it has been shown to be more sensitive to changes in wetting state than geometric contact angles. Secondly, in a pore network modelling study, predicted relative permeabilities using thermodynamic contact angles as a wetting input were found to match experimental values better than when geometric contact angles were used (*Raeini et al.*, 2018). However, the approach gives an average wetting state for a given system, and therefore does not capture spatial variation in wetting state across a given sample. Recent work by *Akai et al.* (2020a) explored utilising thermodynamic contact angle measurements on a pore-by-pore basis, but results were unsatisfying with measurements limited to displacement events confined to an individual pore region. Another drawback of the measure is that it assumes that viscous dissipation is negligible. This is a well founded assumption for imbibition regimes where energy dissipation has been observed to be approximately 10% of applied work, but it is unclear if this assumption is valid in drainage regimes where more applied work is dissipated (*Akai et al.*, 2020a; *Berg et al.*, 2013).

The technique has recently been implemented to observe a wetting alteration during low salinity waterflooding in a carbonate sample (*Selem et al.*, 2021), but has yet to be implemented to observe wetting state during low salinity water flooding in sandstone samples.

Topological Determination of Contact Angle

Sun et al. (2020a,b,c, 2021) have developed an approach where a macroscopic contact angle is produced based on the deficit curvature of the fluid interfaces that are imposed by contacts with other immiscible phases. This method, developed by using integral geometry coupled to thermodynamic laws, provides a universal description of wettability on multiscale surfaces. A macroscopic contact angle, θ_{macro}, can be determined for a ganglion, C, as:

$$\theta_{macro} = \frac{\kappa_d}{4N_c} \tag{2.2}$$

Where N_c is the number of contact loops that the ganglion shared with the solid surface, and κ_d is the deficit curvature of the ganglion.

The method has been shown to be less sensitive to resolution effects than geometric contact angle measurements as it does not rely on the accurate extraction of the three phase contact line, but rather the topological structure of the contact line loops - which can be observed at lower resolutions. θ_{macro} has been determined for a sessile droplet system, and was found to agree strongly with experimentally measure angles, showing that in a simple system, θ_{macro} provides a reliable approximation of intrinsic wettability. However, the method is yet to be tested on more complex morphologically and mineralogically heterogeneous systems (*Sun et al.*, 2020a).

Fluid Surface Coated Area Fraction

Garfi et al. (2020a) have derived a model from equilibrium thermodynamics relating fluid coverage of rock surfaces to wettability and fluid saturation, as follows:

$$A_{so}(S_o) = \frac{1}{\beta}\frac{\sigma_{ow}}{(\sigma_{os} - \sigma_{ws})}\Big(2\int_{S'=0}^{S_o}\kappa dS' - \int_{S'=0}^{S_o}\frac{dA_{ow}}{dS'}dS'\Big) \tag{2.3}$$

Where β is a roughness factor that accounts for the mismatch between the real interfacial area between each fluid and the solid surface and the one measured by imaging. The ratio of interfacial tensions, $\frac{\sigma_{ow}}{\sigma_{os}-\sigma_{ws}}$, is equivalent to $\frac{1}{cos\theta}$ in a single capillary tube. The terms inside the bracket represent the reversible work of desaturation and the creation of oil-water interfacial area, respectively. This shows that the area of solid surface coated by a fluid as a function of fluid saturation $A_{so}(S_o)$ is itself a function of wetting state, and so in an indicative measure of wetting state. By fitting the model to experimental data for a water-wet system, *Garfi et al.* (2020a) calculate a geometrical roughness factor of $\beta \approx 10^0 - 10^3$. This value is consistent with literature roughness factor values which are calculated by comparing Brunauer-Emmett-Teller surface area measurements with and X-ray micro-CT imaging measuremnets (*Lai et al.*, 2015).

Garfi et al. (2020a) show that by presenting the fraction of a mineral surface coated by a given fluid phase as a function of the saturation of that phase, wetting state can be inferred. This is implemented on a subvolume-by-subvolume basis, where an image of a sample can be split into a number of equally sized subvolumes. For each subvolume, oil saturation S_o and the fraction of the solid surface coated by oil A_{fo} is extracted. These values can then be plotted for all subvolumes to present a clear picture of wetting state throughout the sample. An advantage of this method is that it can be used to assess mineral specific wetting state (Fig 2.8). The fraction of the total area of a given mineral group in contact with a fluid (a_{ij}) is calculated as follows:

$$a_{ij} = \frac{A_{ij}}{\sum_i A_{ij}} \tag{2.4}$$

where A_{ij} is the measured surface area per unit of pore volume shared by fluid i with solid j, respectively. These values can then be presented as a function of the saturation of fluid i, S_i for each subvolume (Fig 2.8).

This approach has a number of advantages. Most notably, it is a robust measure as it does not rely upon the accurate measurement of three phase contact lines (which is required for geometric contact angle measurements) or interfacial curvatures (which is required for contact

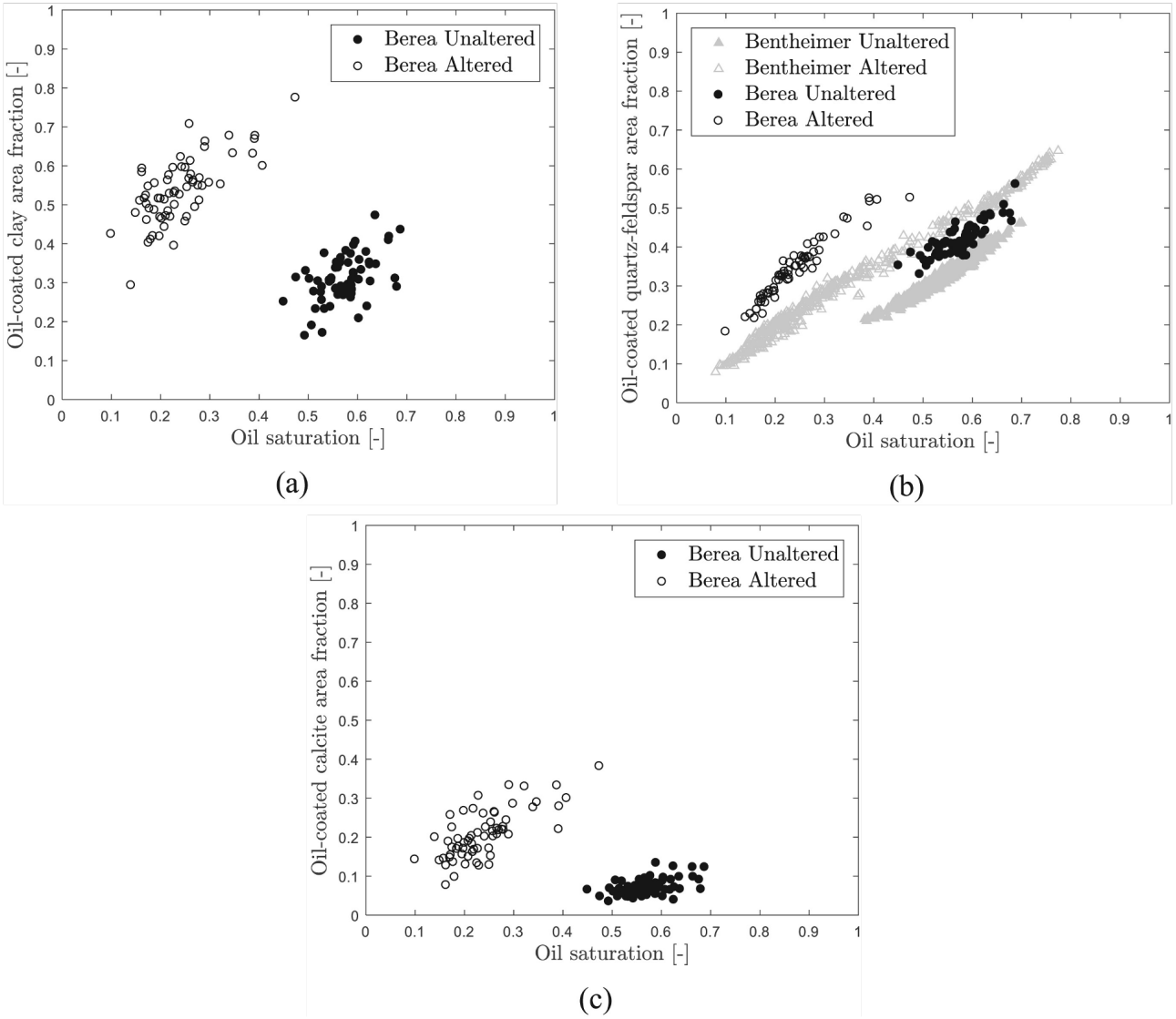


Figure 2.8: Mineral specific Oil-coated area fractions (a_{ij}) computed in one water-wet Berea sample and one Berea sample of altered wetting state for a) Clay minerals, b) quartz and feldspar minerals, and c) Calcite minerals. In all cases, the fraction of mineral surface coated by oil is higher for a given oil saturation in the sample of altered wetting state. This is indicative of more oil-wetting conditions. This effect is particularly prominent on clay and calcite minerals. From *Garfi et al.* (2020a).

angle determination from thermodynamic or topological principles). The method simply relies upon fluid saturation and fluid-solid interfacial area measurements. However, there remains some uncertainty around the utility of the method in systems where sub-resolution water films are present. In such cases, the true determination of oil coated surface area fraction is difficult.

The subvolume-by-subvolume approach allows for spatial variation in wetting to be assessed. Furthermore, the measure can be extended to observe wettability on a pore-by-pore basis, where, for a given fluid, the fluid volume fraction and the fraction of pore surface coated by the fluid is recorded (*Garfi et al.*, 2022). This has been used to show the heterogeneous distribution of wetting state in various samples, and highlights the need for measures of wetting state that are able to capture spatial variability of wetting within a given sample. Lastly, the method allows for mineral specific wetting state to be observed. This is particularly important in the context of low salinity flooding research as clay group minerals are thought to behave differently to other mineral groups. The ability to isolate clay behaviour and assess the pore scale response of clays during low salinity flooding is a potentially powerful tool to better understand the pore scale response of sandstones to low salinity flooding.

2.6.2 Pore structure

It is widely known that pore structure can have a dramatic impact on displacement mechanisms and flow regimes. Pore aspect ratios, pore radii distributions, coordination number, and pore-scale disorder have all been shown to impact displacement mechanisms and fluid distribution during both imbibition and drainage in direct in situ observations, micromodel experiments, and modelling studies (*An et al.*, 2016; *Blunt*, 2017; *Guo et al.*, 2018; *Holtzman*, 2016; *Shams et al.*, 2021; *Singh et al.*, 2019, 2022; *Tanino and Blunt*, 2012; *Xu et al.*, 2014). Most recently, *Singh et al.* (2022) used an X-ray synchrotron facility to constantly image a capillary-controlled drainage-imbibition experiment on an initially brine-saturated carbonate rock sample. The group identified a new type of pore snap-off regime and presented correlations for displacement events as a function of pore-throat geometry. They observed that the throat radius in relation to the pore radius (captured by aspect ratio) involved in a displacement event is the key criterion

(Fig 2.3). Although this was an imbibition experiment, and low salinity flooding is a drainage regime (in a typically oil-wet system), the work gives insight into just how significant the role of pore structure is in determining displacement mechanisms and flow regimes. *Chen et al.* (2021) found that the initial morphology of fluids had a significant impact on oil displacement and production during low salinity flooding. This was in the context of secondary and tertiary low salinity waterflooding but could also be interpreted as an argument for the importance of pore structure. Fluid morphology and dynamics are known to be influenced by pore structure (*Blunt*, 2017; *Guo et al.*, 2018) and therefore, pore structure is likely to play an important role in facilitating additional recovery during low salinity waterflooding. Despite this knowledge, very little research has addressed the impact of pore structure on the efficacy of low salinity waterflooding.

In order to effectively assess the control on pore structure low salinity flooding, experiments across a range of samples with a range of pore geometries and topologies are required. However, until now, pore scale imaging of low salinity waterflooding of clastic rocks has been restricted to experiments on Berea sandstone cores only. Berea is an ideal candidate for low salinity waterflooding experimental studies as it has well documented petrophysical properties, has a significant clay fraction, and has been shown to respond well to low salinity waterflooding in several previous experiments over a range of scales (*Chavez-Miyauch et al.*, 2020; *Khishvand et al.*, 2017; *Romero et al.*, 2013; *Shabaninejad et al.*, 2018). However, the lack of pore scale observations across different clastic rocks has significantly limited our understanding of the interaction between pore structure and low salinity flooding. To further our understanding, pore scale observations are required across a range of samples with varied pore structures.

2.6.3 Mineralogy

As described in *Jackson et al.* (2016a), the general agreement that clays are a necessary condition for favourable recovery during low salinity water flooding is based upon some questionable evidence. General acceptance of the condition emerged after *Tang and Morrow* (1999) concluded that favourable recovery during low salinity flooding was not observed in clean (clay-

free) sandstones. This conclusion was based upon a single low salinity core flood reported in a clean sandstone (which contained an iron oxide coating, that may have altered surface properties of quartz grains throughout the sample). The general assumption that clays were vital for improved recovery during low salinity water flooding in sandstones was then held for subsequent papers published by Morrow and co-workers, and so the overwhelming majority of experiments were carried out on clay-rich sandstone samples (*Loahardjo et al.*, 2007, 2010; *Morrow et al.*, 2011, 1998; *Tang and Morrow*, 2002; *Zhang and Morrow*, 2006; *Zhang et al.*, 2007). This view was later strengthened by *Lager et al.* (2007, 2008a) who showed increased additional recovery with increased kaolonite content in a small number of samples, all of which had a significant clay content. The necessary presence of clay minerals for successful low salinity flooding in sandstones quickly became the accepted view, and so very few low salinity flooding experiments have since been carried out on clay-poor sandstone samples. Following the initial core-scale experiments, a number of groups worked to directly observe the behaviour of oil and clays in the presence of low salinity brine, focusing on the sub pore scale. *Berg et al.* (2010) observed a wettability alteration and oil detachment from a clay surface exposed to low salinity brine in a flow cell. *Cense et al.* (2011); *Mahani et al.* (2015b) both deposited clays on a substrate in all possible orientations within a flow-cell, finding that there was less pinning of oil after exposure to low salinity brine, with a wetting alteration towards more water-wetting state and eventual detachment of oil from clay surface (Figure 2.9). *Nasralla et al.* (2013) imaged oil blobs on mica surfaces, and observed a systematic reduction in contact angles with exposure to lower brine salinities, indicative of a shift to more water-wet conditions. However, despite this body of work, there is an increasing number of studies which suggest that clays may not be essential for additional recovery during low salinity water flooding.

A number of studies have been published suggesting that clays are not essential for a favourable low salinity response in sandstones. Additional recovery during low salinity flooding has been observed in clay-free sandpacks and sandstone samples, and on quartz mineral surfaces (*Hassenkam et al.*, 2011, 2012; *Pu et al.*, 2010; *Suman*, 2014). These studies paved the way to a more thorough examination of the role of clays during low salinity waterflooding. *Liu et al.* (2018) used Atomic Force Microscopy measurements to observe double layer expansion and a

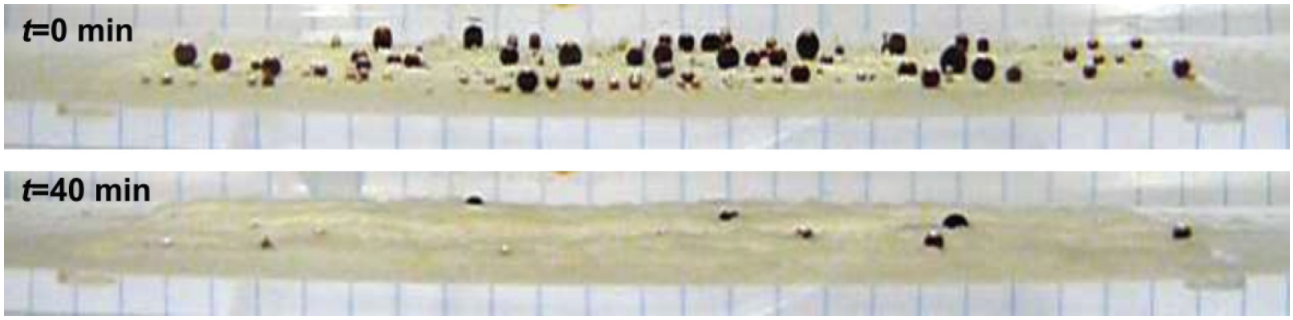


Figure 2.9: Oil droplets displaced from clay surface after exposure to low salinity brine. From *Cense et al.* (2011).

reduction of adhesion forces on quartz surfaces during exposure to low salinity brine. *Bartels et al.* (2017b) used single channel micromodels to assess wettability alteration and oil mobilisation during low salinity waterflooding, observing a positive low salinity response - a reduction in contact angle - for systems containing crude oil regardless of the presence of clays. Additionally, *Shabaninejad et al.* (2018) observed a decrease in oil-quartz and oil-feldspar interfacial area during low salinity flooding of Berea sandstone - indicative of a shift to more water-wetting conditions. *Al-Saedi et al.* (2019a) compared results from tertiary low salinity waterflooding of a sandstone core and clay free sand core. They found that acetate detachment and oil recovery occurred both in the presence and absence of clay during low salinity water flooding. The same group extended this analysis to use four chromatography columns containing varying quantities of quartz and clay minerals to assess the role of clays in the low salinity response. There was strong evidence of ion exchange in the 100% quartz case (*Al-Saedi et al.*, 2019b). Finally, *Wang and Fu* (2018) compared results from 202 tertiary low salinity waterflooding experiments, finding that there was a weak positive correlation between incremental oil recovery and clay content, but that clay content was neither necessary or sufficient for incremental recovery to occur. It, therefore, appears that it is wrong to dismiss the possibility of a favourable response in clay-free or clay-poor sandstones.

Another key uncertainty surrounding the behaviour of clays is how/if any wettability alteration observed on the sub-pore scale (*Berg et al.*, 2010; *Cense et al.*, 2011; *Mahani et al.*, 2015b) translates to fluid redistribution and oil recovery. In situ observations of clays are important for improving understanding of clay behaviour during low salinity waterflooding, as clays have a number of interesting properties which differ from that of other mineralogies. First, it is

known that clays are not distributed evenly throughout most sandstones, with larger pores typically having lower clay contents (*Wang et al.*, 2020; *Xiao et al.*, 2018). Second, the wetting state of clays has been observed to be significantly different to other mineral groups, with clays found to be prone to wettability alteration in the presence of crude oil, leading to very oil-wetting behaviour (*Garfi et al.*, 2020a; *Tabrizy et al.*, 2011). Both of these features are likely to impact the ability for brine to contact clay minerals during low salinity flooding. Last, clays are known to respond differently to low salinity brine depending on their orientation, with clay edges believed to be more sensitive to low salinity brine (*Grim*, 1953; *Secor and Radke*, 1985; *Tombácz and Szekeres*, 2006).

The pore scale in situ behaviour of clays is yet to be directly observed in an oil-wet sample, although sub-pore scale observations have recently been published. *Yesufu-Rufai et al.* (2020) were the first group to make quantitative in situ observations of wettability alteration on clays during low salinity water flooding. The group used Atomic Force Microscopy to measure adhesion forces across a clay-packet in the presence of oil and low salinity brine. The group observed that the orientation of clay packets plays a key role in the reduction of adhesion forces in the presence of low salinity brine. After exposure to low salinity brine, a factor of six reduction in adhesion forces was observed at clay edges, but only an insignificant change was observed on basal planes. This work further highlights the need for in situ observations of the response of a system to low salinity brine with minerals in their natural orientation within the pore space.

With sub-micron resolution over micron scale domains, Atomic Force Microscopy is a key tool in observing wetting behaviour at the sub-pore scale. However, larger domain sizes are needed to inform how changes in wetting state affect the distribution of fluids across a sample. As we have already discussed, Micro-CT X-ray imaging, which provides observations at micron resolution across millimetre scale domains, is a well established technology that has been used extensively to observe changes in wetting state and fluid distribution over pore and pore network scales during low salinity flooding (*Bartels et al.*, 2017a, 2019; *Chen et al.*, 2020; *Sandengen et al.*, 2016). Despite this, the technology has not yet been successfully implemented to assess mineral specific wetting state during low salinity water flooding despite recent research advances

which have shown that this feat is possible. Most notably, *Lai and Krevor* (2014), *Garfi et al.* (2020a), and *Shabaninejad et al.* (2018) have shown that it is possible to segment clay from other mineral groups in X-ray micro-CT images of mineralogically heterogeneous sandstone samples. Moreover, *Garfi et al.* (2020a) have used surface area fractional coverage to assess the wetting state of different mineral groups. There is no reason why these advances in image analysis techniques cannot be applied to low salinity waterflooding research.

2.7 Summary

Low salinity water flooding is an area of extensive scientific research. It is an enhanced oil recovery technique which has the potential to produce large quantities of oil from new and existing hydrocarbon reservoirs. However, there is currently no way to reliably predict which systems will respond favourably to low salinity water flooding. A wealth of observations over the core scale and sub-pore scale has led to a deeper understanding of the underlying mechanisms of low salinity flooding. However, there remains a disconnect between the two scales, with a poor understanding of how wettability alteration and oil detachment on the sub-pore scale leads to increased oil production on the core scale. This is primarily due to a relative lack of pore scale observations of low salinity water flooding. Thanks to advances in X-ray Micro-CT imaging technology, several recent studies have focused on pore scale processes. However, more work must be carried out to close the gap in scales and pave the way for predictive capabilities. In particular, there are three areas that future pore scale experiments should aim to address. Firstly, more robust measures of wetting state should be utilised to understand the spatial distribution of wettability alteration during low salinity flooding, and the effect this has on fluid distribution across scales. Secondly, pore scale observations should be utilised to better grasp the role of pore geometry and topology on the success of low salinity water flooding. Lastly, pore scale imaging should be utilised to observe the in situ behaviour of clays during low salinity waterflooding. Clays are complex and it is known that they have unique distributions with a given sample, and typically are more oil-wetting than other mineral groups in oil-wet systems. It is as yet unclear exactly how these properties affect the behaviour of clays

in real rock samples during low salinity water flooding. Advances in these three areas would represent a leap forward in our understanding of how sub-pore scale fluid-solid interactions during low salinity waterflooding translate to additional oil recovery over core and reservoir scales. Ultimately, this will bring the field a step closer to predicting which crude oil-brine-rock (COBR) systems will respond favourably to low salinity water flooding.

Chapter 3

Materials and Methods

To gather pore scale observations of low salinity flooding, four sets of flow experiments were carried out and imaged using X-ray micro-computed tomography technology. We carried out a flow experiment in an unaltered (water-wet) Berea sample, an altered (oil-wet) Berea sample, an altered (oil-wet) Bunter sample, and an altered (oil-wet) Castlegate sample (see Fig. 3.1). In the following section, the different fluids and rock lithologies are described. Next, experimental protocols and workflows are detailed, followed by a description of image acquisition and analysis workflows.

3.1 Rock Sample and Fluid Properties

3.1.1 Lithologies and Rock Properties

Berea

The Berea samples had a diameter of 6 mm and a length of 20 mm. The imaged porosity of the Berea sample were 0.09 and 0.11 for the unaltered and altered Berea samples respectively (table 3.1). The porosity values are broadly in line with other imaged porosity values of Berea sandstone, which are typically lower than absolute porosity values due to sub-resolution

porosity (*Garfi et al.*, 2020b; *Shabaninejad et al.*, 2018). The estimated absolute permeability value (calculated using PNFlow, as described in section 3.3.6) of the altered Berea sample is 14 mD. Berea sandstone has been used extensively in petrophysical research (*Khilar et al.*, 1983; *Lai and Krevor*, 2014; *Shaw et al.*, 1991). It is predominantly made up of quartz ($> 70\%$) with smaller fractions of feldspar ($< 20\%$) and clays (predominantly kaolonite) ($< 10\%$), as well as small quantities of additional minerals such as pyrite and ankerite (*Lai and Krevor*, 2014). Surveys across Berea samples have shown a range of porosity and permeability values of $0.18 < \phi < 0.25$, and $45 < k < 1000$ mD respectively (*Churcher et al.*, 1991; *Sen et al.*, 1990; *Shabaninejad et al.*, 2018).

The Bunter sample had a diameter of 6mm and a length of 15 mm. The imaged porosity of the Bunter sample was 0.15 (table 3.1). The estimated absolute permeability value (calculated using PNFlow, as described in section 3.3.6) of the Bunter sample was 142 mD. The sample used was cut from a Triassic Sherwood Sandstone core supplied by the British Geological Survey. The mineralogy and petrophysiocal properties of this group varies, but is typically predominantly quartz and feldspar grains, with significant clay content (predominantly kaolonite). Surveys across samples in this group has shown a range of porosity and permeability values of $0.05 < \phi < 0.4$, and $10 < k < 600$ mD respectively (*Hjuler and Kristensen*, 2017; *Olivarius et al.*, 2015; *Schmid et al.*, 2004).

The Castlegate sample had a diameter of 5.5mm and a length of 15mm. The imaged porosity of the Castlegate sample was 0.20 (table 3.1). The estimated absolute permeability value (calculated using PNFlow, as described in section 3.3.6) of the Castlegate sample was 495 mD. The core was cut from a block with average mineralogy of 94 wt% quartz and feldspar, and 6 wt% clay minerals, porosity in the range of $0.2 < \phi < 0.25$, and permeability in the range $550 < k < 950$ mD.

Figure 3.2 shows the pore radius distribution for the three samples. The Berea has a notably narrower distribution, with average values far lower than for the other two samples. The Castlegate and Bunter samples have very similar pore radius distributions.

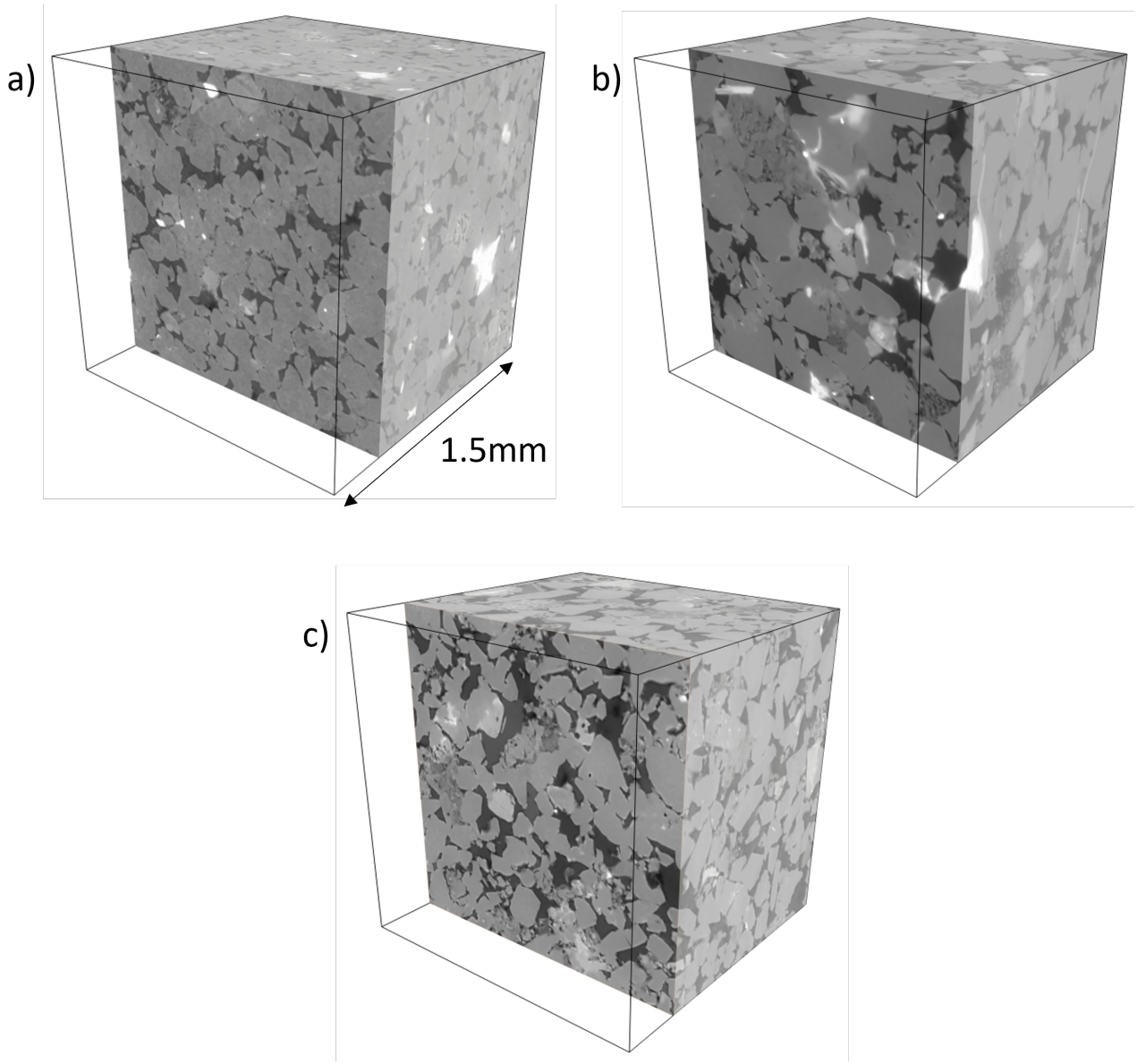


Figure 3.1: X-ray micro-CT images of the three lithologies used in this work: a) Berea sandstone; b) Bunter sandstone; c) Castlegate sandstone. The grey scale is linked to light attenuation, with the darker regions having the lowest density (e.g., pores) and the brightest regions comprising of the most dense materials (e.g., carbonate cement or metal oxides). All images were acquired using an FEI Heliscan micro-CT machine. The voxel sizes are $2.42\mu m$, $2.35\mu m$, and $2.31\mu m$.

Table 3.1: A summary of rock properties for the Berea, Castlegate, and Bunter samples used in this work

	Porosity [-]	Permeability [mD]	Coordination number [-]	Clay Volume Fraction [-]	Sample Diameter [mm]	Sample Length [mm]
Berea	0.11	14	2.5	0.06	6	20
Bunter	0.15	142	2.7	0.06	6	15
Castlegate	0.20	495	3.3	0.08	5.5	15

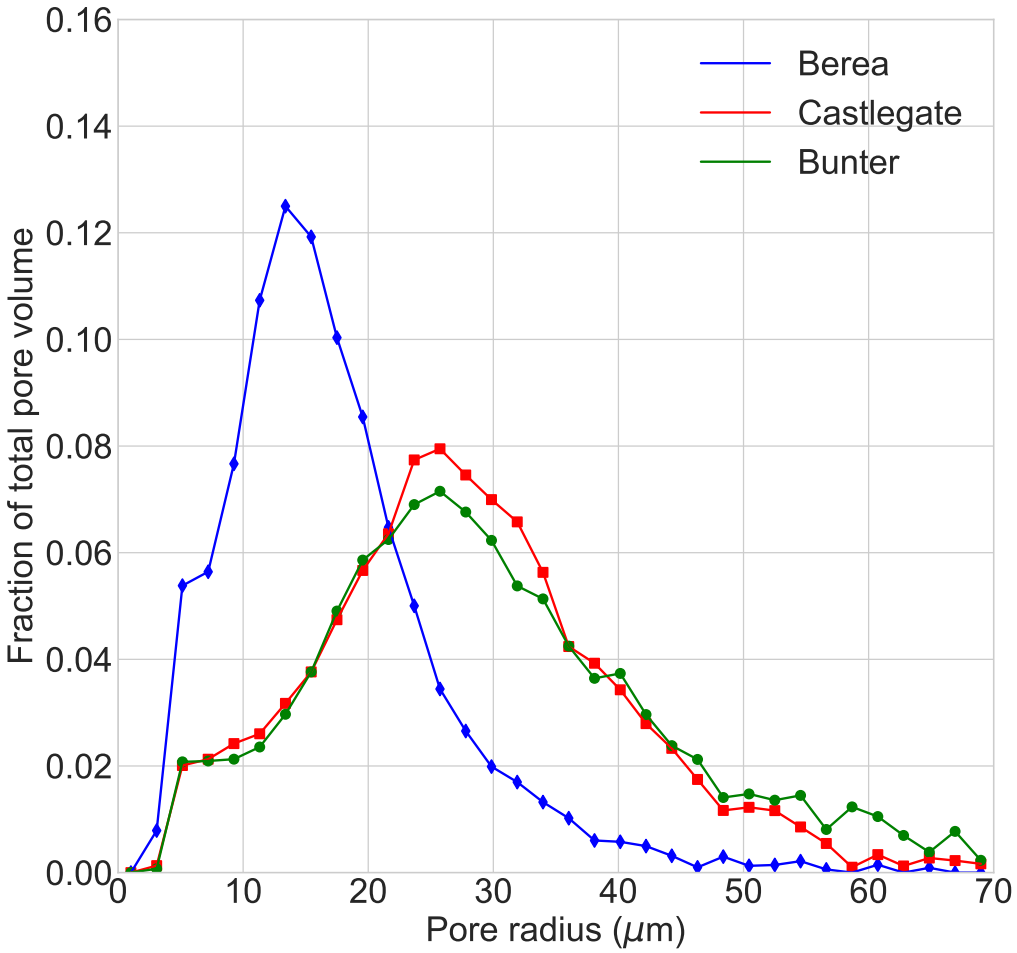


Figure 3.2: Plot of the pore radius distributions as a fraction of total pore volume for each sample. The Berea sample (blue) has a far narrower pore size distribution than the Bunter (green) and Castlegate (red) samples which have a very similar profile. In each case, the pore size distribution is generated using pore network extraction, as described in section 3.3.6

3.1.2 Fluid Properties

In all experiments three distinct fluid phase were used; these were a high salinity brine a low salinity brine and a crude oil. In all experiments exactly the same fluids were used. The properties of each of the fluids are described below.

Table 3.2: The brine recipes for both the high and low salinity brines used in the study. Note that the low salinity brine is simply the high salinity brine diluted by a factor of 69.4. These recipes were supplied by our industry sponsors, BP.

	Dissolved salts [mg/l]	
Salts	**High salinity brine**	**Low salinity brine**
$CaCl_2.2H_2O$	13205	190
$MgCl_2.6H_2O$	2008	29
KCl	744	11
NaCl	57884	834
TDS	73,841	1,064

The oil used in this work is a degassed western hemisphere crude oil with a density of 0.87 kg/m^3 and viscosity 13 mPa s. The oil has a total acid number of 0.01 mgKOH/g and a total basic nitrogen content of 2 mgKOH/g. The Saturates, Aromatics, Resing and Asphaltenes analysis data are Sat=22.00 wt%, Aro=41.00 wt%, Res=20 wt%, and Asp=17 wt%. The oil was doped with 20 wt% iododecane. This dopant concentration represents a trade-off between replicating a realistic reservoir system and the ability to reliably distinguish between phases in X-ray images We chose to add dopant to the oil, as opposed to the brines, to avoid increasing the salinity of the low salinity brine. There remains some uncertainty around the effect of iododecane on interfacial properties. A recent study by *Pan and Trusler* (2022) has shed some light on this. The authors reported that the interfacial tension between iododecance and water was 4.5 $mNm^{-}1$ lower than the interfacial tension between water and decane. The authors concluded that doping decane with iododecane would lead to a decrease in the water-organic phase interfacial tension. This would suggest that introducing 20 wt% iododecane into the

crude oil, acts to decrease the brine-oil interfacial tension. Temperature, salinity, and pressure are all thought to impact crude oil/brine interfacial tension (IFT) values. Additionally, IFT values are time dependant, perhaps due to the diffusion of some components across the interface (*Buckley and Fan*, 2007; *Freer et al.*, 2003; *Moeini et al.*, 2014). It is therefore likely that IFT values do not remain constant throughout the experiments presented here

Two distinct brines were used in all experiments. The first, referred to as high salinity brine, has a total dissolved salts (TDS) of 73,841 and was used as formation water for secondary high salinity water flooding. The second, referred to as low salinity brine, has a TDS of 1,064 and was used for tertiary low salinity waterfloods. Both brine recipes are shown in table 3.2. Note that the low salinity brine is simply the high salinity brine recipe diluted by a factor of 69.4.

3.2 Experimental Workflow

Similar experimental workflows were followed for each of the four flow experiments used for this work. After loading each sample into the core holder, we began flow experiments using the workflows described for each sample below (and summarised in Fig. 3.3). For all flow steps in each sample, a confining pressure of 50 bar was maintained within the core holder. This compresses the Viton sleeve around the core, therefore, preventing fluid bypassing the sample. An inlet pressure of 30 bar was maintained at all times. Each experiment was carried out at ambient temperatures, approximately 25°C.

In three of the four experiments, the wetting state of the samples were altered prior to high and low salinity waterflooding. The purpose of this alteration process was to produce wetting states representative of reservoir conditions which are typically mixed or oil-wet (*Blunt*, 2017). It has been shown that the wetting preference of a rock surface can be altered by the interaction of the solid substrate with surface-active compounds present in crude oil. These compounds can precipitate onto and be adsorbed by the solid surface resulting in a change in local wetting state (*Buckley*, 1998; *Buckley and Liu*, 1998; *Buckley et al.*, 1997). To alter the wetting state of the Berea, Bunter and Castlegate samples, we injected the samples with high salinity brine

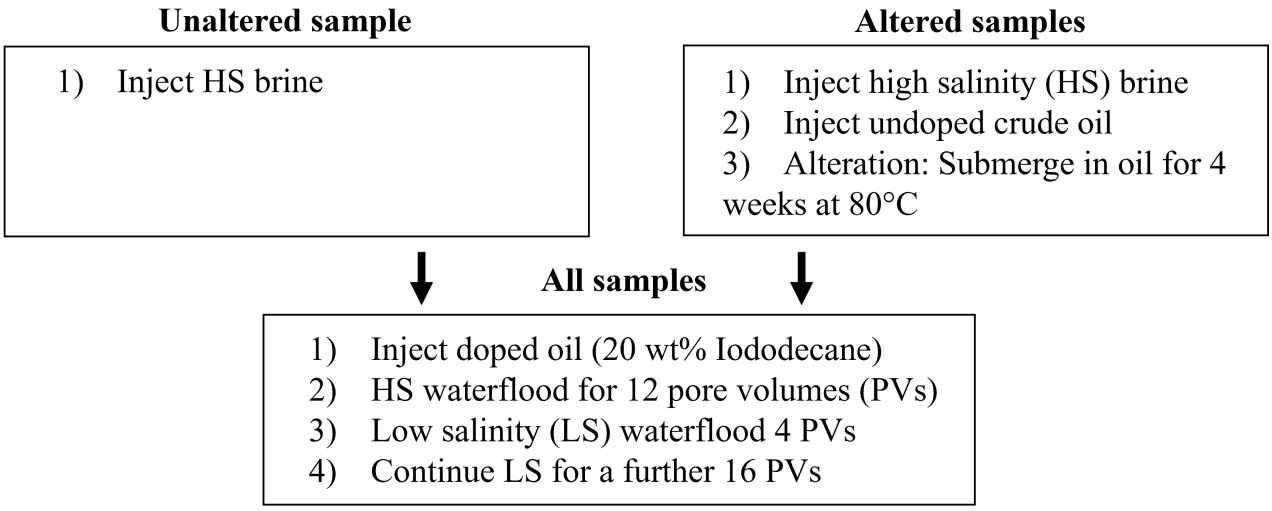


Figure 3.3: An overview of the experimental workflow for all samples (three altered sample and one unaltered sample). A more detailed description of the workflow can be found in the text.

followed by undoped crude oil and submerged the samples in a beaker of crude oil at 80° for four weeks. We assumed that the wetting state of the cores after the wetting alteration process was altered towards a more oil-wetting state (an assumption that is validated in the image analysis).

The core flooding experiments were carried out using the flow-loop shown in Figure 3.4. A carbon fibre Hassler type flow cell was used to keep the rock under pressure with a confining fluid (water). The samples were then placed in a Viton sleeve, and connected to the PEEK tubing of the hydraulic circuit with two steel end pieces. The cell was then placed into an FEI Heliscan x-ray μ-CT so that images could be taken at each stage of each experiment.

3.2.1 Tertiary Low Salinity Water Flooding of Water-Wet Berea Sandstone

We first flooded the dry Berea sample with high salinity brine at 0.2 ml/min for 30 mins to saturate the sample fully. Next, we carried out drainage to establish the initial water saturation, S_{wi}, where undoped crude oil was injected into the sample at a rate of 0.015 ml/min for a total of 10 pore volumes (PV). After drainage, we observed a very low S_{wi} of < 0.05. Subsequently, high salinity brine was injected into the sample at 0.015 ml/min for a total of 12 PV. Next, low

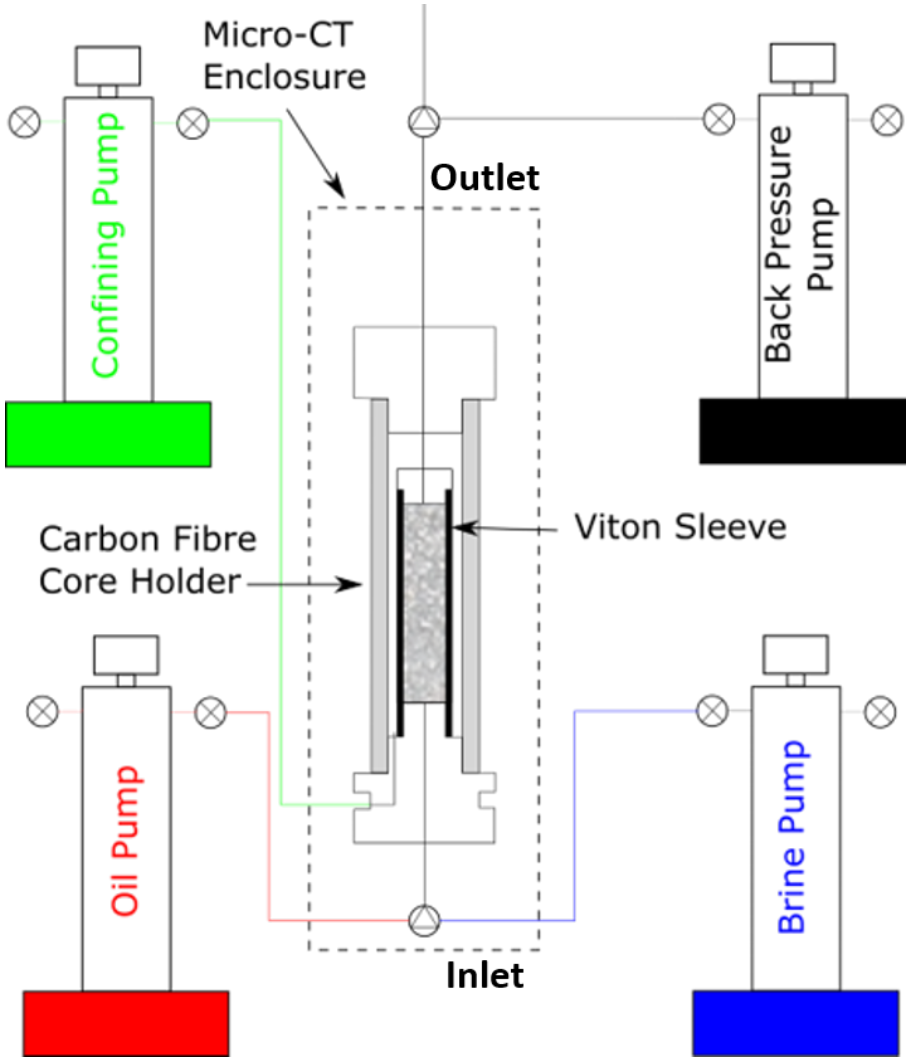


Figure 3.4: Schematic diagram of experimental apparatus for unsteady state flow experiment. Adapted from *Lin et al.* (2018)

salinity brine was injected into the sample at 0.015 ml/min for a total of 4 PV. Finally, a further 16 PV of low salinity brine was injected into the sample at 0.015 ml/min, making a total of 20 PV of low salinity flooding. The Capillary number for the waterfloods of $N_c = v\mu/\sigma$ (where v = darcy velocity of injection, μ = viscosity of injected phase and σ = interfacial tension) = 4×10^{-7} (assuming approximate values of $\mu = 10^{-3}$ Pa.s and $\sigma = 20 \times 10^{-3}$ Nm^{-1}). In order to control both injection pressure and flow rate, for all waterfloods a constant pressure of 30 bar was maintained at the injection pump, and the receiving pump was set to a refill rate of 0.015 ml/min. This resulted in a pressure drop across the core and an average flow rate of 0.015 ml/min.

3.2.2 Tertiary Low Salinity Water Flooding of Altered-Wettability Berea Sandstone

For the altered experiment, We first flooded the dry Berea sample with high salinity brine at 0.2 ml/min for 30 mins to saturate the sample fully. Next, we carried out drainage to establish the initial water saturation, S_{wi}, where undoped crude oil was injected into the sample at a rate of 0.015 ml/min for a total of 10 pore volumes (PV). After drainage, we observed a very low S_{wi} of < 0.05. The wetting state of the core was then altered. The sample was submerged in crude oil for four weeks at 80°C. The alteration process led to a reduction in permeability. This is most likely due to the precipitation of asphaltenes. As a result, an injection flow rate of 0.015 ml/min could not be achieved in the subsequent flow steps with an injection pressure of 30bar. Instead, a constant pressure drop of 25 bar was maintained across the core for all further flow steps in the altered sample. 10 PV of doped crude oil (20wt% iodododecane) was injected into the altered sample to displace the undoped crude oil. 12 PV of high salinity brine were then injected into the sample. Subsequently, 4 PV of low salinity brine were injected into the sample. Finally, a further 16 PV of low salinity brine was injected into the sample. The average flow rate for all waterfloods in the altered sample was approximately 0.001 ml/min, giving an approximate capillary number for the waterfloods of 3×10^{-8}.

3.2.3 Tertiary Low Salinity Water Flooding of Altered-Wettability Castlegate Sandstone

High salinity brine was first injected into the sample at 0.2 ml/min for 30 minutes to saturate the sample fully. Next, we carried out drainage to establish the initial water saturation, S_{wi}, where undoped crude oil was injected into the sample at a rate of 0.015 ml/min for a total of 10 pore volumes (PV). After drainage, we observed a very low S_{wi} of < 0.05. The wetting state of the core was then altered. The sample was submerged in a sealed beaker of undoped crude oil for four weeks at 80°C. Next, high salinity brine was injected into the sample for a total of 12 PV. 4 PV of low salinity brine was then injected, followed by a final 16 PV of low salinity brine injection, making a total of 20 PV of low salinity flooding. A flow rate of 0.015 ml/min was maintained for the doped oil injection and subsequent waterfloods at an injection pressure of 30bar giving an approximate capillary number for the waterfloods of 5×10^{-7}. In order to control both injection pressure and flow rate, for all waterfloods a constant pressure of 30 bar was maintained at the injection pump, and the receiving pump was set to a refill rate of 0.015 ml/min. This resulted in a pressure drop across the core and an average flow rate of 0.015 ml/min.

3.2.4 Tertiary Low Salinity Water Flooding of Altered-Wettability Bunter Sandstone

High salinity brine was first injected into the sample at 0.2 ml/min for 30 minutes to saturate the sample fully. Next, we carried out drainage to establish the initial water saturation, S_{wi}, where undoped crude oil was injected into the sample at a rate of 0.015 ml/min for a total of 10 pore volumes (PV). After drainage, we observed a very low S_{wi} of < 0.05. The wetting state of the core was then altered. The samples were submerged in a sealed beaker of undoped crude oil for four weeks at 80°C. Next, high salinity brine was injected into the samples for a total of 12 PV. 4 PV of low salinity brine was then injected, followed by a final 16 PV of low salinity brine injection, making a total of 20 PV of low salinity flooding. For the Castlegate

and Bunter samples, a flow rate of 0.015 ml/min was maintained for the doped oil injection and subsequent waterfloods at an injection pressure of 30bar giving an approximate capillary number for the waterfloods of 4×10^{-7}. In order to control both injection pressure and flow rate, for all waterfloods a constant pressure of 30 bar was maintained at the injection pump, and the receiving pump was set to a refill rate of 0.015 ml/min. This resulted in a pressure drop across the core and an average flow rate of 0.015 ml/min.

3.2.5 Summary of Experiments

We chose to carry out tertiary low salinity waterflooding experiments, as opposed to secondary waterflooding, so that the extent of additional recovery from low salinity flooding could be more easily determined. In secondary flooding experiments, it is more challenging to attribute any additional oil recovery to brine salinity. We chose 12 pore volumes of high salinity flooding as a trade-off between experimental time and pore volumes injected. We were partly informed by findings by *Khishvand et al.* (2017), who observed no significant change in fluid distribution or wetting state between 5 and 10 pore volumes of high salinity flooding in an altered Berea sandstone core, with the majority of recovery occurring in the first 0.5 pore volumes of high salinity waterflooding. The values of 4 PV and 20 PV of low salinity flooding for each sample were carefully chosen so that both the initial and final response to low salinity flooding could be observed. *Khishvand et al.* (2017) observed an initial shift in wetting state and pore occupancy between 0.5 and 5 PV of low salinity flooding in a Berea sample. We chose a value of 4 PV to be broadly consistent with *Khishvand et al.* (2017), and to maximise the probability of observing oil banking. A further 16 PV of low salinity flooding was carried out to displace any banked oil, and maximise oil recovery.

As stated above, we calculated approximate capillary numbers of 4×10^{-7}, 3×10^{-8}, 5×10^{-7}, and 4×10^{-7} for waterflooding in the unaltered and altered Berea, Bunter and Castlegate experiments respectively. Whilst the value varies between each sample, all waterfloods were carried out in a capillary dominated regime (typically defined as $< 10^{-}6$). The experimental results provide further evidence of a capillary dominated regime. As is discussed in Chapters

4, 5 and 6, we observed relatively high S_o values after waterflooding in all experiments, and no evidence of capillary desaturation. Estimates of capillary numbers for waterflooding in real reservoir systems vary (typically between $10^{-8}-10^{-6}$), but unless there is some intervention (e.g. by drastically lowering interfacial tension) displacement during waterflooding in real reservoirs is capillary dominated at the pore scale (*Blunt*, 2017; *Satter and Iqbal*, 2015).

As discussed above, for each sample, high salinity brine was first injected into the sample at 0.2 ml/min for 30 minutes to saturate the sample fully and undoped crude oil was then injected into the sample at 0.015 ml/min for 10 PV. For all samples, after this drainage process, S_w was < 0.05. This very low water saturation may be a result of the unrealistic drainage process. In real reservoirs, primary oil migration occurs over many millennia due to buoyancy forces where capillary pressure is limited by the height of the oil column. Typically, the capillary pressure during oil migration is not sufficient to invade the smallest pores in a given reservoir, which remain brine saturated. Whilst S_{wi} is thought to vary drastically between reservoirs, it is broadly accepted that values are typically > 0.05 (*Blunt*, 2017). The differences between the experimental drainage process and that of reservoirs, and the resulting differences in fluid saturation and distribution, are important to consider when interpreting results. This will be discussed in chapters 4, 5 and 6.

3.3 X-ray micro-CT Imaging: Acquisition and Processing

3.3.1 Fundamentals of X-ray Micro-CT Imaging

X-ray technology has been widely used to image the internal structures of geological specimens over the last 50 years. The method is based on the attenuation of X-rays as they travel through a target material. This is expressed by Lambert-Beer's law (eq. 3.1):

$$I = I_0 e^{-\int \mu(s) ds} \tag{3.1}$$

where I is intensity at the detector, I_0 is intensity at source, and $\mu(s)$ is the linear attenuation coefficient along the ray path s.

In its infancy, X-ray technology was restricted to producing two-dimensional data. The technique was greatly improved with the advent of computerised transverse axial tomography (CAT or CT), where information is gathered from a number of different directions allowing for a 3D image to be reconstructed. This allows the local value of μ to be found for each point inside the target volume. This technology was first developed in medical imaging (*Gawler et al.*, 1974; *Lcdley et al.*, 1974) but was soon utilised within Earth science (*Coles et al.*, 1991; *Petrovic et al.*, 1982) and has since been used extensively to give unique insight into pore scale processes during multiphase flow in porous media (*Berg et al.*, 2013; *Bultreys et al.*, 2018; *Spurin et al.*, 2019, 2021).

In the basic setup of laboratory micro-CT machines, a sample is placed between a source and a detector. During image acquisition, the sample rotates whilst the source and detector remain stationary (see figure 3.5). Over 360 (or 180) degrees, thousands of radiographs are typically recorded at the detector. The raw data can then be processed using reconstruction algorithms (*Vlassenbroeck et al.*, 2007), to create a 3D volume representing a distribution of the linear attenuation coefficient, μ (*Bultreys et al.*, 2016b).

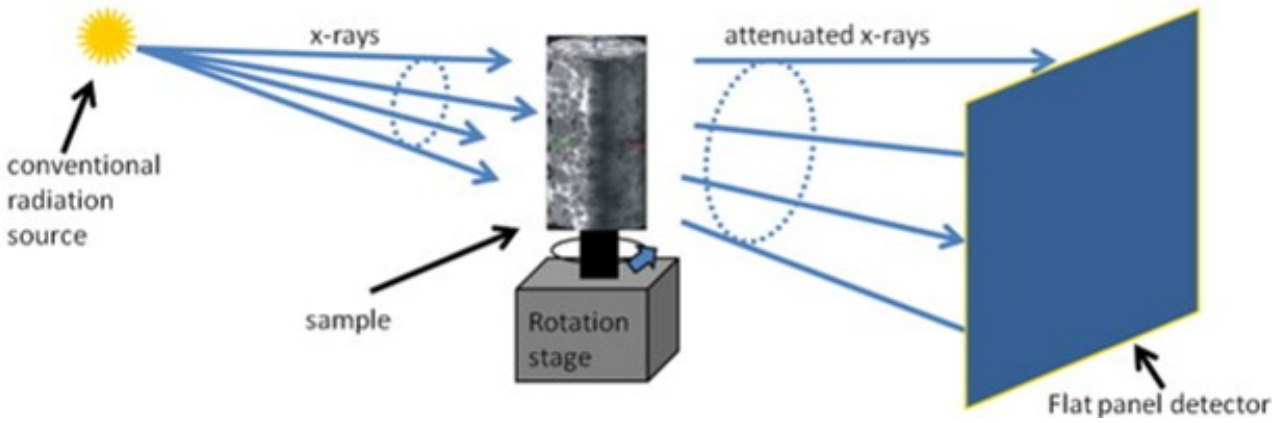


Figure 3.5: Schematic diagram of a typical laboratory micro-CT setup. From *Wildenschild and Sheppard* (2013).

3.3.2 X-ray Micro-CT Acquisition

For all experiments, the samples were imaged using an FEI X-ray micro-CT scanner. The machine has a typical set-up for commercial laboratory based X-ray micro-CT scanners where the X-ray source and detector are fixed, and the sample rotates. The machine uses a 3072 × 3072 pixel flat panel detector, and a source with an energy output ranges of 20 kV to 160 kV and a maximum power output of 8 W. The machine is unique compared to more traditional commercial X-ray Micro-CT scanners in that the sample can move in a helical trajectory during image acquisition. The main advantage of this technique is that a large vertical field of view can be imaged in a single scan, so that no stitching of multiple separate scans is required to image long samples, thus avoiding stitching artifacts. The manufacturer guidelines for optimal image quality are a target current of close to 50 mA during acquisition and a ratio of approximately 40% between the X-ray flux through the sample and the X-ray flux without a sample in place (a clearfield scan). By adjusting filtering, tube current, source voltage and acquisition time, we aimed to achieve the optimal parameters for each scan. Three Dimensional tomograms were then reconstructed from the 2D images by applying an iterative back projection algorithm (provided by the machine manufacturer).

3.3.3 Image Analysis Workflow

Filtering

During each experiment, a section of each sample was scanned at each flow step. The entire imaged region is referred to as the field of view. In each case, a region of the field of view was selected for image analysis. This region is refereed to as the region of interest. In each case, the region of interest was taken from the centre of the field of view, which, in turn, was located in the centre of each sample. For both Berea samples, a region of interest of 1500 × 1500 × 3500 voxels (3.6 × 3.6 × 8.4 mms) was extracted; for the Castlegate, a region of interest of 1425 × 1425 × 2375 voxels (3.3× 3.3 × 5.5 mms); for the Bunter, a region of interest of 1500 × 1500 × 3000 voxels (3.5 × 3.5 × 7.0 mms). Therefore, in the Berea samples, there was a region

of 5.8 mms above and below the region of interest which was not analysed. In the Castlegate sample, there was a region of 4.75 mms above and below the region of interest which was not analysed. In the Bunter sample, there was a region of 4 mms above and below the region of interest which was not analysed.

For each sample, the first image analysis step was to filter all tomograms. Filtering is an important step, which is used to increase signal to noise ratio. There are several filtering options that have been used extensively in the field of porous media (see reviews by *Kaestner et al.* (2008); *Schlüter et al.* (2014)) Non-local means filtering has emerged as the favoured algorithm in recent years. It has been found to retain the contrast of phase boundaries whilst effectively increasing signal to noise ratio (*Buades et al.*, 2005; *Schlüter et al.*, 2014). As such, non-local means filtering has been used in a number of recent works in the field of pore scale imaging (*Alhammadi et al.*, 2017; *Alhosani et al.*, 2020; *Garfi et al.*, 2020a,c; *Scanziani et al.*, 2018; *Spurin et al.*, 2019). For these reasons, non-local means filtering was used in this work. Thermofisher Avizo Fire 2019.1 software was used to carry out the filtering. For all experiments, a search window of 25 pixels, and a similarity of value of 0.3 were used. These correspond to the radius of the search window area in number of voxels, and a weighting factor assigned to each voxel inside the search window during the smoothing procedure, respectively. These values were chosen to avoid excess smoothing and blurring.

Segmentation

For all samples, two separate segmentation workflows were used. As with filtering methods, there are many image segmentation algorithms that are widely used. These can broadly be split into two categories. The first, global thresholding, has been widely used for many years (see review by *Iassonov et al.* (2009)). The second, algorithms which account for spatially varying information within an image, have been found to be superior (*Iassonov et al.*, 2009; *Schlüter et al.*, 2014). One such approach is the watershed algorithm (*Beucher and Meyer*, 1993; *Vincent and Soille*, 1991). Watershed segmentation has been found to perform well in segmenting different mineral groups and pore space in various studies (*Alhosani et al.*, 2020; *Garfi et al.*,

2020a,b; *Leu et al.*, 2014). *Leu et al.* (2014) found that watershed segmentation outperformed both global and hysteresis segmentation methods, giving the most robust estimates of porosity and permeability from images of Berea sandstone. As such, in this work, watershed segmentation is used to segment mineral groups from pore space for each experiment. For each sample, a scan was taken before any dopant was introduced into the oil phase, so that pore space could be easily distinguished from minerals. For each sample, the undoped scan was segmented into 3 groups, pore space and two mineral groups: clay group minerals; and non-clay minerals. We used Thermofisher Avizo Fire 2019.1 software to carry out watershed segmentation, where a number of phases and threshold values that define seeds for each phase were manually inputted. The segmented undoped images for each sample were then registered to subsequent scans with both brine and doped oil present (see Fig. 3.6). The segmented image was used to mask these scans so that just the fluid phases remained. The fluid phases were then segmented using simple global thresholding, with the threshold values determined using the histogram of grey values, where the grey-value corresponding to the local minima between the grey-value peaks for both fluid phases was chosen as the threshold value. This is process was chosen to be an objective, repeatable, workflow.

3.3.4 Estimating Saturation Distribution

First, the fluid saturation distribution in each core was estimated. Once the fluid phases were segmented, the water saturation, S_w, the fractional volume of the water volume in the pore space, was averaged across each of the 3500 horizontal slices. These values were then stacked to produce a saturation profile along the entire length of the imaged region, and averaged to give total water saturation, S_w

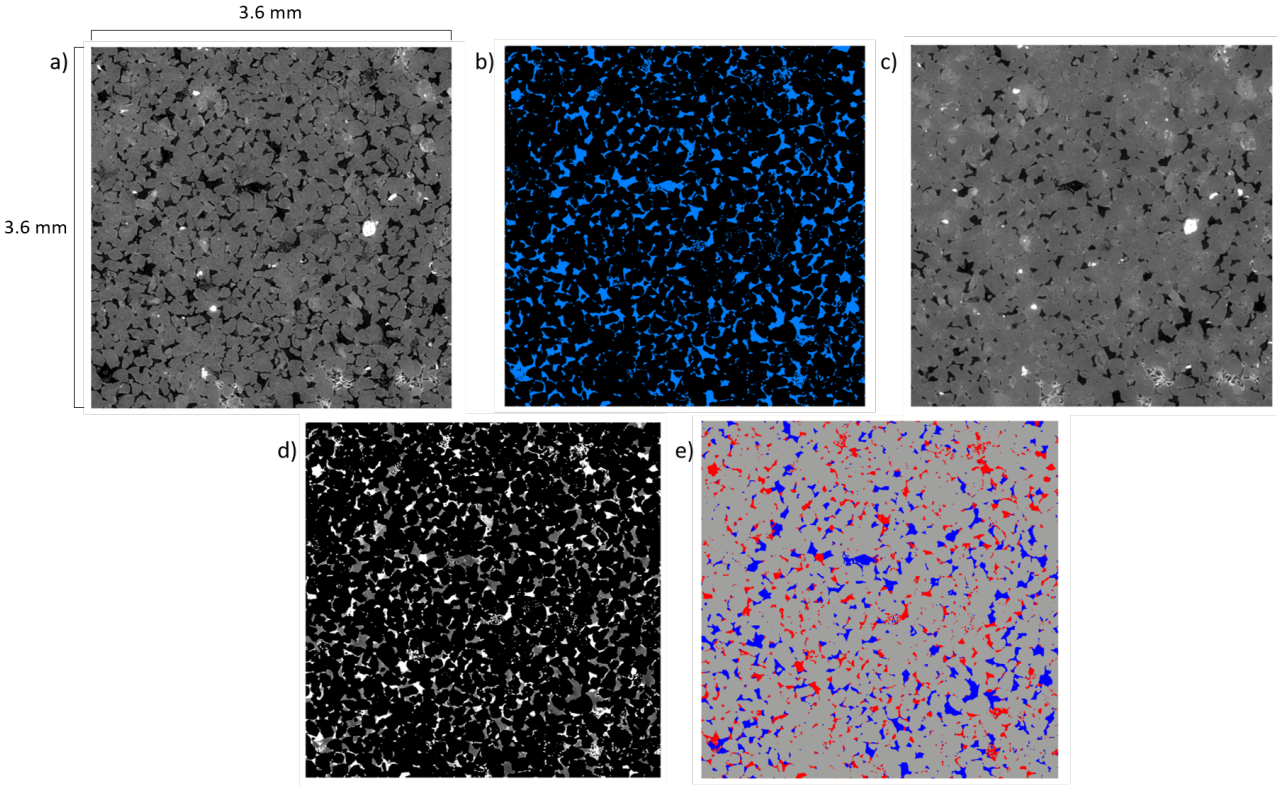


Figure 3.6: A brief overview of the image analysis workflow. a) The undoped scan (filtered) b) The segmented undoped scan (blue = pore space, black = rock) which is then used as a mask for the doped scans c) The scan taken after 20 PV of low salinity water flooding (filtered) d) As in c but masked using b, leaving just the fluid phases (light = oil, dark = brine) e) Segmented LSWF 20PV scan (grey = rock, blue = brine, red = oil)

3.3.5 Surface Area Coverage

Bulk Measurements

We then assessed the fraction of mineral surfaces coated by a fluid phase, A_{fi}, defined as the amount of the solid surface exposed to the pores that is covered a fluid phase, A_i, divided by the total amount of solid surface exposed to the pores, A_T. For oil, $A_{fo} = A_o/A_T$. Following the workflow developed by *Garfi et al.* (2020a), the region of interest in each sample was subdivided into equal sub volumes. For both the unaltered and altered Berea samples, this was 63 equal subvolumes of 500 voxels per side; for the Bunter, there were 54 equal subvolumes of 500 voxels per side for each subvolume; for the Castlegate, there were 45 equal subvolumes of 475 voxels per side. For each subvolume, in each sample, brine-rock interfacial area, oil-rock interfacial area, and fluid saturations were computed. The oil-rock interfacial area as a fraction of total fluid-rock interfacial area was then calculated as a function of saturation for each of the subvolumes in each sample after all flow steps. The resulting cross-plot of A_{fo} and S_o has been demonstrated in *Garfi et al.* (2020a) to provide a robust measure of the wetting state of the system. The more wetting a fluid, the greater fraction of the rock surfaces will be coated by that fluid at a given saturation.

Mineral Specific Measurements

In Chapter 6, we also implemented mineral specific surface area coverage analysis, again following a workflow developed by *Garfi et al.* (2020a). The initial workflow is identical to that of bulk measurements descried above, where each sample is split into equal subvolumes. For each of the subvolumes, we then identified four interface groups, that is, for both mineral groups (clays and non-clay minerals) and both fluid phases (brine and oil). We compared fluid surface coverage of the two mineral groups by recording the fraction of the total area of that mineral group in contact with a fluid:

$$a_{ij} = \frac{A_{ij}}{\sum_i A_{ij}} \tag{3.2}$$

where A_{ij} is the measured surface area per unit of pore volume shared by fluid i with solid j, respectively. We measured the oil-clay interfacial area as a fraction of total fluid-clay interfacial area, and the oil-mineral interfacial area for non-clay minerals as a fraction of total fluid-mineral interfacial area for non-clay minerals. These values were then presented as a function of oil saturation, S_o for each subvolume. This gives a measure of wetting state for the two mineral groups in each sample.

3.3.6 Pore Fluid Occupancy

Next, we evaluated the sizes of the pores occupied by the fluid phases using a pore network abstraction of the pore space, using a workflow first introduced by *Bultreys et al.* (2018). We used a maximal ball network extraction code (*Dong and Blunt*, 2009; *Raeini et al.*, 2017) to extract a network of nodes, representing pores and links, representing throats, from the segmented undoped scans of each sample (Fig. 3.7). Inscribed spheres were fitted to each pore, where the diameter of said spheres represents the pore diameters. The pore occupancy of brine and oil was then quantified by using the segmented images to determine the phase occupying each sphere. From this, we generated a map of fluid distribution throughout the samples after each flow-step. We also created plots of the pore size distribution of oil filled pores and water filled pores. While pore occupancy analysis offers insight into changes in the distribution of fluids throughout each sample, the method may systematically underestimate saturation changes. This is because pore occupancy analysis does not take into account saturation changes in pore corners and oil layers since pore occupancy is decided based on the phase in the centre of a given pore.

In Chapter 6, for all pore elements in all samples, we extracted the mineral surfaces exposed to the pore body and assessed the fraction of the surface made up of clay minerals. From this we split pores up into two groups, clay rich pores (where clay coverage is $> 50\%$) and clay-poor

pores (where clay coverage is $< 50\%$). We then assessed the pore occupancy of these two groups, to give insights into the mineral specific pore occupancy, and the distribution of clay minerals in all samples. The pore occupancy analysis in chapter 6 differs slightly from that of Chapters 4 and 5 in that it does not assess the fluid saturation within a maximal ball in the centre of each pore body and throat, but rather assesses the fluid saturation within the entire pore body or throat.

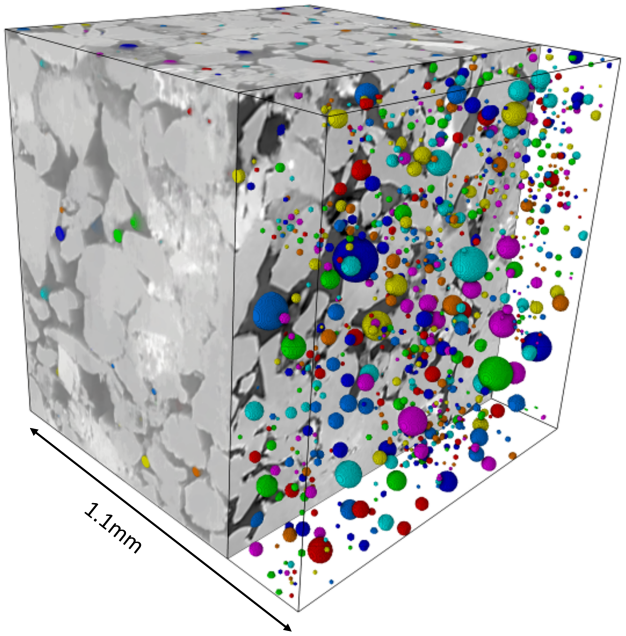


Figure 3.7: Maximum inscribed balls extracted from a subvolume of the Castlegate sample, overlaid on a volume rendering of the subvolume.

To analyse the absolute permeability of each sample, we used PNflow, an open source pore network modelling tool which relies on an assumption of quasi-static capillary dominated flow. The algorithm uses the approach of *Valvatne and Blunt* (2004), as described in *Raeini et al.* (2018), and further validated by *Raeini et al.* (2019) and *Bultreys et al.* (2018). We used the tool to simulate a single phase flow experiment in each sample, giving an estimate of absolute permeability in each case.

In Chapter 5, we analyse the impact of the topology of the largest pores on recovery during low salinity flooding in each sample. We first isolated the largest pores which make up 60% of total pore volume in each sample. This equates to all pores of radius $> 14\mu m$ in the Berea, 25 μm

in the Castlegate, and 24 μm in the Bunter. We chose this cut-off as the minimum pore radius in this group approximately equates to the largest pores in which the oil saturation decreases during low salinity flooding in each sample. Additionally, the average S_w of pores within this group is > 0.5 for all samples after each waterflood. Therefore, the connectivity of these pores is likely to impact the connectivity of the brine in each sample. We then repeated the pore network extraction and single phase flow simulations, described above, for these larger pores only, to obtain the estimates for fluid occupancy and absolute permeability in for the network of largest pores in each sample.

Chapter 4

The Impact of Wetting State on Low Salinity Water flooding

The material from this chapter has been published: *Andrews et al.* (2021)

4.1 Overview and Objectives

As discussed in chapter 2.6.1, understanding how wetting state impacts recovery during low salinity waterflooding is very important. This is the case in the context of both initial wetting state and wettability alteration during low salinity waterflooding itself. Thus far, pore scale observations of low salinity waterflooding have been carried out in Berea sandstone samples with a range of initial wetting states with little thought to the impact of these wetting states on the efficacy of low salinity flooding. Additionally, in pore scale experiments wettability has been exclusively characterised using geometric contact angle measurements which are known to be a noisy measure, sensitive to image analysis workflows and pore geometries. A range of more robust measures of wetting state have been developed recently, but none have yet been used to characterise wetting state during low salinity flooding in a sandstone sample.

The objective of this work is to systematically investigate the role of initial wetting state on

the efficacy of low salinity waterflooding. We compare results of low salinity flooding in one water-wet and one oil-wet Berea sandstone core. We use fluid coated area fraction analysis to characterise the wetting state of two Berea sandstone cores of different initial wetting states. This approach provides the most robust measurements of wetting state during low salinity flooding to date, and gives important insights into the role of initial wetting state and wettability alteration on recovery during low salinity water flooding (see chapter 3.3.5).

4.2 Results

4.2.1 Saturation Distribution

The porosity profiles of the two samples are similar, with a comparable variation of porosity along the samples (fig. 4.1). In contrast, the saturation profiles vary significantly between the two samples. For the experiments with the unaltered rock, $S_w = 0.26$ after 12 PV of high salinity water flooding (Table 4.1, Figure 4.8); this does not change after 4 and 20 PV of low salinity water flooding. This is consistent with fractional flow theory for unaltered systems, where nearly all of the production occurs within the first PV of fluid injected. Additionally, there is little variation in saturation along the core, with all slices in the range $0.16 < S_w < 0.35$ at all locations for all flow steps. The standard deviation was the same for all flow steps with a value of 0.0030.

Table 4.1: Average water saturation, S_w, in the region of interest, and the standard deviation of average S_w across all slices in the region of interest for the unaltered and altered samples, after 12 PV of high salinity flooding (HSWF), 4 PV of low salinity water flooding (LSWF 4PV), and 20 PV of low salinity water flooding (LSWF 20PV). For both samples, there was a very high initial oil saturation with $S_w < 0.05$ prior to waterflooding in both cases. As discussed in chapter 4.2.3 we calculate a standard error of 0.00125 for the saturation measurements in this work

	Unaltered		**Altered**	
	S_w [-]	St.Dev [-]	S_w [-]	St.Dev [-]
HSWF 12 PV	0.260	0.0030	0.382	0.0087
LSWF 4 PV	0.256	0.0030	0.368	0.0080
LSWF 20 PV	0.254	0.0030	0.413	0.0098

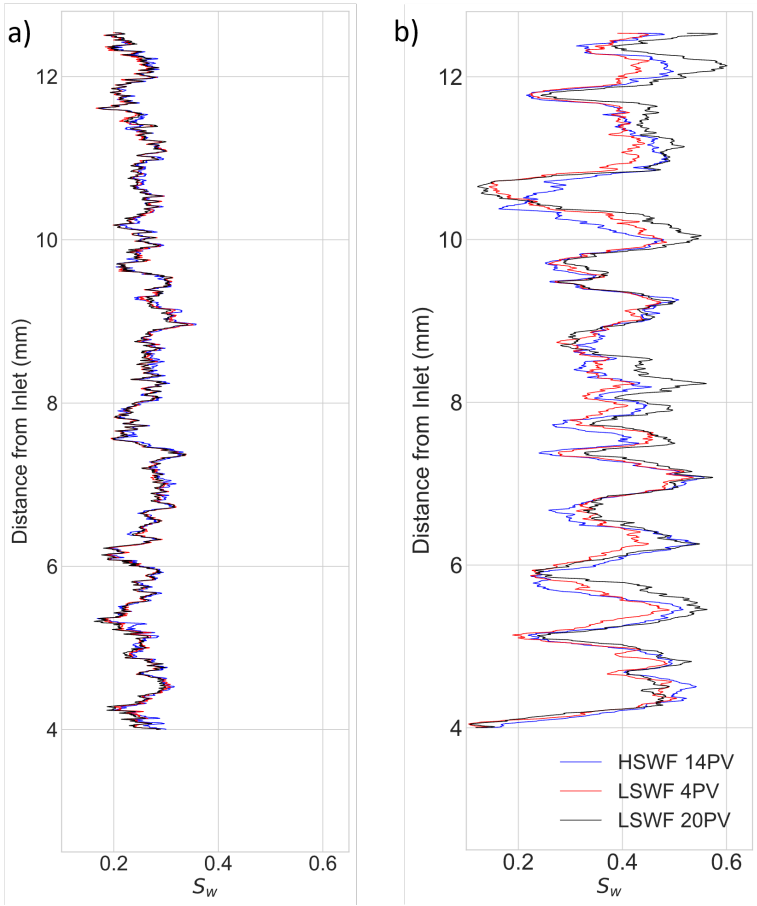


Figure 4.1: Profile of water saturation, S_w, averaged perpendicular to the flooding direction across the entire region of interest (the region at the centre of the sample that is analysed, see chapter 3.3.3) for the a) the unaltered sample b) the altered sample imaged after 12 PV of high salinity flooding (HSWF 12PV), 4 PV of low salinity water flooding (LSWF 4PV), and 20 PV of low salinity water flooding (LSWF 20PV). For the experiments with the unaltered rock, $S_w = 0.26$ after HSWF 12PV. S_w does not change after 4 PV and 12 PV of LSWF. In contrast, the average $S_w = 0.26$ is initially higher in the altered case after HSWF 12PV. There were significant local changes in S_w following LSWF 4PV and LSWF 20PV. Across the region of interest, mean S_w decreased by 0.014 after the first 4 PV of low salinity water flooding. After 20 PV of low salinity flooding, however, S_w increased so that it was 0.031 higher than the value at the end of HSWF 12PV.

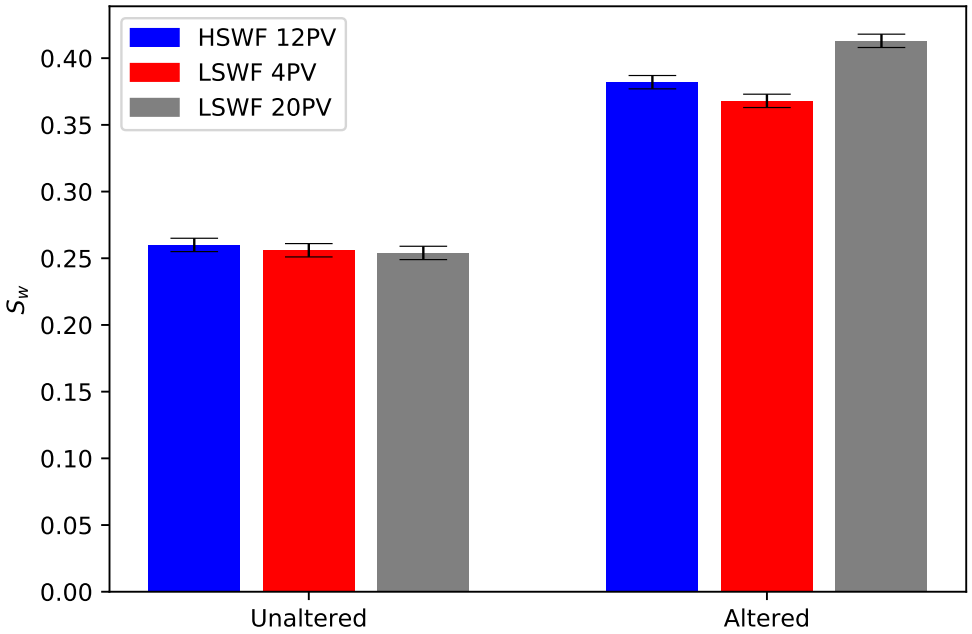


Figure 4.2: S_w values after 12PV of high salinity flooding (HSWF 12PV), 4PV of low salinity flooding (LSWF 4PV), and 20PV of low salinity flooding (LSWF 20PV) for the unaltered and altered Berea samples. As discussed in chapter 4.2.3 we calculate a standard error of 0.00125 for the saturation measurements in this work.

In contrast, the average water saturation is initially higher in the altered case after flooding with high salinity brine. There were also significant local changes in S_w following 4 and 20 PV of low salinity flooding. Across the region of interest (the region at the centre of the sample that is analysed, see chapter 3.3.3), mean S_w decreased by 0.014 after the first 4 PV of low salinity water flooding. This is probably due to the accumulation of oil displaced from elsewhere in the sample, upstream of the region of. As mentioned in Chapter 3.3.3, in both Berea samples, there was a 5.8 mm section of the core that was upstream of the region of interest and not analysed. Given that the volume of this upstream region is 69% of the volume of the region of interest, it is reasonable to assume that oil production from the upstream region during the first 4 PV of low salinity water flooding can explain the increase S_o in the region of interest. There was subsequently significant oil production from the region of interest during 20 PV of low salinity flooding. During 20PV of low salinity flooding S_w increased so that it was 0.031 higher than the value at the end of high salinity water flooding. This net oil recovery of 3 percentage points is broadly consistent with a number of studies carried out at similar conditions, most notably: *Chen et al.* (2020) who observed a recovery of 5 percentage points after tertiary low salinity

flooding in Berea Sandstone; *Lebedeva and Fogden* (2011) who saw a recovery of 7 percentage points during low salinity flooding of a kaolinite coated sandpack; and *Shabaninejad et al.* (2018) who reported a recovery of 3 percentage points in a tertiary low salinity waterflood in a Berea sandstone sample.

One notable feature of the altered sample saturation profiles is the variability in S_w along the length of the core, oil is much more heterogeneously distributed than in the unaltered case. For each flow step, the standard deviation of the saturation values along the core were approximately three times greater than for the unaltered case (see table 4.1). This could be a reflection of heterogeneity in the pore scale wetting state subsequent to the alteration with crude oil.

4.2.2 Surface Area Fractional Coverage

Figure 4.3 plots the surface area fractional coverage for 63 subvolumes for all flowsteps in both samples. This analysis provides a clear measure of wetting state, where the more wetting a fluid, the greater fraction of the rock surfaces will be coated by that fluid at a given saturation (see chapter 3.3.5). The area fractions exhibit distinct wetting states for the altered and unaltered samples. This indicates that the ageing process was successful in altering the wetting state in the altered sample (*Garfi et al.*, 2020a). In the unaltered case, points lie below the $A_{fo} = S_o$ line (where A_{fo} is the fraction of mineral surfaces coated by oil, see chapter 3.3.5). At no point does the proportion of oil coating mineral surfaces exceed the proportion of oil filling the pore space (the oil saturation). This is indicative of a preference for water to wet the rock surface. Conversely, for the altered case, all points lie above the $A_{fo} = S_o$ line showing a preference for oil to wet the rock surface.

In the unaltered case there is no significant change in oil-coated area fraction between the steps flooding with high and low salinity brine. This shows that there is no significant shift in wetting state during low salinity flooding when the rock is initially water-wetting. The precision of the points, with many shifting very little in either saturation or area coverage, also provides an indication of the reproducibility of the image analysis workflow.

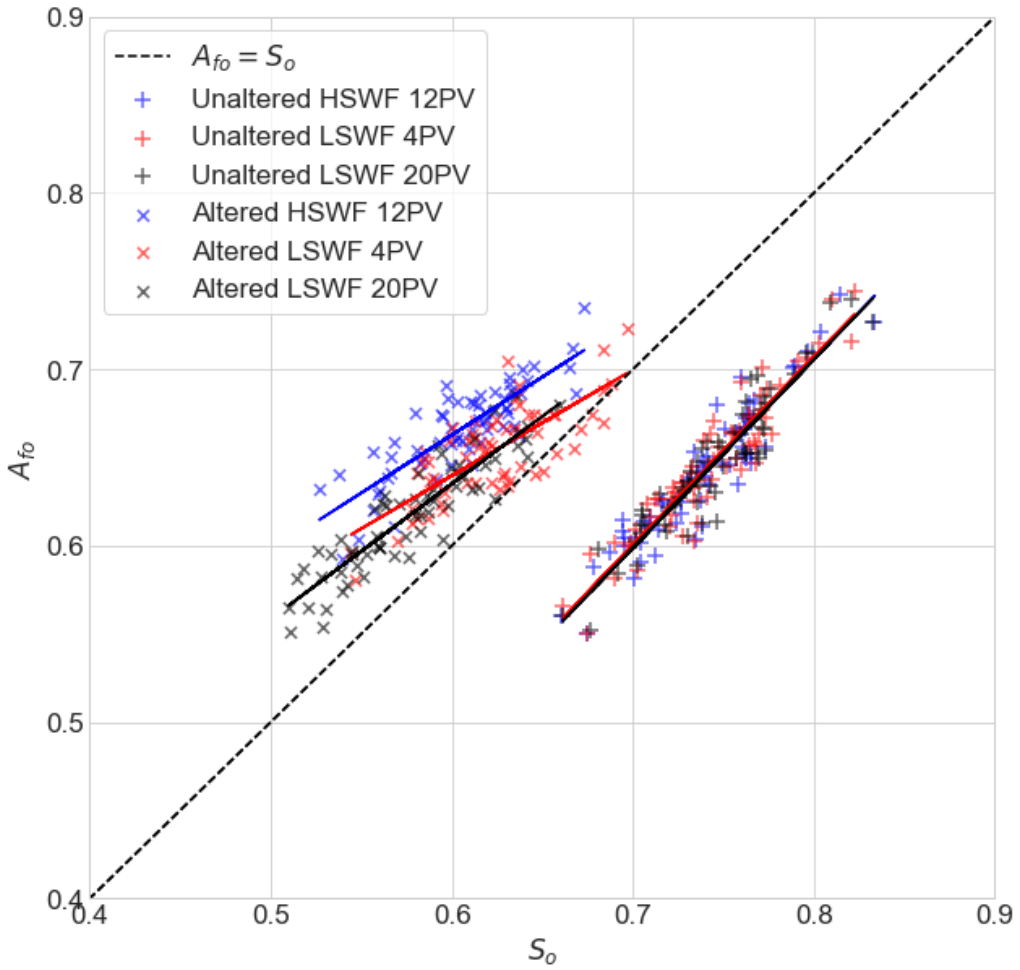


Figure 4.3: Oil-coated area fractions computed for both the unaltered sample and the altered sample, imaged after high salinity water flooding (HSWF), 4 PV of low salinity water flooding (LSWF 4PV), and 20 PV of low salinity flooding (LSWF 20PV). In the unaltered case, points lie below the $A_{fo} = S_o$ line. This is indicative of a preference for water to wet the rock surface. Conversely, for the altered case, all points lie above the $A_{fo} = S_o$ line showing a preference for oil to wet the rock surface. In the unaltered case there is no significant change in $A_{fo}(S_o)$ between the flow steps. In the altered case, $A_{fo}(S_o)$ shifts towards $A_{fo} = S_o$ after LSWF 4PV, a shift towards more water-wetting conditions. After LSWF 20PV, there is a shift parallel with $A_{fo} = S_o$ which represents a decrease in S_o but not a change in wetting state.

With the altered sample, there are shifts in the data indicative of a movement towards a more water wetting state. After 4 PV of low salinity flooding, $A_{fo}(S_o)$ shifts towards $A_{fo} = S_o$, so that for a given oil saturation, there is a lower fraction of the rock surface coated by oil. This is indicative of a shift towards more water-wetting conditions. After 20 PV of low salinity flooding, there is a shift roughly parallel with $A_{fo} = S_o$ which represents a decrease in S_o but not a change in wetting state. This shows that, although the wetting state is altered in the first 4 PV of low salinity flooding, it does not result in oil production until further flooding.

The decrease in A_{fo} in the altered case is consistent with qualitative observations by (*Chen et al.*, 2020) who reported water film propagation and enlargement during low salinity water flooding, leading to the detachment of oil from the rock surface and, therefore, a decrease in A_{fo}. These results also broadly agree with pore-scale observations of a change in wetting state during low salinity flooding made using contact angle measurements (*Khishvand et al.*, 2017; *Qin et al.*, 2019), and sub-pore scale observations of wetting alteration during low salinity flooding using atomic force microscopy (*Hassenkam et al.*, 2016; *Yesufu-Rufai et al.*, 2020).

However, our results show a small shift towards a more water-wet state while the rock remains oil-wetting. This is not a shift to an entirely water wetting system.

4.2.3 Pore and Throat Occupancy

Shifts in wetting states are also reflected in the distribution of fluids throughout the samples. We investigate the spatial distribution of brine saturated pores and throats for all flow steps in both samples. Figure 4.4 shows the contribution of different pore and throat size ranges to the total volume of brine within a $1500 \times 1500 \times 2000$ subvolume at the centre of the region of interest for all flow steps in both samples.

Global Pore Occupancy

In the unaltered case, a larger proportion of small pores are occupied by brine than the proportion of large pores which are occupied by brine (Fig. 4.4a). This is expected as in a unaltered

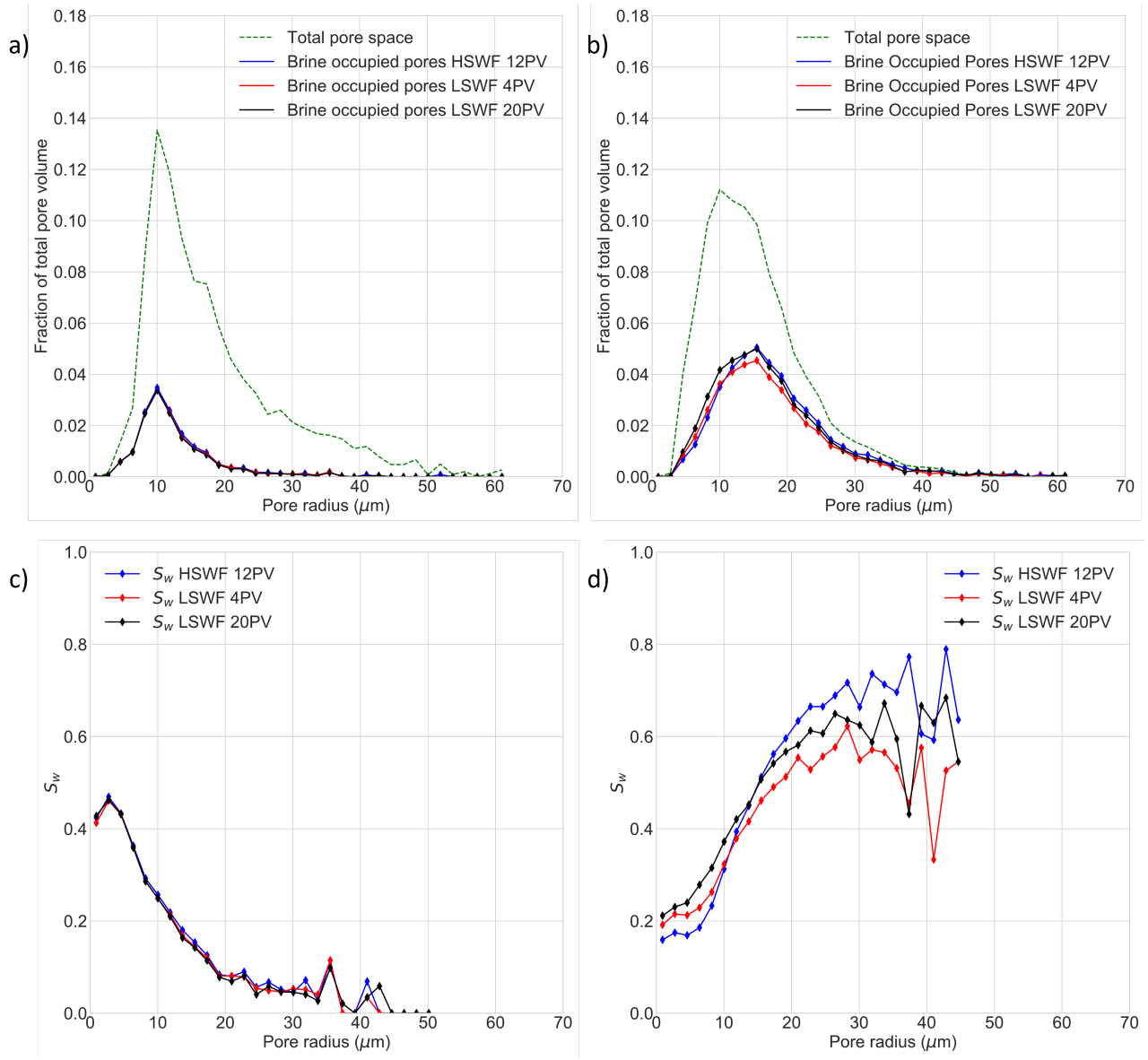


Figure 4.4: The size distribution for all brine saturated pores (bodies and throats) in a) the unaltered sample b) the altered sample, and the total brine saturation (S_w) in pore radii bins, for c) the unaltered sample d) the altered sample, imaged after 12 PV of high salinity water flooding (HSWF 12PV), 4 PV of low salinity water flooding (LSWF 4PV), and 20 PV of low salinity flooding (LSWF 20PV). In the unaltered case, there is no significant shift in pore occupancy following either LSWF 4PV or LSWF 20PV. In the altered sample, there is a subtle shift in the pore occupancy after both LSWF 4PV and LSWF 20PV. After LSWF 4PV, there is a small increase in brine volume in the smallest pore and throat elements (radius $< 10\mu$m). This is outweighed by a decrease in brine volume within larger pore and throat elements ($12 <$ radius $< 25\mu$m). After LSWF 20PV, there is a further increase in brine volume in the smallest pore and throat elements (radius $< 10\mu$m). There is also an increase in brine volume within the larger pore and throat elements ($12 <$ radius $< 25\mu$m) compared to after LSWF 4PV, however, the brine saturation in this pore size range remains lower than values after HSWF.

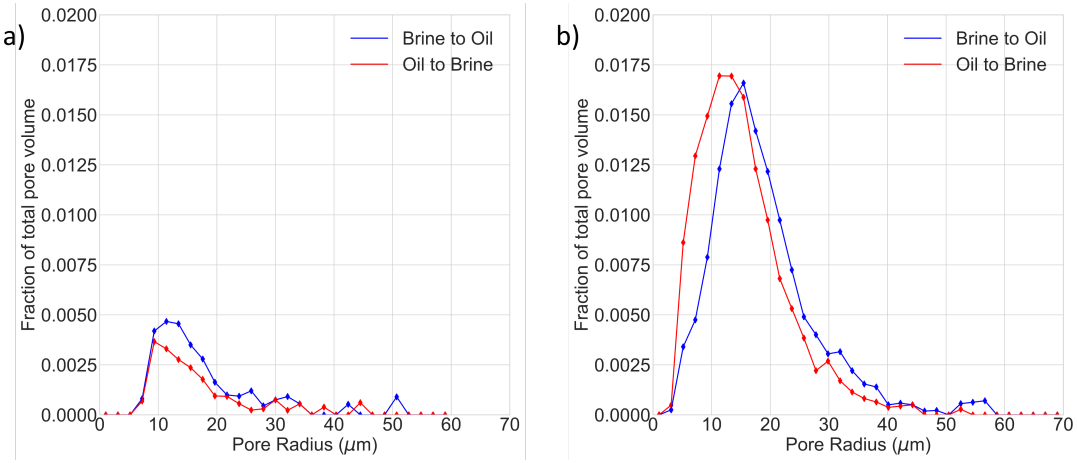


Figure 4.5: The size distribution for all pores (bodies and throats) where saturation changed from oil to brine (red) or brine to oil (blue) between HSWF and LSWF 20PV, for a) the unaltered sample b) the altered sample. In the unaltered case, there are relatively few pores where saturation changes from oil to brine or brine to oil. In the altered case, however, there are many more redistribution events. In the smaller pores (radius $< 19\mu$m) oil to brine events (where brine displaced oil during low salinity flooding) outweigh brine to oil events (where oil displaced brine during low salinity flooding), the opposite is true for larger pores (20 $<$ radius $< 35\mu$m).

system, oil may only invade small pores at high capillary pressure. Conversely, in the altered case, brine saturated pores span a wider range of radii, with the majority of the largest pores being occupied by brine (Fig. 4.4b).

In the unaltered case, there is no significant shift in pore occupancy following either 4 or 20 PV of low salinity water flooding. In the altered sample, there is a subtle shift in the pore occupancy after both 4 and 20 PV of low salinity water flooding. After 4 PV of low salinity water flooding, there is a decrease in brine volume within larger pore and throat elements (12 $<$ radius $< 25\mu$m). This probably represents the accumulation of oil displaced from the smallest pores within the field of view as well as oil from elsewhere in the sample. After 20 PV of low salinity water flooding, there is a small increase in brine volume in the smallest pore and throat elements (radius $< 10\mu$m). There is also an increase in brine volume within the larger pore and throat elements (12 $<$ radius $< 25\mu$m) compared to the observations after 4 PV of low salinity water flooding, however, the brine saturation in this pore size range remains lower than saturation after high salinity water flooding. This means that some, but not all, of the additional oil which accumulated within the larger pores during the first 4 PV of low salinity

water flooding was displaced.

The subtle changes in pore-occupancy do not fully reveal the large volume of fluid redistribution taking place within the pores. To better understand the extent of such events, we isolated pores where a change in pore occupancy occurs between the high salinity waterflood and 20 PV of low salinity water flooding. Figure 4.5 shows the size distribution of pores in which pore occupancy changed between the flow steps, that is to say, pore elements in which brine displaced oil or vice versa. As expected, in the unaltered case (fig. 4.5a), there are relatively few pores where saturation changes from oil to brine or brine to oil. In the altered case (fig. 4.5b), however, there are many more redistribution events. Even in pore radii bins in which no or little net change of pore occupancy occurs (e.g. 19-20 μm), there are numerous like for like changes in saturation. Approximately, 20% of pores ranging in radius from 19-20 μm changed in saturation from oil to brine or vice versa. In the smaller pores (radius $< 19\mu$m) oil to brine events outweigh brine to oil events, the opposite is true for larger pores ($20 <$ radius $< 35\mu$m).

It is important to note that the initial distribution of fluids has an important control over pore occupancy changes during waterflooding. As discussed in Chapter 3.2.5, S_{wi} was < 0.05 for both samples, with the smallest pores predominately oil saturated. In real reservoirs, it is unlikely that the smallest pores will be oil saturated due to the large capillary pressure that is needed for oil invasion of smaller pores during primary oil migration (*Blunt*, 2017). The results presented here, show that oil is primarily produced from the smallest pores during low salinity flooding in the altered Berea sandstone. It is likely that fewer of these smallest pores would be initially oil saturated in real reservoirs, and, therefore, there would less opportunity for low salinity brine to displace oil from them. Therefore, the observed additional recovery during low salinity flooding in the altered Berea sample may be larger than would be expected in a similar sample with a more realistic initial fluid distribution.

As discussed in Chapter 3.3.6, it is important to note that pore occupancy analysis may systematically underestimate saturation changes. To more accurately assess the volume of mobilised and retrapped oil, we calculate the volume of oil that is mobilised after low salinity flooding, defined as the total fraction of oil displaced by brine after 20 PV of low salinity flooding. We

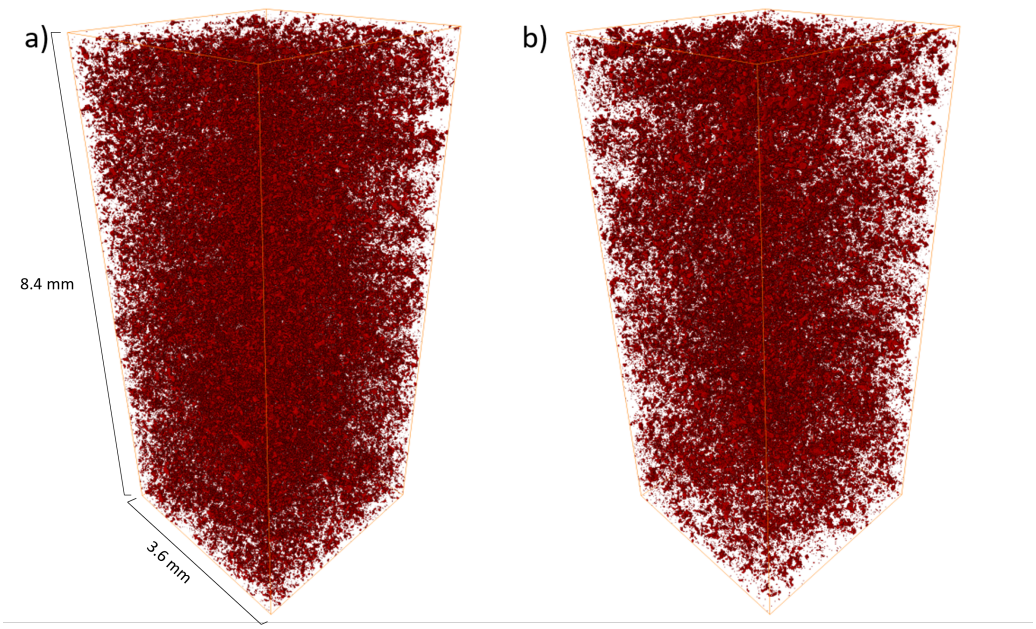


Figure 4.6: A volume rendering of a) Oil displaced during twenty pore volumes of low salinity water flooding (LSWF 20PV) in the altered sample. Only 20% of this displaced oil is produced, the rest is redistributed and retrapped within the core, as shown in b).

compare this to bulk changes in saturation to calculate the fraction of the mobilised oil that is produced. We observe that 22% of the oil in place on completion of high salinity water flooding is displaced after 20 PV of low salinity water flooding, but less than a quarter of this displaced oil is produced or transported out of the region of interest (Fig 4.6). This means that, on completion of 20 PV of low salinity water flooding, the volume of redistributed oil is 4 times greater than the volume of produced oil. This ratio is consistent with findings by (*Sohrabi et al.*, 2017) who observe a ratio of five between redistributed and produced oil using computational fluid dynamic simulations of tertiary low salinity water flooding in a 2D domain. These results show that a complex redistribution of fluids can occur during low salinity water flooding as a result of a shift in the wetting state, without a corresponding change in bulk saturation. This implies that a wetting state shift is not sufficient to determine production. Furthermore, a low salinity effect may occur in a rock as a redistribution of fluids at the pore and pore-network scale, but may not be observed in typical core-scale experiments where only saturation is monitored. This could, therefore, be a significant contributor to the confusion around core flooding analysis of low salinity floods.

As we observed very little fluid redistribution during 4 or 20 PV of low salinity waterflooding in

the unaltered sample, we can use the results to estimate the uncertainty of the measures used in this study. We observed very small changes in average saturation, area fraction and pore occupancy measurements between the three waterfloods, indicating that the image analysis workflow is robust and repeatable. S_w values of 0.260, 0.256 and 0.254 were recorded after high salinity water flooding, 4 PV of low salinity water flooding and 20 PV of low salinity waterflooding, respectively. This gives a mean value of 0.257, and a standard error of 0.00125. The average A_{fo} value for all subvolumes was calculated as 0.641, 0.646 and 0.646 after high salinity water flooding, 4 PV of low salinity water flooding and 20 PV of low salinity waterflooding, respectively. This gives a mean value of 0.644 and a standard error 0f 0.00118. These standard errors are an order of magnitude lower than the shifts in S_w and A_{fo} observed during low salinity flooding in the altered sample. This highlights the robust nature of the image analysis workflows used in this work and gives confidence that the shifts observed in the altered sample reflect physical changes in the sample and not uncertainty in the image analysis techniques.

Local Pore Occupancy

To give insight into the spatial variation of pore occupancy in the altered sample, we carry out further pore occupancy analysis on selected subvolumes of $1500 \times 1500 \times 300$ voxels in size (fig. 4.7). Two of these subvolumes (subvolumes a and c) were selected in areas with significant net oil production after 20 PV of low salinity water flooding, based on figure 4.1. The other two subvolumes (subvolumes b and d) were chosen in areas with a comparatively small change in saturation after 20 PV of low salinity water flooding. The results of this localised pore occupancy analysis are shown in figure 4.7.

In subvolumes a and c, where there is significant net oil production, there is a pronounced increase in S_w in the small and medium pores. This increase is not associated with a decrease in S_w in the larger pores, meaning that displaced oil is transported out of the subvolumes. In subvolume b and d, where there is no net oil production, there is a smaller increase in S_w within the smallest pores. This increase is balanced by a small decrease in S_w in the largest pores so that there is no or limited net production of oil from the subvolumes, but rather a

Table 4.2: Water saturation, S_w, values for subvolumes a,b,c, and d after high salinity water flooding (HSWF), 4 PV of low salinity water flooding (LSWF 4PV), and 20 PV of low salinity flooding (LSWF 20PV)

	S_w [-]			
	Subvolume a	**Subvolume b**	**Subvolume c**	**Subvolume d**
HSWF 12 PV	0.294	0.355	0.376	0.412
LSWF 4 PV	0.308	0.357	0.361	0.413
LSWF 20 PV	0.340	0.373	0.448	0.437

redistribution. Irrespective of net saturation changes, the pore occupancy changes are indicative of a significant shift in wetting state towards more water-wet. The profile is similar to those presented in both experimental (*Bartels et al.*, 2017a; *Khishvand et al.*, 2017) and modelling (*Sohrabi et al.*, 2017) studies, with a pronounced oil reduction range in the small and medium pores.

In all subvolumes, S_w increases in the smallest pores and throats ($< 13\mu m$) after both 4 and 20 PV of low sanity water flooding. In subvolumes a and c, this effect is more pronounced, particularly after 20 PV of low salinity water flooding where S_w increases significantly in pores $< 15\mu m$ radius. In subvolume c, there is a pronounced decrease in S_w in pores of radius $> 13\mu m$ after 4 PV of low salinity water flooding, probably due to the accumulation of oil displaced from outside of the region of interest. However, this additional oil remains connected and is displaced during 20 PV of low salinity water flooding, after which S_w within the pores $> 13\mu m$ radius is comparable to the S_w following the high salinity water flood.

This analysis highlights the non-uniform nature of the low salinity effect, which varies spatially throughout the core. While the wetting alteration appears widespread throughout the pore space, the local pore structure plays a leading role in whether or not this results in oil production, or alternatively, if mobilised oil is trapped again.

4.2.4 Displacement Processes in The Pores

In previous studies x-ray μ-CT imaging has been used to observe both the expansion of water layers (*Chen et al.*, 2020) and brine snap-off events (*Khishvand et al.*, 2017) during low salinity

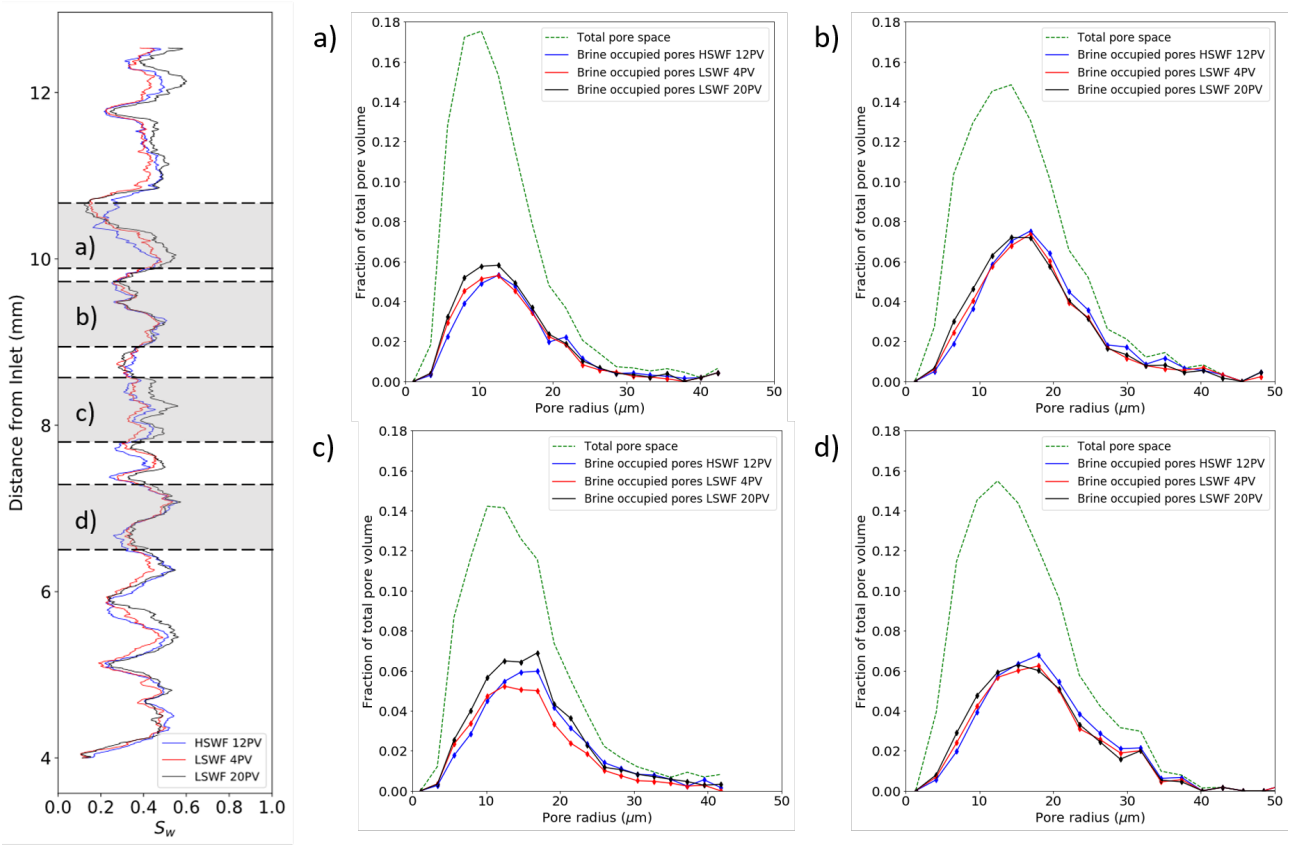


Figure 4.7: The size distribution for all brine saturated pores in 4 carefully selected sub volumes within the altered sample imaged after high salinity water flooding (HSWF), 4 PV of low salinity water flooding (LSWF 4PV), and 20 PV of low salinity flooding (LSWF 20PV). In subvolumes a and c, there is a pronounced increase in S_w in the small and medium pores after LSWF 20PV, and no decrease in S_w in the larger pores, so that there is net oil production from the subvolumes. In subvolumes b and d, where there is no or little net oil production after LSWF 20PV, there is a smaller increase in S_w within the smallest pores and a small decrease in S_w in the largest pores.

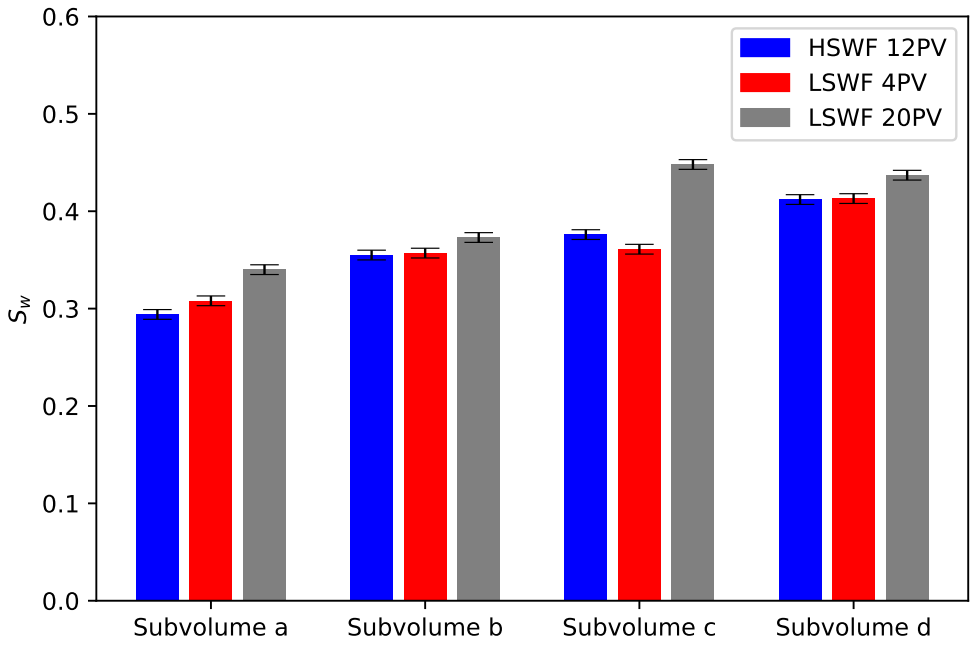


Figure 4.8: S_w values after 12PV of high salinity flooding (HSWF 12PV), 4PV of low salinity flooding (LSWF 4PV), and 20PV of low salinity flooding (LSWF 20PV) in subvolumes a,b,c, and d. As discussed in Chapter 4.2.3, we estimate a standard error of 0.00125 for the saturation measurements.

water flooding as a consequence of a wettability alteration. Using the same method, both of these features are also observed in this study. A more water-wet system encourages brine to proliferate in layers in the corners of pores which, when these layers expand to critical size within a given pore or throat, can become unstable, leading to a snap-off event (*Blunt*, 2017). Such events are, as expected, prevalent in the unaltered case and are probably a key factor for the high S_{or} observed. After HSWF in the altered case, there is little evidence of any snap-off events, indicating the absence of water-wetting areas. However, after 20 PV of low salinity water flooding, some snap-off events are observed throughout the sample, indicating more water-wetting behaviour. Evidently, in some areas, the wettability alteration during low salinity flooding in the altered sample, was sufficient to create water-wetting conditions in some pores and throats. This is further evidence of the wettability alteration observed in figure 4.3. These snap-off events have the effect of breaking up oil ganglia (fig. 4.9), and in some cases, where all of the throats surrounding an oil-saturated pore are snapped-off, can lead to the entrapment of oil in the centre of pores (fig. 4.10c). This trapping may help to explain the increase of oil saturation in the largest pores after 20 PV of low salinity water flooding, oil is

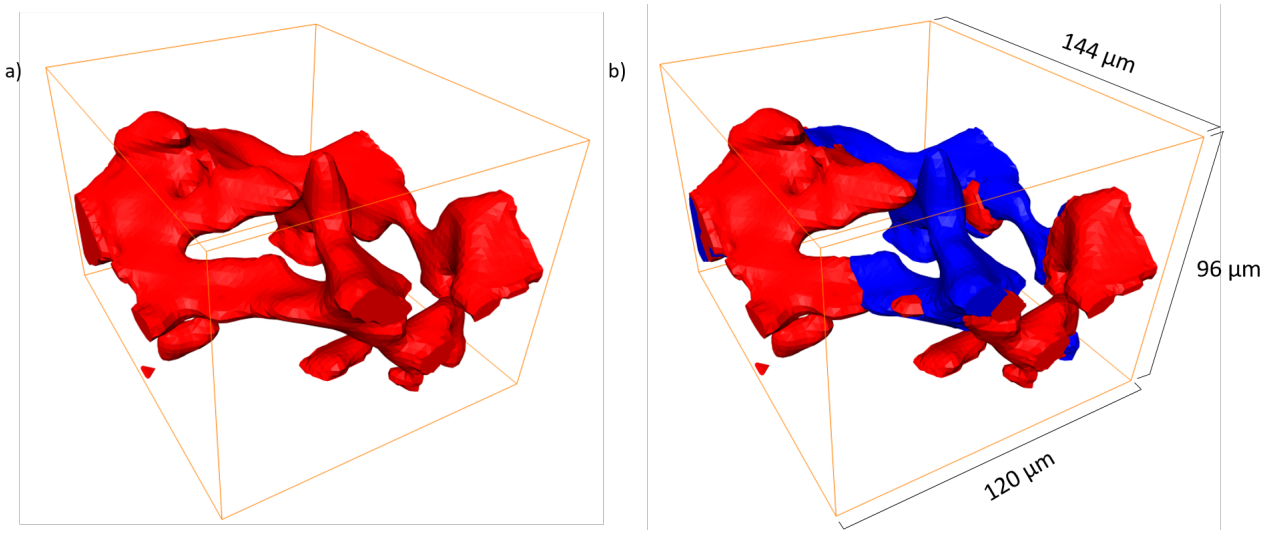


Figure 4.9: A brine snap-off event in the altered sample where oil connected across multiple pores is broken up. The configuration of oil (red) and brine (blue) in a subvolume after a) high salinity water flooding b) 20 PV of low salinity water flooding. The rock is transparent in each case.

transported to these pores and subsequently snapped-off and, therefore, trapped.

We have shown that LSWF can alter the wetting state of a sample where there is an initial preference for oil to wet the rock surface, and consequently, can lead to the displacement of residual oil. However, the local displacement of oil does not guarantee production. In agreement with *Aziz et al.* (2019); *Bartels et al.* (2017a) we observe the majority of initially displaced oil to be re-trapped. The extent of this re-trapping varies throughout the sample. Significant production is observed in some areas, and in others little to no oil is produced. The extent of this re-trapping is crucial in determining oil production, and so it is crucial to gain a better understanding of the controls of this process. As described above, much of the re-trapping is probably due to snap off events in brine (fig. 4.10). A more water wetting system leads to more snap-off events (*Blunt*, 2017). However, the geometry of pores and throats is also known to impact the occurrence of snap-off events as well as other pore scale displacement events. In particular, the aspect ratio (ratio of the pore to throat radius) of a pore space has been shown to strongly correlate with the occurrence of pore-filling and snap-off events during imbibition (*Singh et al.*, 2019, 2022; *Tanino and Blunt*, 2012). Additionally, pore radii, coordination number, pore size distribution, and pore scale disorder have all been shown to impact flow regimes and displacement efficiency during both imbibition and drainage (*An et al.*,

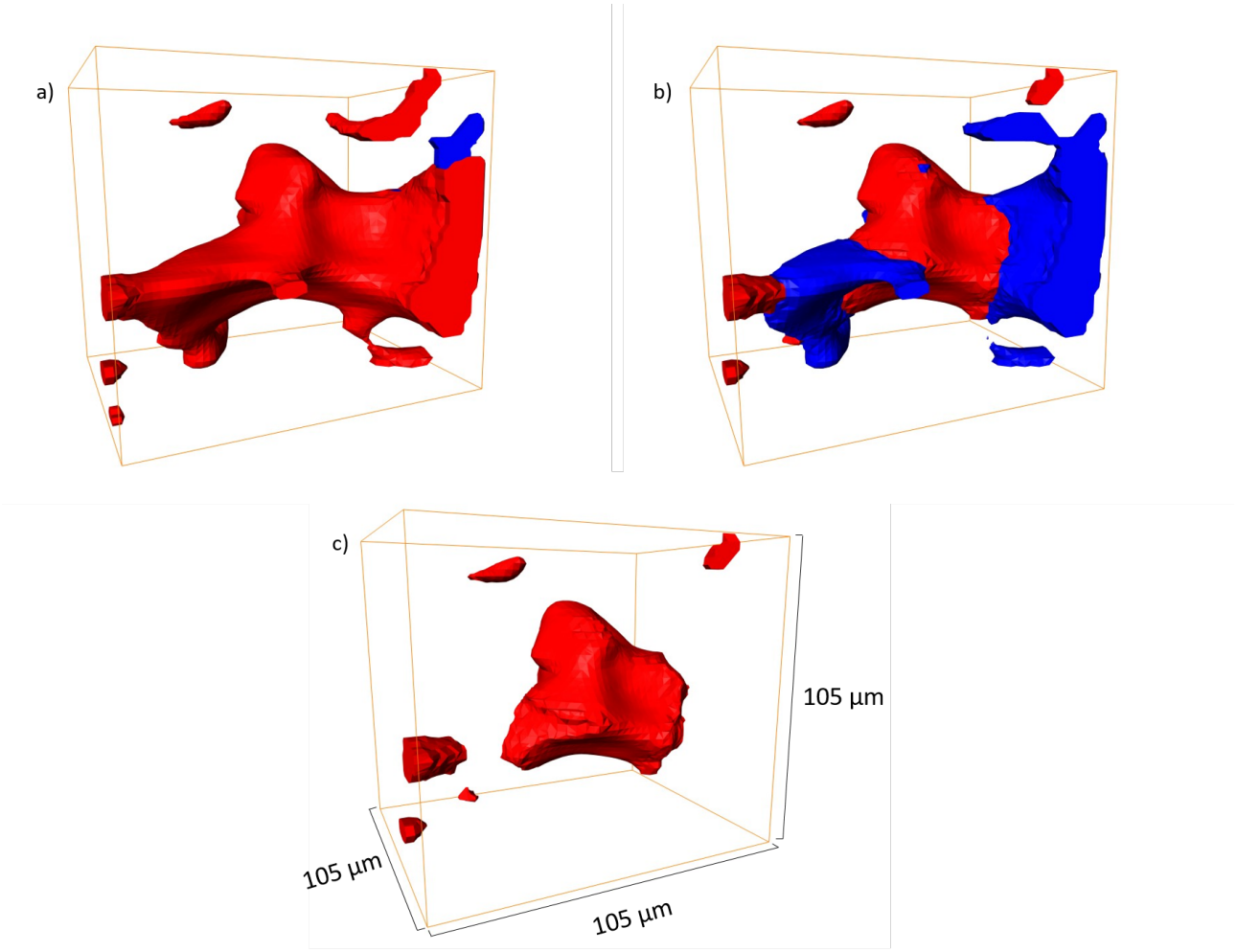


Figure 4.10: A brine snap-off event in the altered sample where oil is trapped. The configuration of oil (red) and brine (blue) in a subvolume after a) high salinity water flooding b) 20 PV of low salinity water flooding. The rock is transparent in each case, and the water is transperent in c) to isolate the trapped oil.

2016; *Blunt*, 2017; *Holtzman*, 2016; *Tanino and Blunt*, 2012; *Xu et al.*, 2014). We, therefore, hypothesise that the geometry of a pore space directly impacts the extent of re-trapping of oil during low salinity water flooding, and hence the extent of production.

4.3 Conclusions

In this chapter, we observed the displacement of crude oil from Berea sandstone during flooding with high and low salinity brine in cores with both an unaltered (water-wet) and an altered wetting state. Our main findings are as follows:

- The fluid saturation profiles and the average saturation changes are distinct for water wet and altered rocks. In the unaltered rock, oil was trapped at a relatively high saturation ($S_o = 0.74$), uniformly distributed throughout the sample after flooding with high salinity brine. This saturation did not change significantly after subsequent flooding with low salinity brine; There was no low salinity effect. In contrast, oil was trapped heterogeneously throughout the altered rock sample at a lower saturation (S_o= 0.62) after high salinity flooding. Subsequent flooding with low salinity brine resulted in a 3 percentage point enhancement to oil production.

- The wetting state shifts in response to low salinity brine in the altered sample while no such change was observed in the unaltered sample. In the altered sample, we observe a shift in the solid surface area covered by the oil phase indicative of a change from an oil-wetting state to less oil-wetting, but not to a water-wetting state. This change is also reflected in the observed variation in fluid pore occupancy, where water preferentially displaces oil in small pores in response to the low salinity effect.

- In the altered sample, changes in fluid pore occupancy in response to low salinity brine were found to vary across the core. In subvolumes with net oil production, the behaviour of brine invading the small and medium pores and throats was pronounced. In subvolumes with little to no net oil production, the invasion of small and medium pores was far less significant, and oil saturation in the largest pores increased.

- In the altered sample, we directly observe snap-off events after low salinity water flooding, behaviour indicative of a more water-wet system. We observe that in some areas, snap off events can lead to the trapping of oil ganglia at the centre of pores. This mechanism may help to explain the large amount of retrapping of mobilised oil that we observed in the altered sample.

- The combined impact of this was that a shift in the wetting state resulted in a large amount of oil being redistributed, but only a small amount of oil produced. In other words, most of the oil mobilised as a result of low salinity flooding is re trapped. This implies that a wetting state shift is not sufficient to determine production. Low salinity flooding can cause a complex redistribution of fluids at the pore and pore-network scale, but may not lead to improved recovery. The combined role of wetting alteration and pore structure must be evaluated for the prediction of a low salinity effect. This has significant implications for typical core-scale low salinity flooding experiments where only saturation is monitored.

- The success of low salinity water flooding depends on both the ability of the low salinity flood to alter the wetting state from more oil-wetting to more water-wetting and the pore structure to facilitate the production of mobilised oil. Further work should be carried out to better constrain what controls the extent of oil re trapping during low salinity flooding. We hypothesise that particular features of the geometry and topology of a pore space plays a leading role.

Chapter 5

The Impact of Pore Structure on Low Salinity Water flooding

5.1 Objectives

So far we have shown that initial wetting state has a strong control on displacement during low salinity waterflooding, with more oil-wetting conditions more favourable compared to water-wet conditions. We have also hypothesised that pore structure controls displacement during low salinity flooding. In this chapter, we further explore the impact of pore structure on displacement during low salinity water flooding.

It is widely understood that pore structure can have drastic impacts on displacement mechanisms, fluid distribution and flow regimes during multiphase flow. However, the impact of pore structure on low salinity response in sandstones has not yet been examined. One reason for this is that all pore scale investigations of low salinity water flooding in sandstones have been carried out using Berea sandstone samples, and so results over only a very narrow range of pore structures are available. In this chapter, we compare results from the altered Berea sample presented in Chapter 4, with tertiary low salinity waterflooding of Bunter and Castlegate sandstone samples of altered wetting states. These samples, Berea, Bunter and Castlegate sandstones (as described in section 3.1.1) have similar mineralogy but different pore structures. The objective

of this chapter is to explore the role of pore structure in facilitating, or, conversely, limiting, a favourable response during low salinity water flooding.

5.2 Pore Scale Observations

5.2.1 Saturation Distribution

Table 5.1 and Figure 5.1 present S_w values for each of the three samples after each waterflood step. After 20PV of low salinity flooding, there is a 3, 4, and 1 percentage point additional recovery in the Berea, Bunter and Castlegate samples respectively. Fig 5.2 shows the saturation profiles for each of the three samples after each waterflood step. In all samples, there is significant variation in S_w along the length of the samples for all waterfloods. In the Berea and Bunter samples, a significant decrease in S_w is observed in some sections towards the top of the imaged region, away from the inlet, after 4 PV of low salinity water flooding. This probably represents an accumulation of oil displaced from upstream of the imaged region during the 4 PV of low salinity flooding. This effect is most significant in the Berea sample, where there is a 1 percentage point increase in oil saturation in the region of interest after 4 PV of low salinity flooding in the Berea sample. In both samples, after 20 PV of low salinity flooding, the majority of this accumulated oil is produced from the region of interest. As a result, there is an additional oil production of 3 and 4 percentage points in the Berea and Bunter samples after 20 PV of low salinity waterflooding. These values are consistent with multiple studies carried out on sandstones at similar conditions: *Lebedeva and Fogden* (2011) observed an additional recovery of 7 percentage points during low salinity flooding of a kaolinite coated sandpack; *Chen et al.* (2020) reported a recovery of 5 percentage points after tertiary low salinity flooding in Berea Sandstone; and *Shabaninejad et al.* (2018) observed a recovery of 3 percentage points in a tertiary low salinity waterflood in a Berea sandstone sample.

In the Castlegate sample, there is little change in average S_w after 4 and 20 PV of low salinity water flooding, with 1 percentage point additional recovery after 20 PV of low salinity water-

Table 5.1: Average water saturation, S_w, in the region of interest, for all samples, after 12 PV of high salinity flooding (HSWF), 4 PV of low salinity water flooding (LSWF 4PV), and 20 PV of low salinity water flooding (LSWF 20PV). Additionally, ΔS_w relative to HSWF 12PV is presented for all samples after LSWF 4PV and LSWF 20PV. In all cases, there was a very high initial oil saturation with $S_w < 0.05$ prior to waterflooding. As discussed in Chapter 4.2.3, we estimate a standard error of 0.00125 for the saturation measurements. In all samples, the changes in S_w during low salinity waterflooding are an order of magnitude higher than the standard error of the measurement.

	Berea		Bunter		Castlegate	
	S_w	ΔS_w relative to HSWF 12PV	S_w	ΔS_w relative to HSWF 12PV	S_w	ΔS_w relative to HSWF 12PV
HSWF 12PV	0.382		0.429		0.389	
LSWF 4PV	0.368	-0.014	0.439	0.01	0.397	0.008
LSWF 20PV	0.413	0.031	0.467	0.038	0.400	0.011

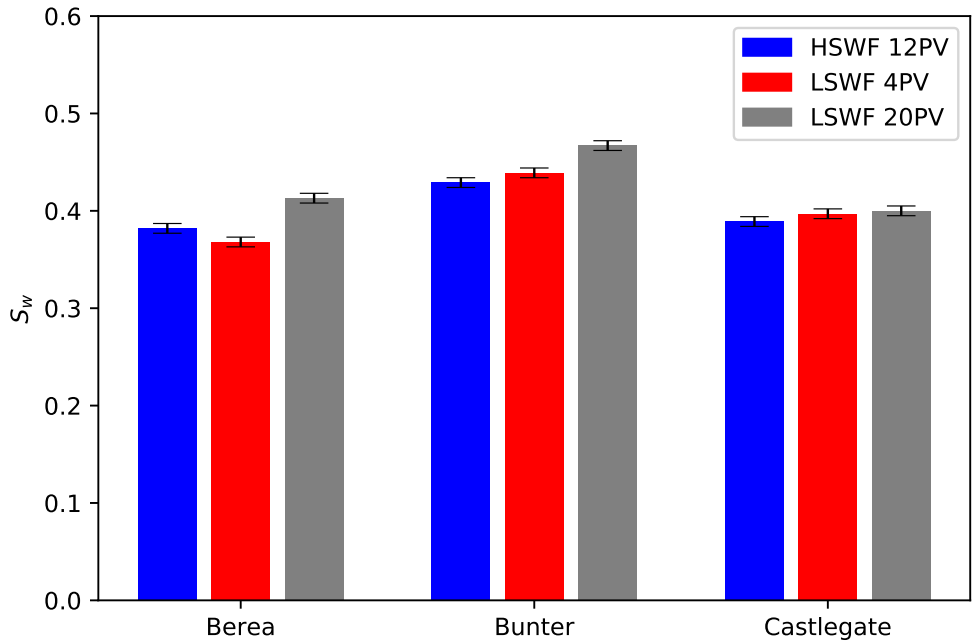


Figure 5.1: S_w values after 12PV of high salinity flooding (HSWF 12PV), 4PV of low salinity flooding (LSWF 4PV), and 20PV of low salinity flooding (LSWF 20PV) for the Berea, Bunter and Castlegate samples. As discussed in Chapter 4.2.3, we estimate a standard error of 0.00125 for the saturation measurements.

flooding. Additionally the local changes in S_w values after 4 and 20 PV of low salinity flooding are significantly smaller than the changes observed in both the Berea and Bunter samples. As discussed in Chapter 4, we estimate a standard error of 0.00125 for the saturation measurements. In all samples, the changes in S_w during low salinity waterflooding are an order of magnitude higher than the standard error of the measurement.

5.2.2 Surface Area Fractional Coverage

In Chapter 4, we applied a workflow developed by *Garfi et al.* (2020a) to use bulk fluid surface area coverage measurements to show a wettability alteration during low salinity flooding in the Berea sandstone sample. Here, we also apply this analysis to the Bunter and Castlegate samples (fig. 5.3).

After high salinity water flooding, the fraction of mineral surface area coated by oil at a given saturation, $A_{fo}(S_o)$, is lower in the Berea sample than for the Bunter and Castlegate samples. For the Berea sample, $A_{fo}(S_o)$ values lie close to the 1:1 line after high salinity flooding. In contrast, $A_{fo}(S_o)$ values are significantly higher in both the Bunter and Castlegate sandstones. This suggests that the Berea sample is less oil wetting after aging than the other two samples.

In the Berea sample, after 4 PV of tertiary low salinity flooding, there is a shift to lower $A_{fo}(S_o)$ values, so that for a given S_o there is a lower fraction of oil coating the mineral surfaces. This indicates a shift to more water-wet conditions. After 20 PV of tertiary low salinity flooding, there is no further shift in $A_{fo}(S_o)$ values beyond what was observed after 4 PV. However, there is a significant decrease in oil saturation, that is, in the Berea sandstone, low salinity flooding was characterised by a rapid wetting state shift, followed by oil production over longer timescales.

The Bunter sandstone responds similarly as the Berea sandstone. There is a significant shift to lower $A_{fo}(S_o)$ values after 4 PV of tertiary low salinity flooding. Between 4 and 20 PV of tertiary low salinity flooding there is no further shift in $A_{fo}(S_o)$, however, there is a significant decrease in the oil saturation. Similarly to the Berea sandstone, in the Bunter sandstone,

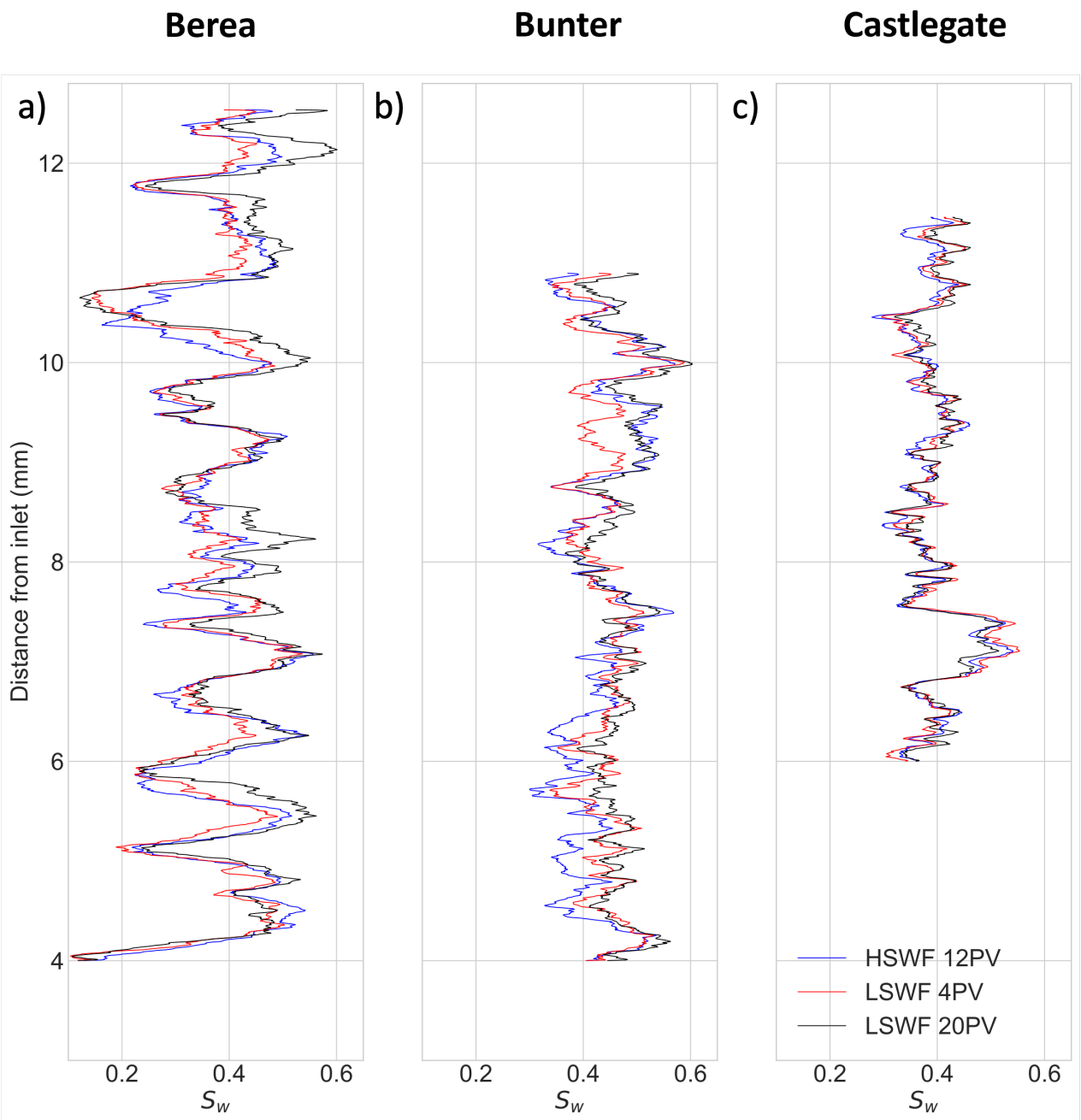


Figure 5.2: Profile of water saturation, S_w, averaged perpendicular to the flooding direction across the region of interests of a) Berea sandstone b) Bunter sandstone c) Castlegate sandstone after 12 PV of high salinity water flooding (HSWF 12PV), 4 PV of low salinity water flooding (LSWF 4PV), and 20 PV of low salinity water flooding (LSWF 20PV).

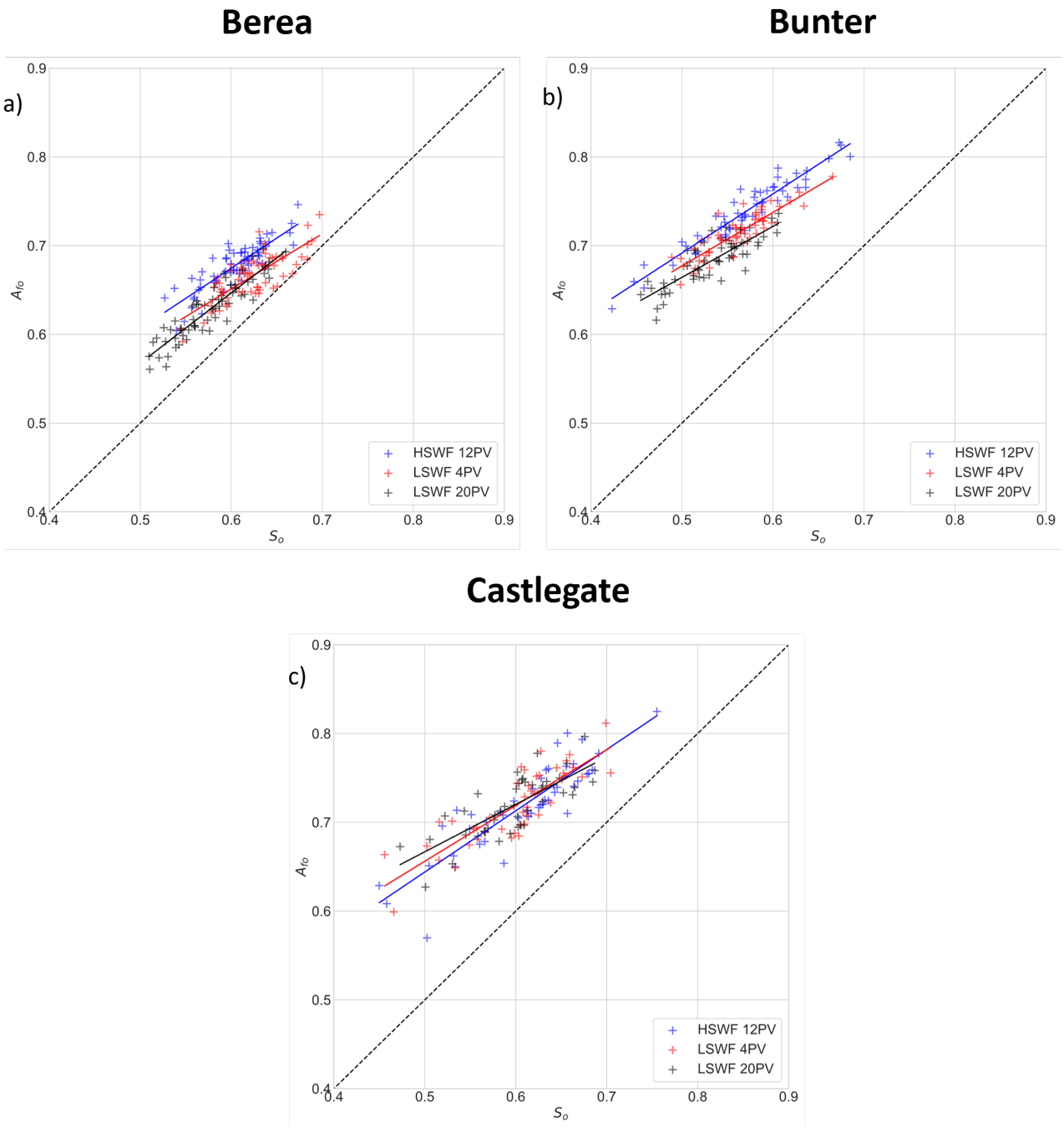


Figure 5.3: Oil-coated area fractions, imaged after high salinity water flooding (HSWF), 4 PV of low salinity flooding (LSWF 4PV), and 20 PV of low salinity flooding (LSWF 20PV), for a) Berea b) Bunter and c) Castlegate. As discussed in chapter 4, we calculate a standard error for the A_{fo} measurements 0f 0.00118

low salinity flooding causes a rapid wetting state shift, followed by oil production over longer timescales.

In the Castlegate sample, there is no significant shift in $A_{fo}(S_o)$ values after either 4 or 20 PV of low salinity water flooding. There is also very little oil production throughout the flooding. This suggests no systematic wettability alteration within the sample. As discussed in chapter 4, we calculate a standard error for the A_{fo} measurements 0f 0.00118. The changes in A_{fo} during low salinity flooding in both the Berea and Bunter samples are an order of magnitude greater than the standard error.

Observations of wettability alteration in the Berea and Bunter sandstone samples are broadly consistent with a wealth of observations of wettability alteration during low salinity water-flooding across a range of scales, from AFM to field scale (*Berg et al.*, 2010; *Cense et al.*, 2011; *Mahani et al.*, 2015b; *Nasralla et al.*, 2013; *Vledder et al.*, 2010; *Yesufu-Rufai et al.*, 2020). More specifically, these findings agree with pore scale observations of wetting alteration during low salinity water flooding of Berea sandstone using manual contact angle measurements (*Khishvand et al.*, 2017), and observations of water-film propagation during low salinity flooding of Berea sandstone (*Chen et al.*, 2020).

5.2.3 Global Pore Occupancy

Changes in wetting state impact the distribution of fluids throughout a sample. Here, we investigate the spatial distribution of brine saturated pores and throats after each flow step in each sample, to infer changes in wetting state, and analyse the effect of low salinity water flooding on fluid occupancy. Figure 5.4 shows the contribution of different pore and throat size ranges to the total volume of brine within the region of interest of imaged in each sample.

After high salinity waterflooding, the Bunter and Castlegate samples have very similar pore occupancy profiles, with $< 20\%$ of the smallest pores brine saturated, and $> 80\%$ of the largest pores brine saturated (fig. 5.4e and 5.4f). This is indicative of an oil-wet system, where it is preferable for brine to occupy the largest pores, and oil the smallest (*Blunt*, 2017). Pore

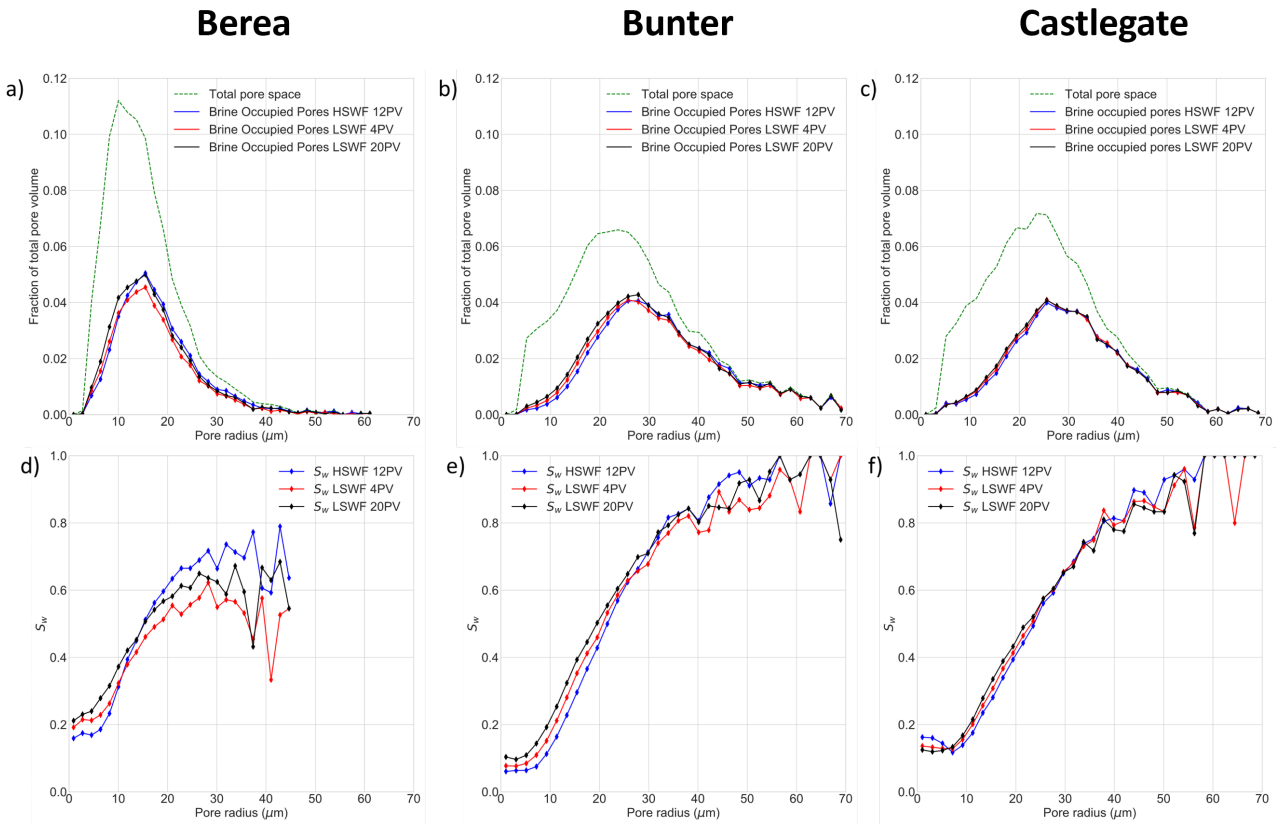


Figure 5.4: The size distribution for all brine saturated pores (bodies and throats) in a) Berea b) Bunter c) Castlegate, and the total brine saturation (S_w) in pore radius bins, for d) Berea e) Bunter f) Castlegate, imaged after 12 PV of high salinity water flooding (HSWF 12PV), 4 PV of low salinity water flooding (LSWF 4PV), and 20 PV of low salinity flooding (LSWF 20PV).

occupancy after high salinity water flooding differs in the Berea sample as although $< 20\%$ of the smallest pores are brine saturated, $< 80\%$ of the largest pores are also brine saturated (fig. 5.4d). It, therefore, appears that the Berea sample is not as strongly oil-wet as the other two samples. This agrees with the surface area fraction analysis (Fig. 5.3), which showed that the Berea sample is less oil-wetting compared to the Bunter and Castlegate samples, signified by lower average A_{fo} values for a given S_o in the Berea sandstone.

In both the Berea and Bunter samples, there is a significant shift in pore occupancy in the smallest pores after low salinity waterflooding. In the Bunter sample, there is a significant increase in brine saturation in pores with radius $< 30\mu m$ after 4 PV of low salinity waterflooding, and then again after 20 PV of low salinity waterflooding. We observe the same effect in the Berea, but with pores of radius $< 15\mu m$.

In the Castlegate sample, we observe a far smaller, yet systematic, increase in brine saturation in pores with radius $< 25\mu m$ after both 4 and 20 PV of low salinity waterflooding. The smaller changes in pore occupancy observed in the Castlegate sample after low salinity waterflooding is expected based on the lack of pervasive and systematic wettability alteration observed using surface area fractional coverage analysis (see fig 5.3). We cannot rule out smaller local shifts in wetting state, which may explain the small shift in pore occupancy observed in the Castlegate sample.

There is little significant change in the pore occupancy of the larger pores in the Bunter and Castlegate samples (radius $> 30\mu m$ and $> 25\mu m$ respectively) after low salinity flooding. However, in the Berea sample there is a significant decrease in the brine saturation in pores of radius $> 15\mu m$ after low salinity water flooding. This is particularly prominent after 4 PV of low salinity waterflooding, where, on average, S_w decreases by over 10 percentage points in pores of radius $> 20\mu m$ radius. Some of this redistributed oil is produced after 20 PV of low salinity waterflooding, however, S_w remains significantly lower after 20 PV of low salinity waterflooding than after high salinity waterflooding.

The systematic and consistent nature of pore occupancy changes in the smallest pores of each sample are striking. Although the effect is smaller in the Castlegate sample, in each case, there

is an increase in water saturation in the smallest pores after both 4 and 20 PV of low salinity waterflooding. This change is consistent with a wettability alteration towards more water wet conditions and in broad agreement with literature. Pore occupancy results agree with experimental studies across both sandstones and carbonates (*Bartels et al.*, 2017a; *Khishvand et al.*, 2017; *Selem et al.*, 2021) and modelling (*Aziz et al.*, 2019) results which show an oil reduction range in the small and medium pores during low salinity waterflooding. In all cases, this effect is thought to directly result from a wettability alteration to more water-wetting conditions during low salinity flooding. The alteration allows water to more-easily enter smaller pores and throats because of the support of capillary forces (*Aziz et al.*, 2019; *Bartels et al.*, 2017a).

As discussed in Chapter 4.2.3, the initial distribution of fluids in each sample may have a control over pore occupancy changes during waterflooding. S_{wi} was < 0.05 for all three samples presented in this chapter, with the smallest pores predominately oil saturated. In real reservoirs, it is unlikely that the smallest pores will be oil saturated due to the large capillary pressure that is needed for oil invasion of smaller pores during primary oil migration (*Blunt*, 2017). In this work, pore occupancy results show that oil is primarily produced from the smallest pores during low salinity flooding in each sample. However, it is likely that fewer of these smallest pores would be initially oil saturated in real reservoirs, and, therefore, there would less opportunity for low salinity brine to displace oil from them. Therefore, the observed additional recovery during low salinity flooding in each sample may be larger than would be expected in similar samples with a more realistic initial fluid distribution.

5.2.4 Fluid Mobilisation and Redistribution

To further investigate changes in pore occupancy, we isolated pores where pore occupancy changed between the high salinity waterflood and 20 PV of low salinity water flooding. In other words, we isolated pores where either brine displaced oil or oil displaced brine during 20 PV of low salinity water flooding. Figure 5.5 shows the size distribution of pores in which pore occupancy changed between the flow steps for each sample.

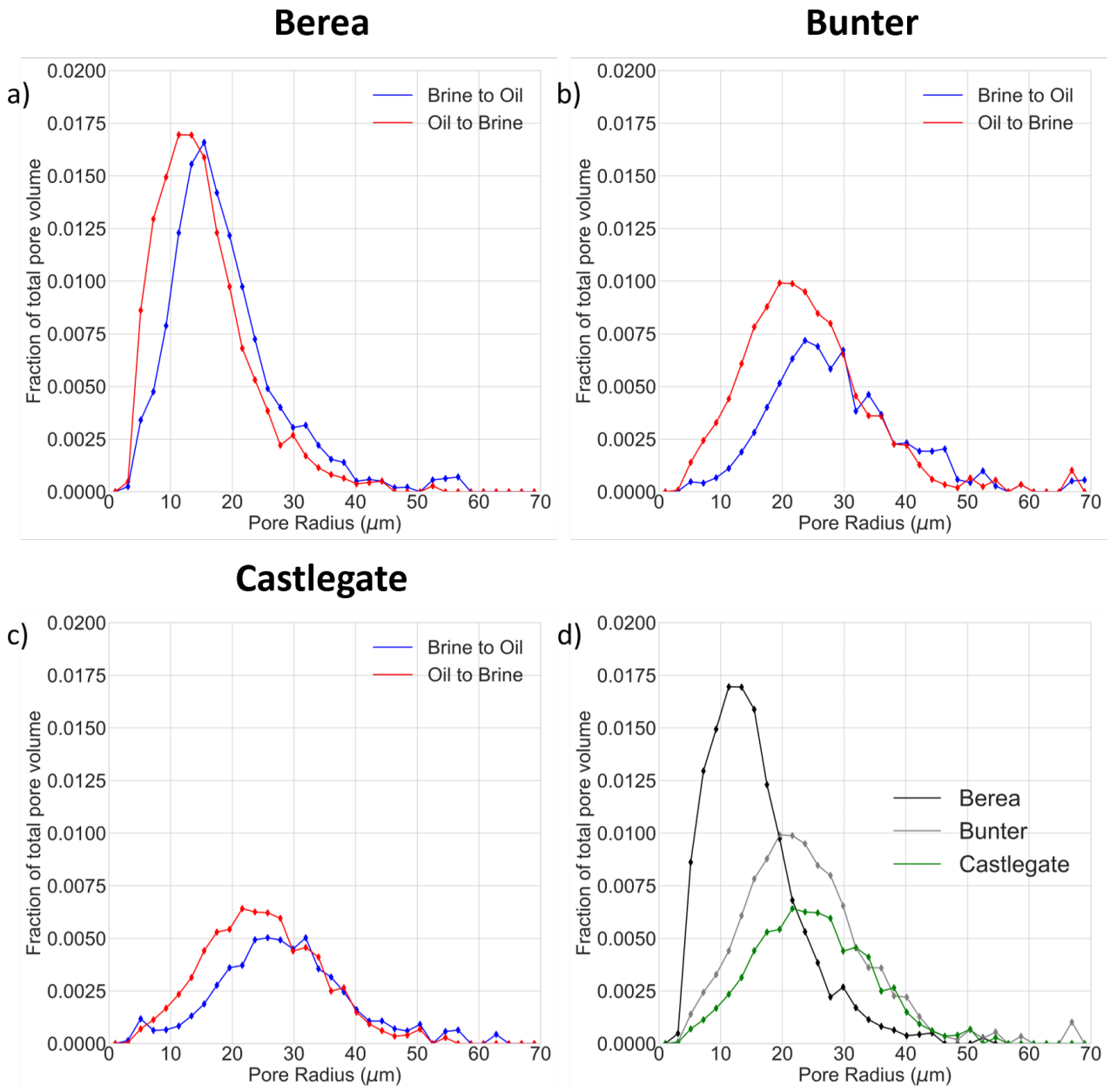


Figure 5.5: The size distribution for all pores (bodies and throats) where saturation changed from oil to brine (red) or brine to oil (blue) between HSWF and LSWF 20PV, for a) the Berea sample b) the Bunter sample c) the Castlegate sample d) oil to brine events in all samples. In all cases, there are more oil to brine events than brine to oil events in the medium and small pores. This effect is most significant in the Bunter sample. In the Berea sample, there are more brine to oil events than oil to brine events in the larger pores. This effect is not observed on the same scale in the Bunter and Castlegate samples. There are fewest oil to brine events in the Castlegate sample, indicative of less oil mobilisation during low salinity water flooding.

There is a significantly higher volume of oil to brine events in the small pores ($< 15\mu$m in the Berea, $< 30\mu$m in the Bunter) in the Berea sample than in the Bunter sample, which in turn has a significantly higher volume of oil to brine events than the Castlegate sample. This is most clear in Fig 5.5d which compares oil to brine events for each sample. Pores where an oil to brine event occurred account for 14% of Berea pore volume, 11% of Bunter pore volume, and 7% of Castlegate pore volume.

Despite fewer oil to brine events in the Bunter sandstone compared to the Berea, we have shown that the Bunter sandstone has the highest additional recovery after low salinity waterflooding (Table 5.2). This appears to be because in the Bunter sample a smaller percentage of the mobilised oil is re-trapped in the larger pores. In the Berea sample, for pores $> 15\mu$m radius, brine to oil events outweigh the oil to brine events, in other words there is a net increase in S_o in the largest pores in the Berea sample. This represents a redistribution of oil from smaller to larger pores in the Berea sample. This effect is not observed in either the Bunter or Castlegate samples.

As discussed in Chapter 3.3.6, it is important to note that pore occupancy analysis may systematically underestimate saturation changes. To more accurately assess the volume of mobilised and retrapped oil, we calculate the volume of oil that is mobilised after low salinity flooding, defined as the total fraction of oil displaced by brine after 20 PV of low salinity flooding. We compare this to bulk changes in saturation to calculate the fraction of the mobilised oil that is produced. Table 5.2 shows volumes of mobilised and produced oil for each sample after 20 PV of low salinity waterflooding. In the Berea and Bunter sandstones, we observe that similar fractions of the oil in place after high salinity flooding is mobilised during low salinity flooding, with values of 22% and 20%, respectively. In contrast, in the Castlegate sample, 11% of the oil in place after high salinity flooding is mobilised during low salinity waterflooding.

The difference in overall recovery between the Berea and Bunter samples is due to a significant difference in the fraction of mobilised oil that is produced. In the Berea, 20% of mobilised oil is produced, in the Bunter, 32% of the mobilised oil is produced. This results in a slightly higher recovery in the Bunter sandstone despite a slightly lower proportion of the oil in place after

Table 5.2: The fraction of the oil in place after high salinity water flooding that is mobilised during 20 PV of low salinity water flooding in the Berea, Bunter and Castlegate samples, and the fraction of this mobilised oil that is produced.

	Fraction of OOIP mobilised [-]	Fraction of mobilised oil produced [-]	Additional recovery [percentage points]
Berea	0.22	0.20	3
Bunter	0.20	0.32	4
Castlegate	0.11	0.13	1

high salinity flooding being mobilised during low salinity waterflooding. The pore occupancy plots give insight into why this is the case (figs 5.4 and 5.5). As described above, some of the oil displaced from the smallest pores in the Berea is re-trapped in the largest pores. This leads to a lower fraction of mobilised oil produced and hence a lower additional oil recovery after low salinity waterflooding. We do not observe this effect in the Bunter sample.

5.2.5 Linking Observations to Pore Geometry and Topology

There were different responses to low salinity flooding in each sample, despite similar mineralogy. It is likely that pore structure was the controlling factor in the varied responses. Pore structure has been shown to impact displacement mechanisms and flow regimes in various systems with aspect ratios, connectivity, pore radius distributions, coordination number, and pore-scale disorder controlling behaviour during both imbibition and drainage (*An et al.*, 2016; *Blunt*, 2017; *Holtzman*, 2016; *Singh et al.*, 2019; *Tanino and Blunt*, 2012; *Xu et al.*, 2014). However, the role of pore structure in facilitating additional recovery during low salinity flooding has yet to be investigated thoroughly. In this section, we present evidence to show the topology of the largest pores may be important in determining the volume of oil mobilisation and production during tertiary low salinity water flooding.

A notable difference in the pore structure of each sample is the connectivity of the largest pores. Figure 5.6 shows a volume rendering of the largest pores accounting for 60% of total pore volume in each sample. As discussed in chapter 3.3.6, we chose this cut-off as the minimum pore radius in this group approximately equates to the largest pores in which the oil saturation decreases during low salinity flooding in each sample. Additionally, the average S_w of pores

Table 5.3: Absolute permeability values calculated across all pores, and the network of largest pores in the Berea, Bunter and Castlegate samples. As discussed previously the 'largest pores' are those that comprise 60% of the pore volume

	Permeability [mD]	Permeability of largest pores [mD]
Berea	14	0
Bunter	142	0
Castlegate	495	27

within this group is > 0.5 for all samples after each waterflood. Therefore, the connectivity of these pores is likely to impact the connectivity of the brine in each sample. In figure 5.6, areas of the same colour represent connected network of pores. For example, in the Castlegate sample sample we observe a connected network of large pore which spans the region of interest. In the Berea sample, the large pores are poorly connected, with the largest connected cluster of large pores accounting for only 20% of the total volume of large pores in the Berea sample. In the Castlegate sample, the vast majority of the largest pores are connected across the region of interest, this connected pathway makes up 89% of the total volume of the largest pores in the castlegate sample. In the Bunter sample, there are two distinct behaviours, in the upstream section, the large pores are poorly connected, similar to the Berea sample, and in the downstream section there is a connected pathway of large pores, similar to the Castlegate sample. The largest connected cluster of large pores in the Bunter sample makes up 57% of the total volume of large pores and is located in the upper section of the sample. In both the Berea and Bunter samples the network of the largest pores do not connect across the region of interest, and so the permeability calculated across both networks is zero. In contrast, we calculate an absolute permeability value of $27mD$ across the network of the largest pores in the Castlegate samples (Table 5.3) using PNflow as described in section 3.3.6.

The connectivity of the largest pores in each sample controls the brine distribution and, therefore, the mobilisation or bypassing of oil during low salinity waterflooding. The largest brine blob in the Castlegate region of interest after high salinity waterflooding accounts for 60% of total brine volume, and connects in a continuous pathway across the region of interest (Figure 5.7). This is probably a result of the well connected large pores in the Castlegate sample, that allow for a well established, stable pathway for brine to flow across the region of interest (fig.

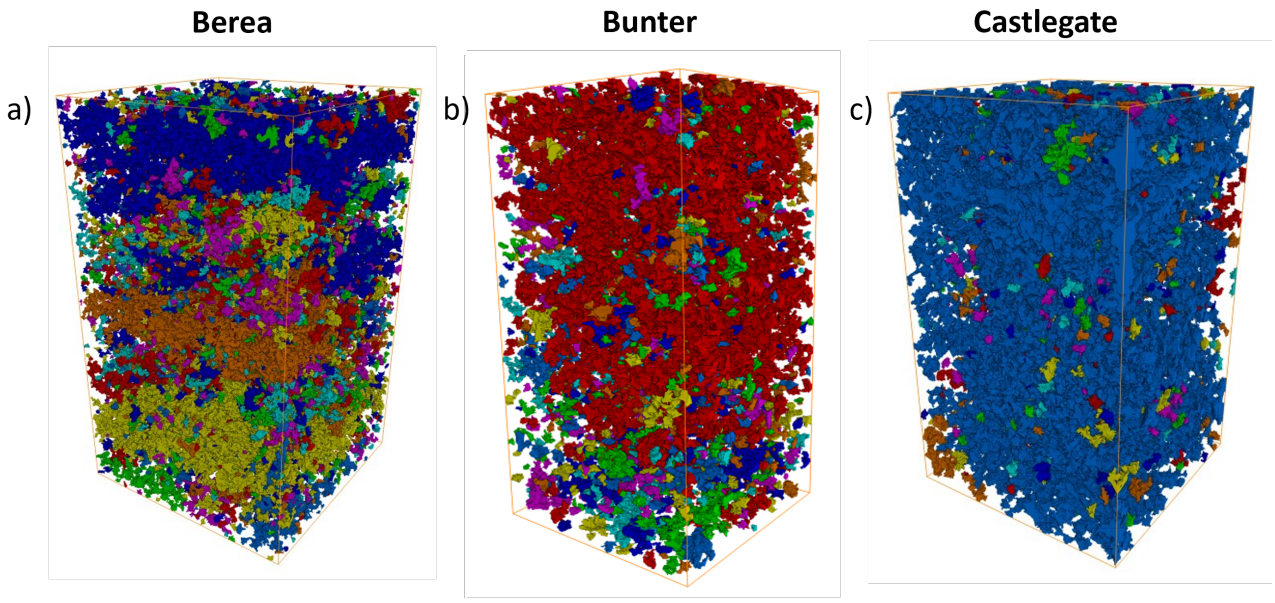


Figure 5.6: Volume rendering of largest pores accounting for 60% of pore volume for a)Berea b) Bunter c) Castlegate Each colour represents a separate disconnected region of pores. The Castlegate sample has the most connected large pores with the majority of the pores connected in a single pathway across the region of interest. The Berea and Bunter samples have much poorer connectivity across the largest pores. This is also reflected in the permeability values presented in table 5.3

5.7). During subsequent low salinity flooding, brine can flow across the preexisting connected pathway of brine, bypassing oil. As a result, it is not favourable for capillary trapped oil to be mobilised during low salinity flooding in the Castlegate sample (*Chen et al.*, 2021; *Gandomkar and Rahimpour*, 2015; *Pinerez Torrijos et al.*, 2016; *Winoto et al.*, 2012; *Zhang and Morrow*, 2006). In contrast, in the Berea and Bunter samples, there is no connectivity across the region of interests in the brine phase after high salinity waterflooding. Due to a poorly connected network of large pores, brine must invade smaller pores and throats to connect across the samples during high salinity waterflooding. These smaller pores and throats are susceptible to subsequent oil invasion via both distal and local oil snap off events - which have been observed in previous experiments to disconnect brine clusters (*Alhosani et al.*, 2020; *Berg et al.*, 2013; *Blunt*, 2017; *Roof*, 1970). As a result, during low salinity flooding, brine must invade oil-saturated pores and throats to connect across the Berea and Bunter samples. In the Berea and Bunter samples, the tertiary low salinity waterflood behaves somewhat more like a secondary low salinity waterflood as there is no existing brine pathway for low salinity brine to follow and so, it is more favourable for capillary trapped oil to be displaced by invading low salinity

brine (*Chen et al.*, 2021). This effect, coupled with a wettability alteration (fig. 5.3), which can occur when low salinity brine contacts oil saturated pores and oil coated mineral surfaces, makes oil mobilisation and production more favourable in the Berea and Bunter samples. In the Berea and Bunter samples 22% and 20% of the oil in place after high salinity waterflooding is displaced during low salinity flooding, respectively. In the Castlegate sample, this figure is just 11% (Table 5.2). The connectivity of large pores appears to control brine distribution during and after secondary high salinity waterflooding, which in turn controls oil mobilisation and production during subsequent tertiary low salinity waterflooding.

This effect of pore topology also explains the varying degrees of oil mobilisation in different parts of the Bunter sample. The sample can be split into two discrete sections: the downstream (upper) section, where larger pores are well connected, and the upstream (lower) section, where larger pores are poorly connected. The boundary between these two sections is closely matched by a change in additional recovery after low salinity waterflooding as observed in the saturation profile (Fig 5.8). In the downstream section, where large pores are well connected, there is an additional recovery of 1 percentage point after 20 PV of low salinity flooding. In contrast, in the upstream section, there is an additional recovery of 6 percentage points. The three largest brine blobs after both high salinity and low salinity waterflooding are observed in the downstream section of the region of interest. These differences are probably due to the different pore structures observed. In the downstream section, well connected large pores allow for the creation of more stable brine pathways during high salinity flooding and therefore relatively small volumes of oil mobilisation during subsequent low salinity flooding. Conversely, in the upstream section, poorly connected large pores decrease brine connectivity after high salinity flooding and, therefore, increase oil mobilisation during low salinity flooding. Indeed, we observe that the difference in additional oil recovery between the two sections is because of differences in the volume of oil mobilisation during low salinity flooding. There are significantly fewer oil to brine events in the downstream section compared to the upstream section (Figure 5.9). Pores which changed from oil occupied to brine occupied during 20 PV of low salinity flooding make up 14% of the total pore volume in upstream section and 10% of total pore volume in downstream section. The evidence from local differences in pore topology and production in

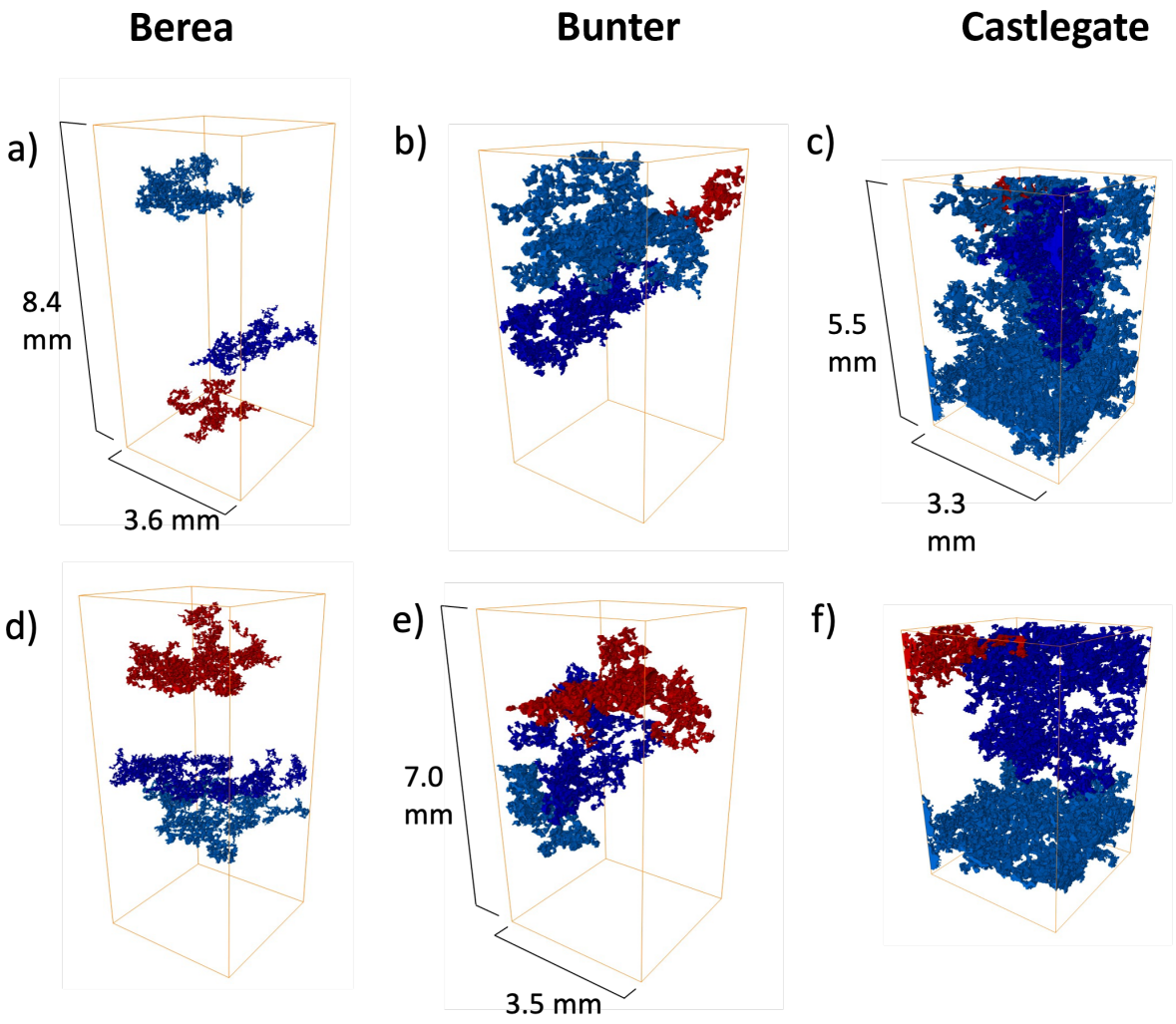


Figure 5.7: Volume rendering of the three largest brine blobs after high salinity water flooding for a) Berea b) Bunter c) Castlegate and after 20 PV of low salinity waterflooding for d) Berea e) Bunter f) Castlegate. In the Berea and Bunter samples there is no connected cluster of brine across the region of interest after either HSWF 12PV or LSWF 20PV. In the Castlegate sample there is a connected pathway of brine across the region of interest after HSWF 12PV, this is broken up after LSWF 20PV, but Castlegate still has the largest brine clusters.

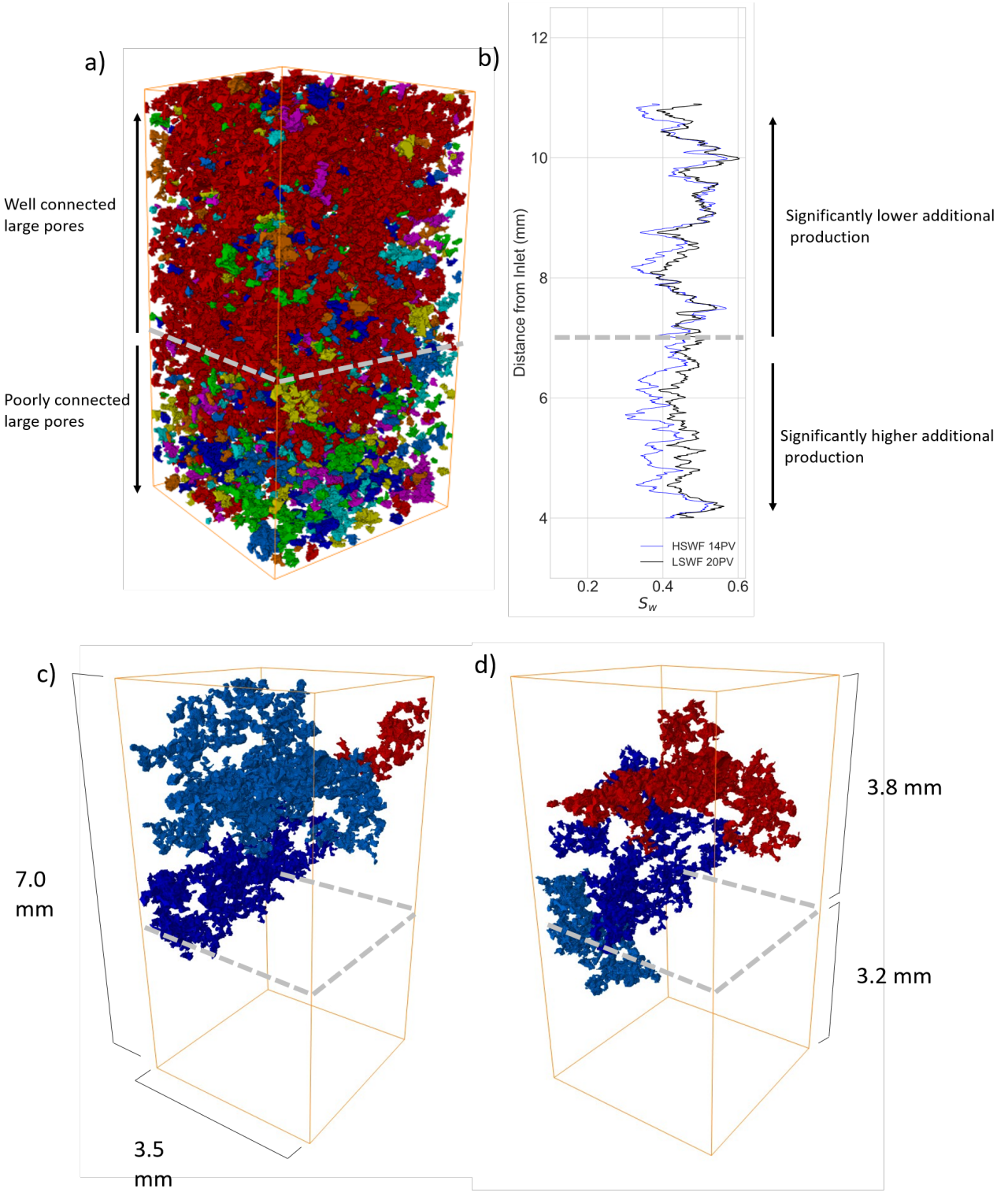


Figure 5.8: a) Volume rendering of the largest pores which make up 60% of the pore space in the Bunter sandstone. Different colours represent disconnected clusters of large pores. b) Saturation profile for the Bunter sandstone c) Volume rendering of the largest 3 brine blobs after 12PV of high salinity flooding in the Bunter sandstone and d) Volume rendering of the largest 3 brine blobs after 20PV of low salinity flooding in the Bunter sandstone. The sample can be broadly be split into two halves (denoted by the grey dotted line). In the downstream (upper) section, the largest pores are well connected, there is lower additional recovery after LSWF 20PV and all three of the largest brine blobs are present. In the upstream (lower) section, there is poor connectivity in the largest pores, and significantly higher additional recovery after LSWF 20PV

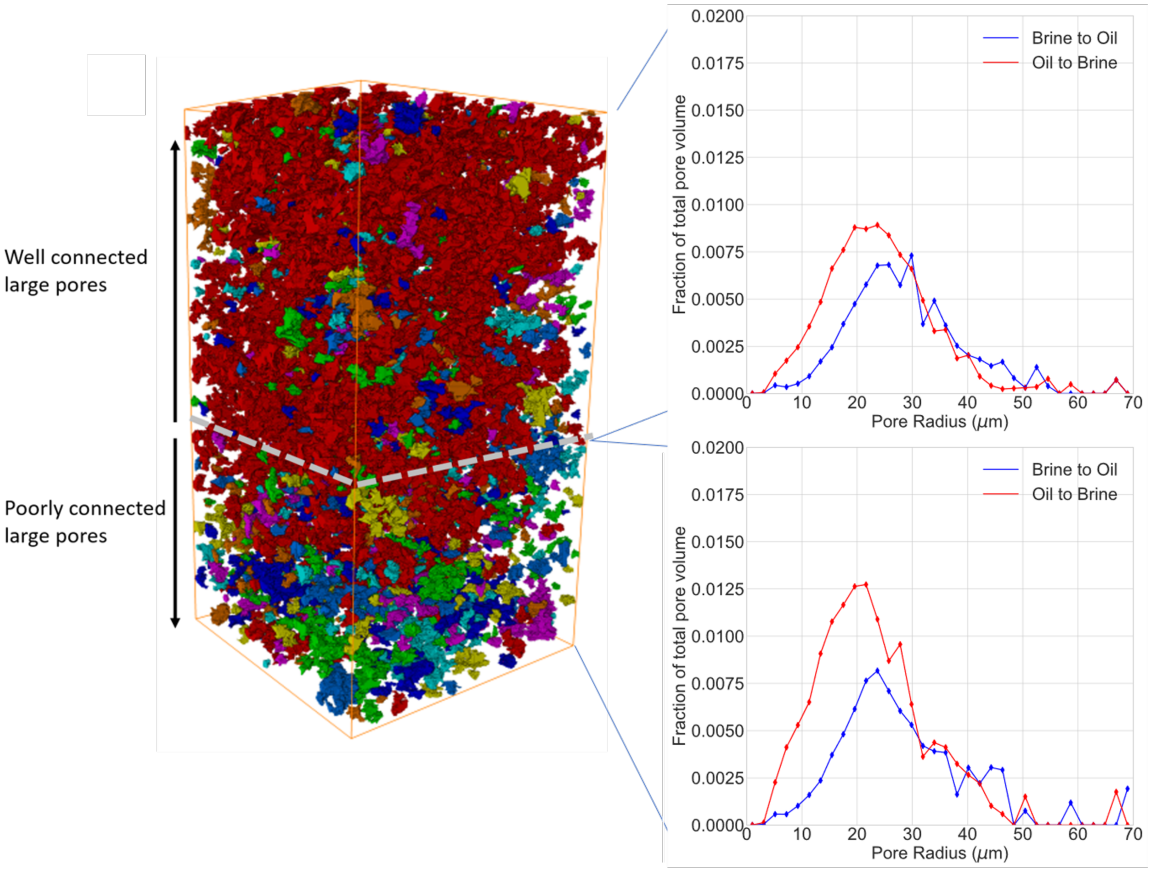


Figure 5.9: Volume rendering of largest pores that make up 60% of pore space in Bunter sandstone. The grey dotted lone marks the boundary between two sections - the upper (downstream) section where larger pores are well connected, and the lower (upstream) section where larger pores are poorly connected. For each section the size distribution for all pores (bodies and throats) where saturation changed from oil to brine (red) or brine to oil (blue) between HSWF and LSWF 20PV changes are plotted, is plotted for each section.

the Bunter sample further highlights the impact of pore structure on oil production during low salinity water flooding.

5.3 Conclusions

In this work, we present the first systematic comparison of pore scale behaviour during low salinity waterflooding in sandstones. We used X-ray micro-CT imaging to observe unsteady state tertiary low salinity waterflooding in Berea, Castlegate, and Bunter sandstone samples all of altered wetting state. Our main findings are as follows:

- Significant additional oil production of 3 and 4 percentage points occurred during low salinity flooding in the Berea and Bunter samples respectively. In contrast, we observe an additional recovery of only 1 percentage point during low salinity waterflooding in the Castlegate sample.

- There was a significant wettability alteration towards more water wet conditions in the Berea and Bunter samples, which responded well to low salinity waterflooding. This wettability alteration led to significant pore occupancy changes in the Berea and Bunter samples, with significant increase in S_w in smaller pores during low salinity waterflooding. There was no systematic wettability alteration observed in the Castlegate sample. We observe a similar yet smaller shift in pore occupancy in the Castlegate sample.

- There were different volumes of oil mobilisation during low salinity flooding in each sample. In the Berea 22% of the oil in place after high salinity flooding was mobilised during low salinity water flooding, this value was 20% and 11% for the Bunter and Castlegate samples respectively. In the Berea, a significant proportion of this mobilised oil was retrapped in the largest pores, so that, the additional recovery was higher in the Bunter sandstone despite having a lower fraction of mobilised oil during low salinity water flooding.

- We hypothesise that pore structure, and in particular the topology of the largest pores, had a significant impact on recovery in each of the samples. In the Castlegate sample, the largest pores are well connected across the sample resulting in a stable, connected pathway of brine across the largest pores during high salinity waterflooding, which makes oil mobilisation unfavourable during subsequent low salinity flooding. In the Berea and Bunter sandstone, the largest pores are more poorly connected. We hypothesise that in the Berea and Bunter samples, during high salinity water flooding, brine is forced to flow into the small pores and throats during waterflooding, distal and local oil snap off events then break up the brine clusters. During low salinity waterflooding there is no established path for the brine to follow, and so oil mobilisation is more favourable.

Pore structure played an important role in the low salinity response in each sample. Here we have proposed that pore topology can impact the volume of oil mobilisation during tertiary low salinity waterflooding. This, however, does not explain other phenomena, for example, the re-trapping of oil in the largest pores of the Berea sample. There is a complex relationship between pore structure and production. This work acts to highlight this point and offer the first insights into this relationship. Future work should further investigate the relationship between pore structure and recovery, with the ultimate goal of including pore structure in any exhaustive list of necessary conditions for successful low salinity water flooding.

Chapter 6

The Impact of Sandstone Mineralogy on Low Salinity Water flooding

6.1 Objectives

So far, we have shown that wetting state and pore structure are important in determining fluid displacement and oil recovery during low salinity waterflooding. We have not yet examined how mineralogy can interact with these properties to impact production. There is general agreement that clays are necessary for favourable recovery during low salinity water flooding in sandstones. This belief is based largely on measurements of saturation and capillary pressure during core scale experiments on a range sandstone samples, and sub-pore scale observations of oil detachment from clays on artificial surfaces within flow cells. However, there is a growing body of literature which suggests that clays are likely not required for a favourable low salinity response, and there have not yet been any in situ pore scale observations of oil detachment from clay in the presence of low salinity brine.

In this chapter, we carry out further analysis of the experimental datasets presented in Chapter 5. We implement mineral specific surface area fractional coverage analysis to give the first pore scale in situ measurements of mineral specific wettability during low salinity flooding. Building upon chapter 5, we also assess how mineralogy interacts with pore structure to impact

production during low salinity waterflooding. This work offers unique insights into the role of clays during low salinity flooding and casts further doubt on the belief that clays are essential for a favourable low salinity response in sandstones.

6.2 Pore Scale Observations

6.2.1 Clay distribution

As shown in Table 3.1, all 3 samples have a significant clay fraction (fig 6.1), with clay volume fractions of 6%, 6% and 8% for Berea, Bunter, and Castlegate samples respectively. However, the percentage of the pore volume made up of clay-rich pores differs significantly between each sample. Clay-rich pores make up 7% of total pore volume in the Berea sample, 14% of pore volume in the Bunter sample, and 4% of total pore volume in the Castlegate sample. Figure 6.2 shows the fraction of pores in each sample that are clay-rich ($> 50\%$ clay coverage) for different pore radii (see Chapter 3.3.6 for method). In all samples, smaller pores are preferentially clay-rich where $> 50\%$ of pores with radius $< 7\mu m$ are clay-rich in each sample. In all samples, large pores are preferentially clay-poor, this is most pronounced in the Berea and Castlegate samples, where $< 5\%$ of pores with radius $> 15\mu m$ are clay-rich. In the Bunter sample, the smallest pores are also more likely to be clay-rich, with $> 60\%$ of the smallest pores being clay-rich. In contrast with the other two samples, a significant fraction, specifically 15% of pores $> 35\mu m$ radius are clay-rich in the Bunter sample.

6.2.2 Mineral-Specific Surface Area Fractional Coverage

Figure 6.3 shows mineral-specific surface area fractional coverage values for all three samples after 12 PV of high salinity water flooding and then after 20 PV of low salinity water flooding. In each sample, the $A_{fo}(S_o)$ values for clay are distinct from that of the other minerals for all flow steps. For a given S_o, we observe that the fraction of clay surfaces coated by oil is significantly higher than the fraction of non-clay mineral surfaces coated by oil. These results

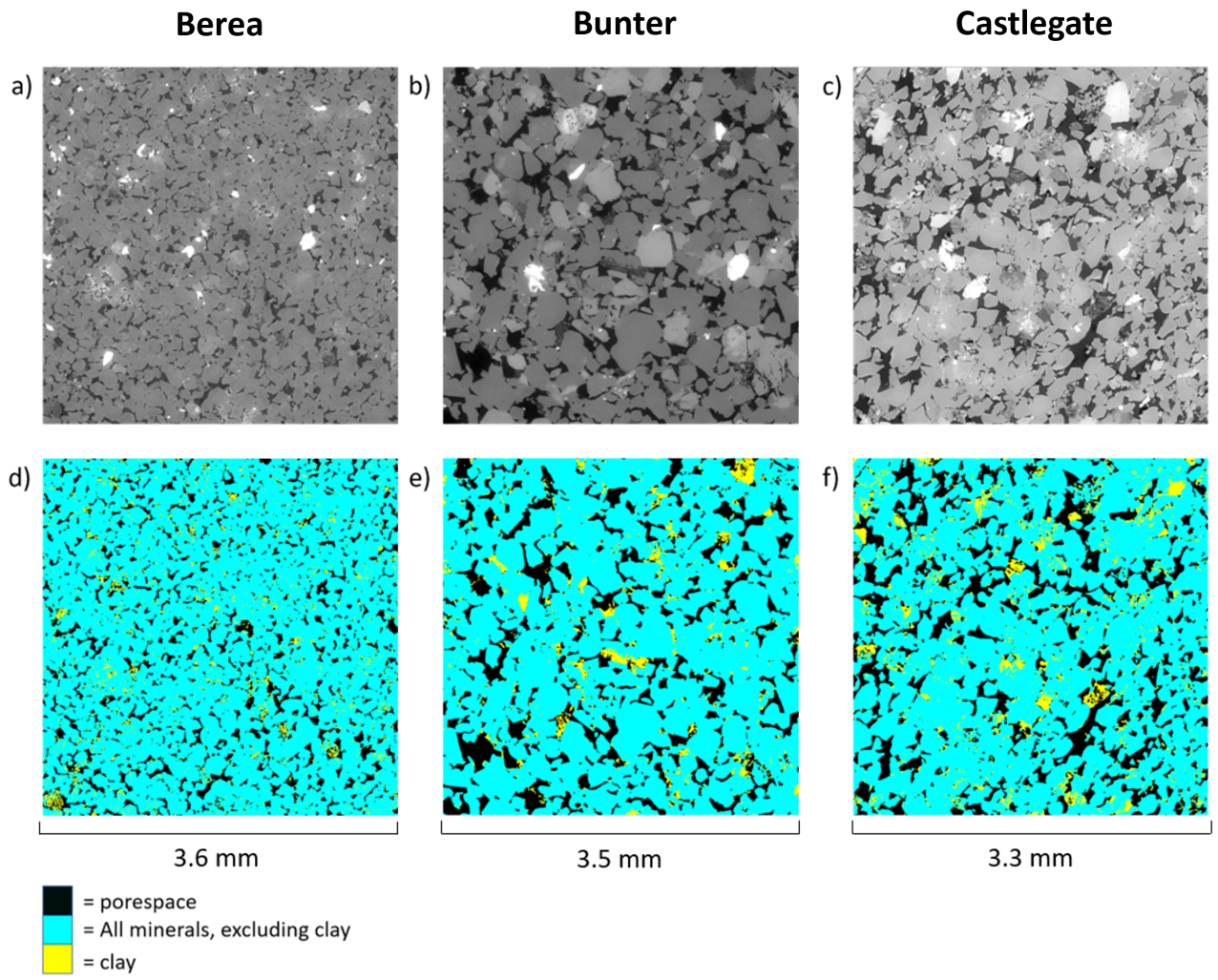


Figure 6.1: A slice of the X-ray micro-CT image of the a) Berea sample b) Castlegate sample and c) Bunter sample, before the injection of doped oil. In each case the darkest colour represents the pore space. In each case, the bright spots represent small quantities of highly attenuating metallic minerals. The corresponding slices for the segmented images of the d) Berea sample, e) Castlegate sample, and f) Bunter sample are also shown, where black represents the pore space, yellow represents clay minerals, and blue represents non-clay minerals.

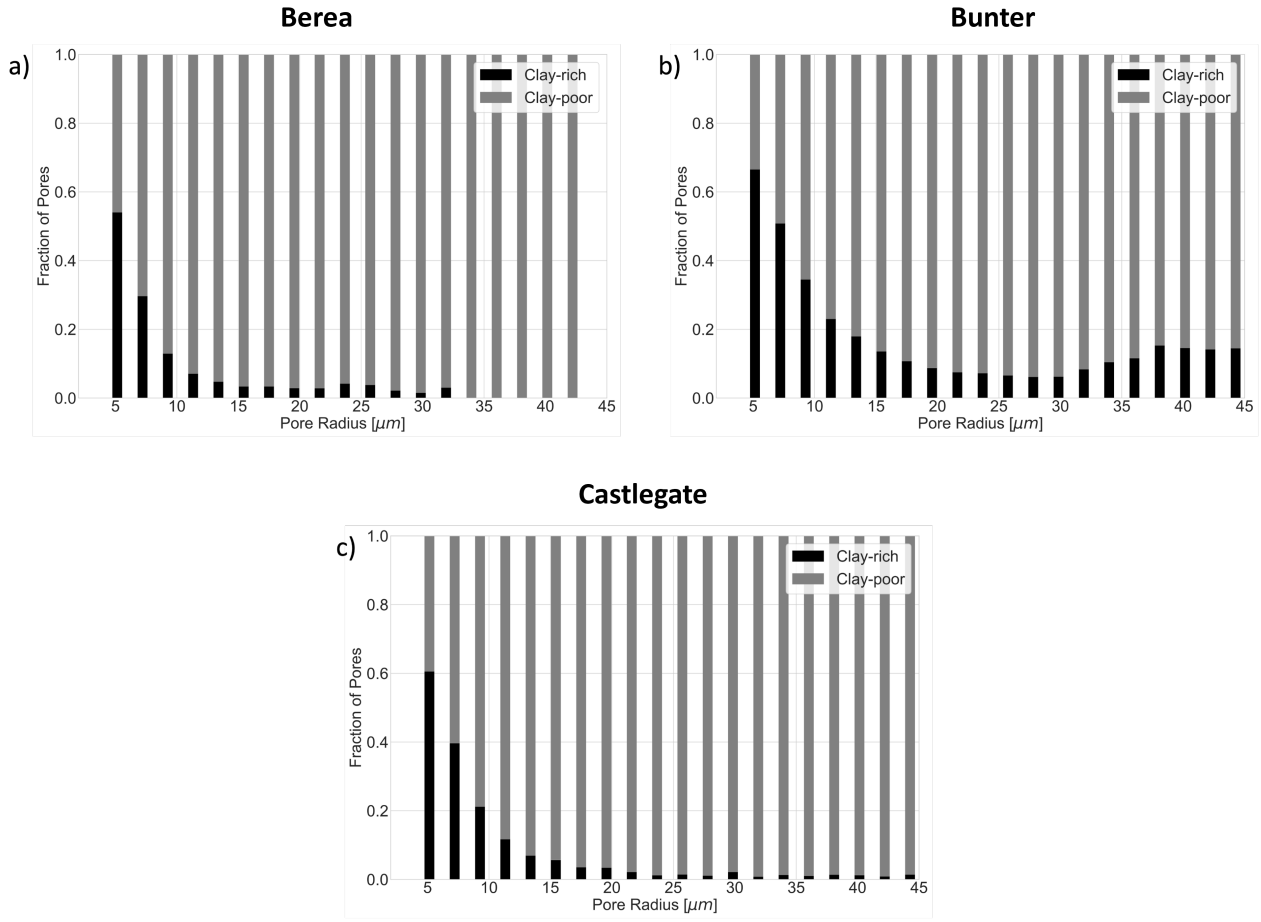


Figure 6.2: The fraction of clay-rich ($>$ 50%clay coverage) pores in different radii bins for a)Berea b) Bunter c) Castlegate samples. In each case, the smaller pores are preferentially clay-rich. In the Berea and Castlegate samples there are very few clay-rich large pores ($> 15\mu m$). In contrast, in the Bunter sample, a larger fraction of larger pores are clay-rich, approximately 15% of pores ($> 35\mu m$) are clay-rich. Clay-rich pores make up 7% of total pore volume in the Berea sample, 14% of pore volume in the Bunter sample, and 4% of total pore volume in the Castlegate sample.

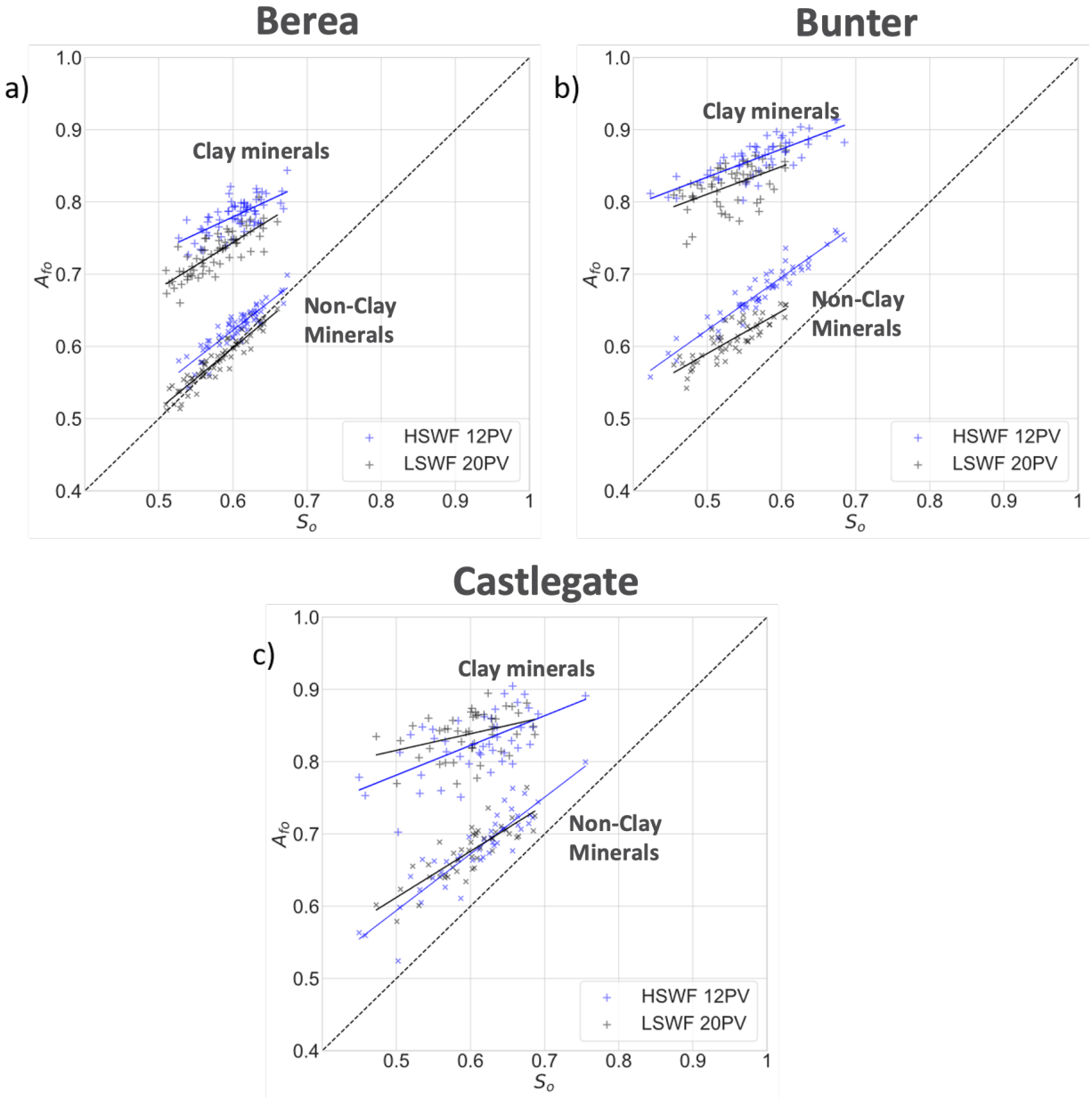


Figure 6.3: mineral-specific oil-coated area fractions, imaged after high salinity water flooding (HSWF), 4 PV of low salinity flooding (LSWF 4PV), and 20 PV of low salinity flooding (LSWF 20PV), for a) Berea b) Castlegate and c) Bunter. For each sample $A_{fo}(S_o)$ values are plotted for both clay surfaces and the surfaces of non-clay minerals. In each case $A_{fo}(S_o)$ values are greater for clays than non-clay minerals. There is a significant decrease in $A_{fo}(S_o)$ values for both mineral groups after LSWF 4PV in the Berea and Bunter samples. After LSWF 20PV there is no significant change in $A_{fo}(S_o)$ values in either the Berea or Bunter samples relative to the state at LSWF 4PV, but there is a significant change to lower S_o values. In the Castlegate sample, there is no clear shift in $A_{fo}(S_o)$ values for either mineral group after either LSWF 4PV or LSWF 20PV. As discussed in chapter 4, we calculate a standard error for the A_{fo} measurements 0f 0.00118.

show that clays are more oil-wetting than non-clay minerals in all three samples. This finding is consistent with observations by *Garfi et al.* (2020a), who reported higher fractional oil coverage on clays than for quartz and feldspar within a Berea sample of altered wettability, and *Tabrizy et al.* (2011) who found powdered kaolonite to be more prone to wettability alteration during exposure to crude oil than quartz and feldspar. Whilst clay-minerals are more oil-wetting than non-clay minerals for all samples, there are significant differences in the wetting state of clay-minerals between the three samples. $A_{fo}(S_o)$ values for clay minerals are lower in the Berea sample than for Bunter and Castlegate samples, this is indicative of less oil-wetting behaviour. This difference may be due to subtle differences in clay mineralogy, pore structure or the distribution of clays throughout the samples. The potential relationships between pore structure, clay distribution, wetting state and additional recovery during low salinity flooding are discussed further in section 6.2.4.

We observe that $A_{fo}(S_o)$ values for both mineral groups are lower in the Berea sample than for the Bunter and Castlegate samples after either waterflood. This suggests that both mineral groups in the Berea sample are initially less oil wetting than in the Bunter and Castlegate samples. In the Berea sample, after 20 PV of tertiary low salinity flooding there is a shift to lower $A_{fo}(S_o)$ values in both mineral groups, so that for a given S_o there is a lower fraction of oil coating the mineral surfaces. This behaviour is most significant for clay minerals. This indicates a shift to more water-wet conditions in both mineral groups with a more pronounced shift in clay minerals. In the Bunter sandstone, there is a significant shift to lower $A_{fo}(S_o)$ values in both mineral groups after 20 PV of tertiary low salinity flooding (LSWF 20PV). This wettability alteration in the Bunter sample is greater on non-clay minerals than for clay minerals. In the Castlegate sample, there is no significant shift in $A_{fo}(S_o)$ values in either mineral group after 20 PV of low salinity water flooding. This indicates no pervasive and systematic wettability alteration during low salinity waterflooding within the Castlegate sample. As discussed in chapter 4, we calculate a standard error for the A_{fo} measurements 0f 0.00118. The changes in A_{fo} during low salinity flooding for both mineral groups in both the Berea and Bunter samples are an order of magnitude greater than the standard error.

Observations of wettability alteration during low salinity flooding in the Berea and Bunter

sandstone samples are broadly consistent with a wealth of observations of wettability alteration during low salinity waterflooding across a range of scales (*Berg et al.*, 2010; *Cense et al.*, 2011; *Chen et al.*, 2020; *Khishvand et al.*, 2017; *Mahani et al.*, 2015b; *Nasralla et al.*, 2013; *Shabaninejad et al.*, 2018; *Vledder et al.*, 2010; *Yesufu-Rufai et al.*, 2020). More specifically, observations of wettability alteration on clay minerals in the Berea sample, and to a lesser extent, the Bunter sample are consistent with several studies using flow cells to observe oil detachment on clay basal planes (*Berg et al.*, 2010; *Nasralla et al.*, 2013), the detachment of oil droplets from clays deposited on a glass substrate (*Cense et al.*, 2011; *Mahani et al.*, 2015b), and in-situ observations of oil detachment from clays in the presence of low salinity brine using Atomic Force Microscopy (*Yesufu-Rufai et al.*, 2020). Observations of wettability alteration on non-clay minerals in the Berea and Bunter sandstone samples agree with a growing body of research that suggests that significant wettability alteration can occur on quartz and feldspar grains during low salinity flooding. (*Al-Saedi et al.*, 2019a,b; *Bartels et al.*, 2017b; *Liu et al.*, 2018; *Shabaninejad et al.*, 2018).

6.2.3 Pore Occupancy

To understand the effect of any wetting alteration on fluid distribution throughout each sample and further understand the role of mineralogy in the low salinity response, we next assess pore occupancy. In Chapter 5, we presented pore occupancy analysis for all pores within the region of interest of each sample. Here, we extend that analysis by observing mineral-specific pore occupancy - analysing the pore occupancy of clay-rich pores ($> 50\%$ clay coverage) and clay-poor pores ($< 50\%$clay coverage) separately. This allows for the role of clays in pore occupancy changes to be investigated.

Figure 6.4 shows S_w values for clay-rich and clay-poor pores of a range of radii for all three samples. In all cases, clay-rich pores have lower S_w values than clay-poor pores across all pore radii after high salinity waterflooding. There is a shift to higher S_w values in the smallest clay-poor pores of each sample during low salinity waterflooding. This effect is largest in the Bunter and Berea samples. However, there is a small but systematic increase in S_w values in

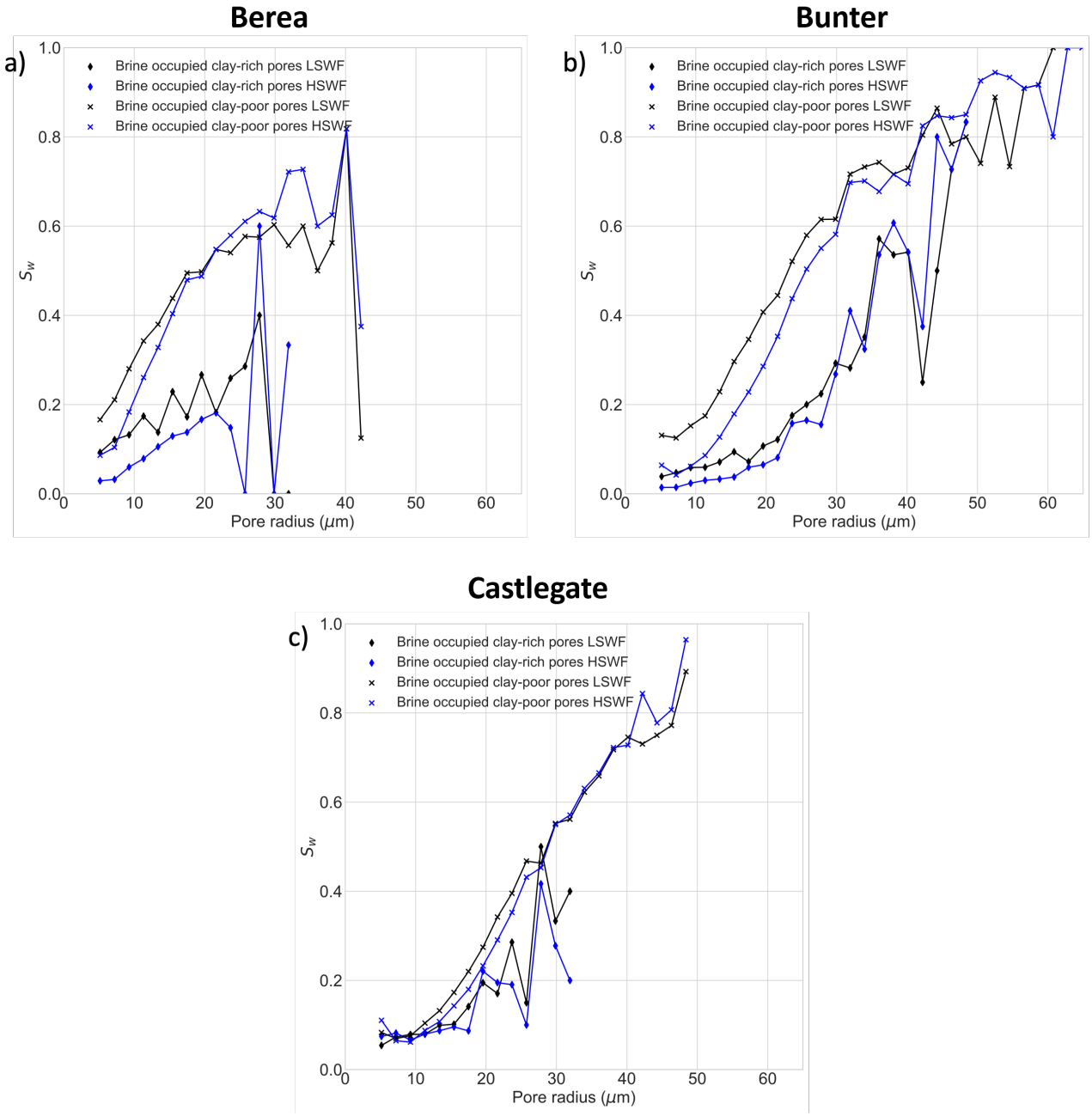


Figure 6.4: The total brine saturation (S_w) in pore radii bins for clay-poor ($< 50\%$ clay coverage) and clay-rich pores ($> 50\%$ clay coverage) in the a) Berea b) Bunter c) Bunter samples, imaged after 12 PV of high salinity water flooding (HSWF 12PV) and 20 PV of low salinity flooding (LSWF 20PV). In all samples, there is an increase in S_w in small clay-poor pores, this is most significant in the Berea and Bunter samples. In the Berea sample, the largest shift in S_w is observed in small and medium sized clay-rich pores (pore radius¡25μm). For the Bunter and Castlegate samples, S_w increases in small pores during low salinity flooding is greater in clay-poor pores than in clay-rich pores

the smallest Castlegate clay-poor pores. In clay-rich pores, there is a significant increase in S_w across a large range of pore sizes in the Berea sample. In the Castlegate and Bunter samples, there are smaller shifts in S_w values in clay-rich pores during low salinity flooding.

We observe that clay-poor pores account for the vast majority of oil displacement events following low salinity waterflooding in each sample. Figure 6.5 shows pore occupancy of clay-poor and clay-rich pores in each sample for a range of pore radii as a fraction of total pore volume. There is a significant increase in brine saturation in the smallest clay-poor pores for each sample (pore radius $< 18\mu m$ in the Berea sample, $< 30\mu m$ in the Bunter sample, and $< 28\mu m$ in the Castlegate sample). This effect is largest in the Berea and Bunter samples. Observations of pore occupancy changes in small and medium pores during low salinity flooding are consistent with a range of studies. Experimental studies across both sandstones and carbonates (*Bartels et al.*, 2017a; *Khishvand et al.*, 2017; *Selem et al.*, 2021) and modelling studies (*Aziz et al.*, 2019) observe that brine saturation increases in the smallest pores during low salinity water flooding. This effect is thought to be the result of a wettability alteration to more water-wetting conditions. The alteration allows water to more-easily enter smaller pores and throats because of the support of capillary forces (*Aziz et al.*, 2019; *Bartels et al.*, 2017a).

To more clearly present changes in pore occupancy, we isolate clay-rich and clay-poor pores where pore occupancy changed between the high salinity waterflood and 20 PV of low salinity water flooding. Figure 6.6 shows the size distribution of pores in which pore occupancy changed between the flow steps for each sample.

We observe significantly more oil-to-brine events (pores where brine displaced oil during low salinity flooding) in clay-poor pores than in clay-rich pores for all samples. This effect is most significant in the Bunter and Castlegate samples. In each sample, oil-to-brine events outweigh brine-to-oil events (pores where oil displaced brine during low salinity flooding) in small and medium clay-poor pores, indicating the net production of oil from these pores. The signal in clay-rich pores is less consistent. In the Berea sample, oil-to-brine events far outweigh brine-to-oil events for clay-rich pores of radius $< 25\mu m$, with three times more oil-to-brine events than brine-to-oil events for $5 <$ pore radius $< 12\mu m$. In the Castlegate sample, there are very few

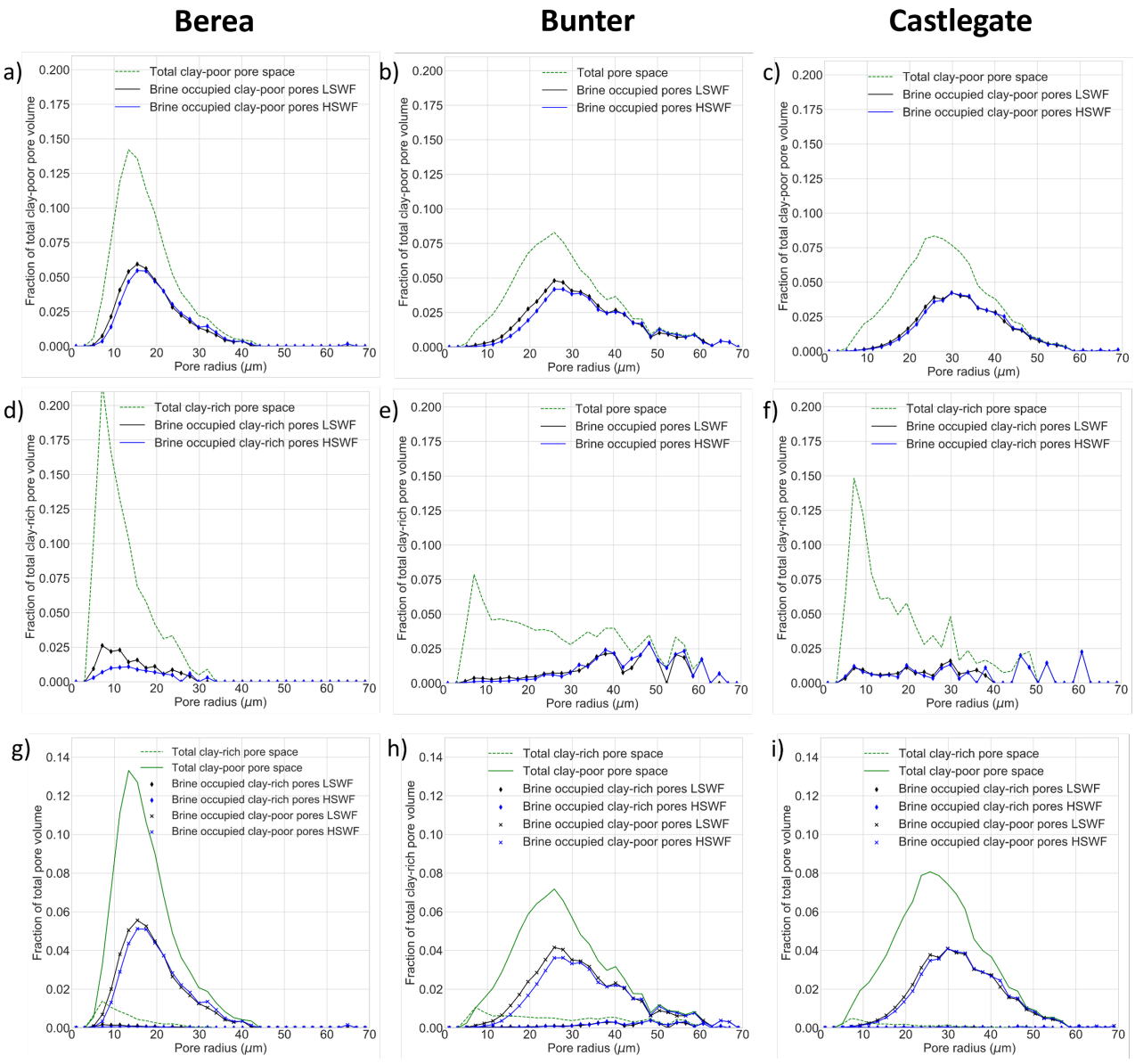


Figure 6.5: The size distribution for all brine saturated clay-poor pores (bodies and throats) in the a) Berea b) Bunter c) Castlegate samples, and the size distribution for all brine saturated clay-rich pores (bodies and throats) in the d) Berea e) Bunter f) Castlegate samples after high salinity water flooding (HSWF) and low salinity flooding (LSWF). A comparison of the size distribution for all brine saturated clay-poor and clay-rich pores is presented for g) Berea, h) Bunter and i) Castlegate. In all samples, there is an increase in brine volume in the small and medium clay-poor pores after LSWF, this is most significant in the Berea and Bunter samples. There is also an increase in brine volume in the small and medium clay-rich pores in the Berea and Bunter samples. In all cases clay-poor pores are more abundant than clay-rich pores account for the majority of total pore occupancy changes by volume.

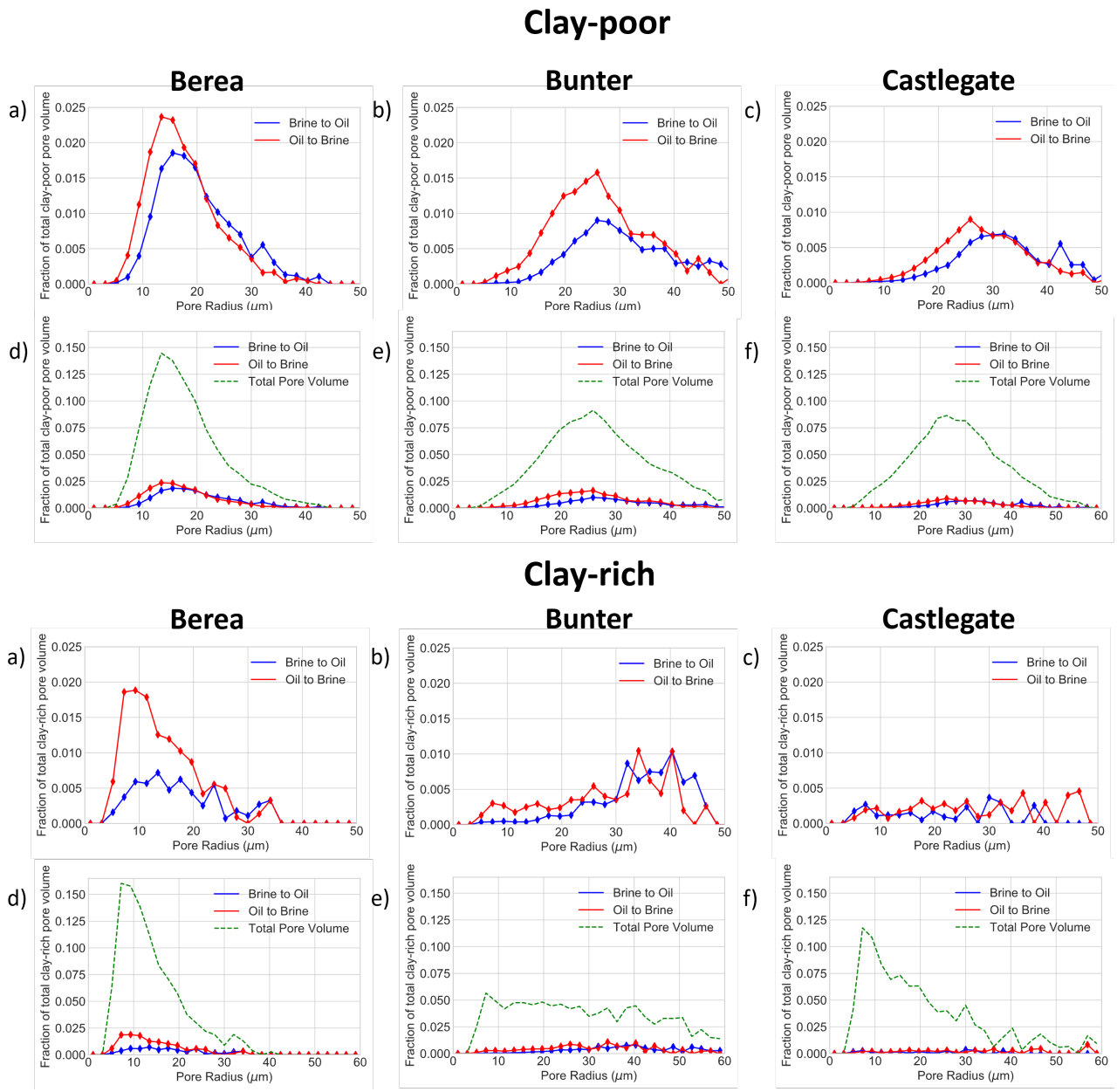


Figure 6.6: The size distribution for all clay-poor pores where saturation changed from oil to brine (red) or brine to oil (blue) between HSWF and LSWF 20PV, for a) the Berea sample b) the Castlegate sample c) the Bunter sample, and the size distribution for all clay-rich pores where saturation changed from oil to brine (red) or brine to oil (blue) between HSWF and LSWF 20PV, for d) the Berea sample e) the Castlegate sample f) the Bunter sample. In all cases, there are more oil to brine events than brine to oil events in the medium and small clay-pore pores. There are fewer oil-mobilisation event clay-poor pores

redistribution events in the clay-rich pores during low salinity flooding. A similar response is observed in the Bunter sample, but with a small increase in oil-to-brine and brine-to-oil events for larger clay-rich pores.

For clay-rich pores in the Berea sample, there is a large increase in brine saturation in small pores with the fraction of pores of radius $< 12\mu m$ occupied by brine more than doubling during low salinity flooding. In contrast, in the Bunter and Castlegate samples there is are far smaller changes in pore occupancy in clay-rich pores across all pore radii. In both samples, the relative pore occupancy changes in clay-poor pores are significantly greater than in clay-rich pores. When coupled with the fact that clay-rich pores only account for a small fraction of total pore space in each sample, it is clear that oil production from clay-rich pores in the Bunter and Castlegate samples is very small. This is clear in Figure 6.5g, 6.5h, and 6.5i which show the relative importance of pore occupancy changes in pores of each mineral group. We can analyse this affect quantitatively (Fig 6.7). In the Berea sample, clay-rich pores make up 7% of pore volume and account for 15% of the total additional recovery during low salinity flooding. In the Bunter sample clay rich pores make up 14% of total pore volume and account for 5% of the total additional recovery during low salinity flooding. In the Castlegate sample, clay rich pores make up 4% of total pore volume and account for 3% of the total additional recovery during low salinity flooding. Even in the Berea sample, where there is a pronounced wettability alteration on clay minerals and significant pore occupancy changes in clay-rich pores, the majority of oil production occurs from clay-poor regions of the pore space.

In Figure 6.5, we observe that brine saturation in clay-rich pores is low for all samples. To quantitatively assess this signal, we record S_o values for all clay-rich and clay-poor pores (table 6.1). For all samples, clay-rich pores have a significantly higher S_o than clay-poor pores after both high salinity flooding and low salinity flooding. This effect is most prominent in the Berea and Castlegate samples, with S_o in clay-rich pores > 20 percentage points higher than in clay-poor pores after both high and low salinity flooding for both samples. In the Bunter sample, probably because a larger fraction of large pores are clay-rich (fig 6.2), S_o values in clay-rich pores are lower than for the other two samples. However, S_o values are still significantly higher in clay-rich pores than in clay-poor pores, with a difference of 16 and 18 percentage points

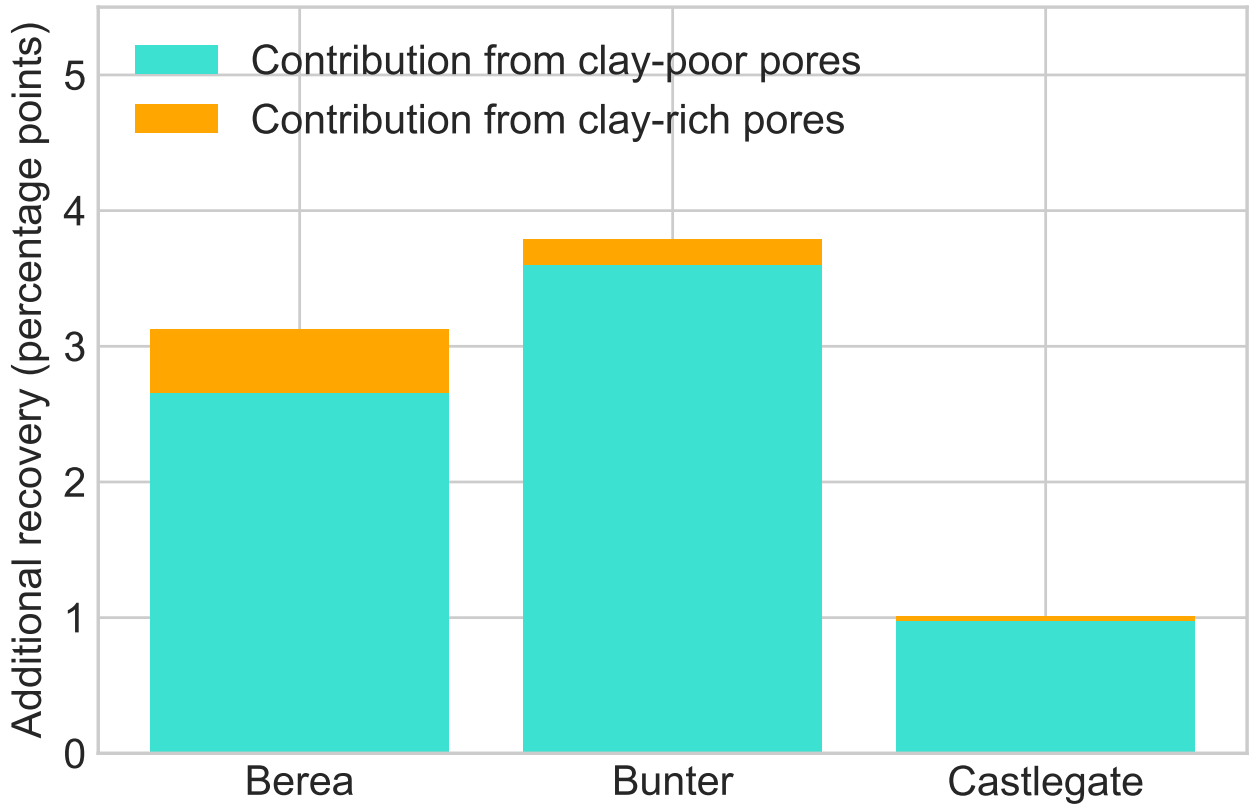


Figure 6.7: Bar chart showing the contribution of clay-rich and clay-poor pores to additional recovery during low salinity flooding in each sample. Clay-rich pores account for 15% of additional production in the Berea sample, 5% of additional production in the Bunter sample, and 3% of additional production in the Castlegate sample. Therefore, in all samples, clay-poor pores account for the majority of oil production.

Table 6.1: S_o values for clay-poor pores (< 50% clay coverage), clay-rich pores (> 50% clay coverage) and very clay-rich pores (> 90% clay coverage) for all samples after both high salinity water flooding and low salinity waterflooding. In all cases there are significantly higher S_o values in clay-rich pores than clay-poor pores.

	Clay-poor pores		Clay-rich pores		Very Clay-rich pores	
	S_o HSWF	S_o LSWF	S_o HSWF	S_o LSWF	S_o HSWF	S_o LSWF
Berea	0.60	0.57	0.89	0.82	0.98	0.93
Bunter	0.55	0.50	0.73	0.72	0.96	0.96
Castlegate	0.57	0.56	0.80	0.79	0.97	0.96

after high and low salinity flooding, respectively. The higher S_o values in clay-rich pores in all samples are to be expected as we have shown that clays are preferentially present in the smallest pores (Fig 6.2) and are more oil-wetting than non-clay minerals in all samples (Fig 6.3). These effects combine to make brine invasion in clay-rich pores very unfavourable as in an oil-wet system, brine invasion preferentially occurs in larger less oil wetting pores (*Blunt*, 2017).

The high S_o in clay-rich regions is even more prominent when only considering very clay-rich pores (pores with > 90% clay coverage). Very clay-rich pores are almost entirely oil saturated after high salinity flooding for all samples, with S_o values of 0.98, 0.96, and 0.97 in the Berea, Bunter, and Castlegate samples respectively (Table 6.1). After low salinity waterflooding, there is no significant change in S_o in very clay-rich pores in either the Castlegate or Bunter sample, so that very clay-rich pores remain almost entirely oil saturated. In contrast, there is a 5 percentage point decrease in S_o in the very clay-rich Berea pores during low salinity waterflooding. In the Bunter and Castlegate samples, very clay-rich pores remain almost entirely oil saturated throughout the duration of the experiment. These observations are further illustrated in Figures 6.8, 6.9, and 6.10 which show direct observations of fluid occupancy in clay aggregates within subvolumes of the Berea, Bunter, and Castlegate samples, respectively.

We can directly observe the behaviour of clays in each sample, with significant oil displacement from very clay-rich regions of the Berea sample, but no significant oil displacement from very clay-rich pores in the Bunter and Castlegate samples. Figures 6.8, 6.9 and 6.10 show subvolumes of the Berea, Bunter and Castlegate samples, respectively. In each figure, the undoped

scan is presented to show mineralogy, as well as the fluid configuration after both high and low salinity waterflooding. In all cases, there are large clay-aggregates present (highlighted by black boxes). In each case, these regions are completely oil saturated after high salinity waterflooding. In the Berea sample, there is significant oil displacement from a clay-aggregate (highlighted by a dashed black box) during low salinity waterflooding. A second clay aggregate is also shown. This second aggregate remains oil saturated during low salinity waterflooding. In the Bunter and Castlegate samples, after low salinity water flooding, there is no change in the oil configuration within the clay aggregates, so that low salinity brine does not contact the clays at any point throughout the experiment. There are significant fluid occupancy changes in clay-poor pores during low salinity water flooding in all samples (highlighted by solid grey boxes). This highlights the more unstable nature of clay-poor pores throughout the experiments, and echos results presented in Fig. 6.5 and which show more significant pore occupancy changes in clay-poor pores than for clay-rich pores.

6.2.4 Clays as a Screening Criterion

We observe that the majority of oil displacement in each sample occurs in clay-poor pores. Clay-rich regions of the pore space are preferentially oil saturated throughout the duration of high and low salinity waterflooding. This shows that clay-rich pores behave differently to clay minerals on planar surfaces where oil detachement during low salinity waterflooding is often observed (*Bartels et al.*, 2017b; *Berg et al.*, 2010; *Cense et al.*, 2011; *Mahani et al.*, 2015b; *Nasralla et al.*, 2013; *Song and Kovscek*, 2015). This finding casts doubt on the generally accepted view that oil detachment from clay is the primary mechanism of recovery during low salinity water flooding and that clays are essential for favourable recovery during low salinity flooding (*Berg et al.*, 2010; *Nasralla et al.*, 2013; *Song and Kovscek*, 2015; *Yesufu-Rufai et al.*, 2020).

Whilst we have shown that clays were not primarily responsible for additional recovery during low salinity waterflooding in any of the 3 samples, we have observed that clays responded differently in the different samples. In the Berea sample, there was a significant wettability

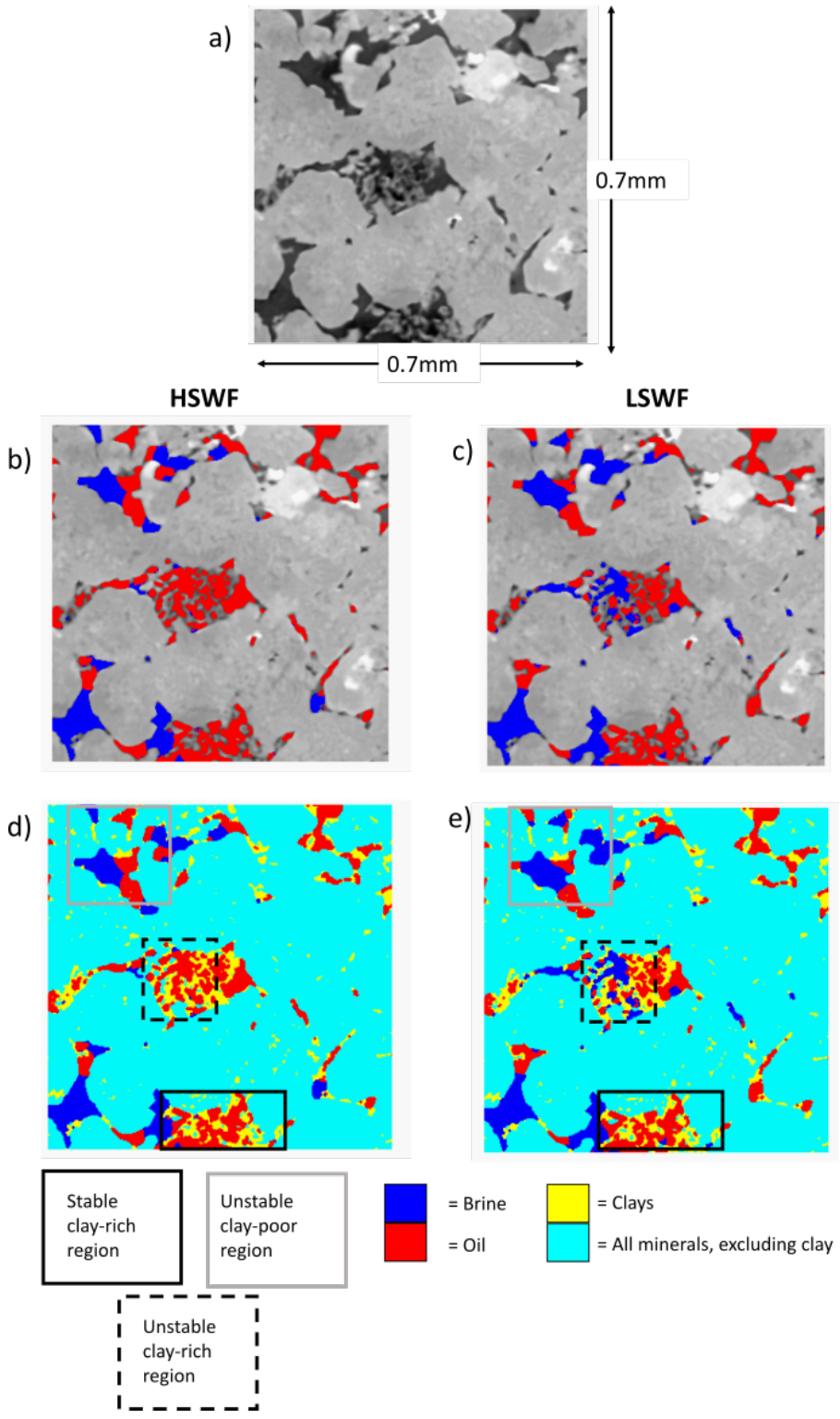


Figure 6.8: Direct observations of mineralogy and fluid distribution within a subvolume of the Berea sample. a) Undoped scan of slice through subvolume b) raw scan of minerals presented with segmented fluid phases (blue = brine, red = oil) after high salinity water flooding c) raw scan of minerals presented with segmented fluid phases (blue = brine, red = oil) after low salinity water flooding d) Segmented minerals (turquoise = bulk minerals, yellow = clays) and segmented fluid phases (blue = brine, red = oil) after high salinity waterflooding e) Segmented minerals (turquoise = bulk minerals, yellow = clays) and segmented fluid phases (blue = brine, red = oil) after low salinity water flooding, stable clay-rich areas of the pore space are represented by solid black boxes, unstable clay-rich regions are represented by dashed black boxes, unstable clay-poor regions are represented by grey boxes.

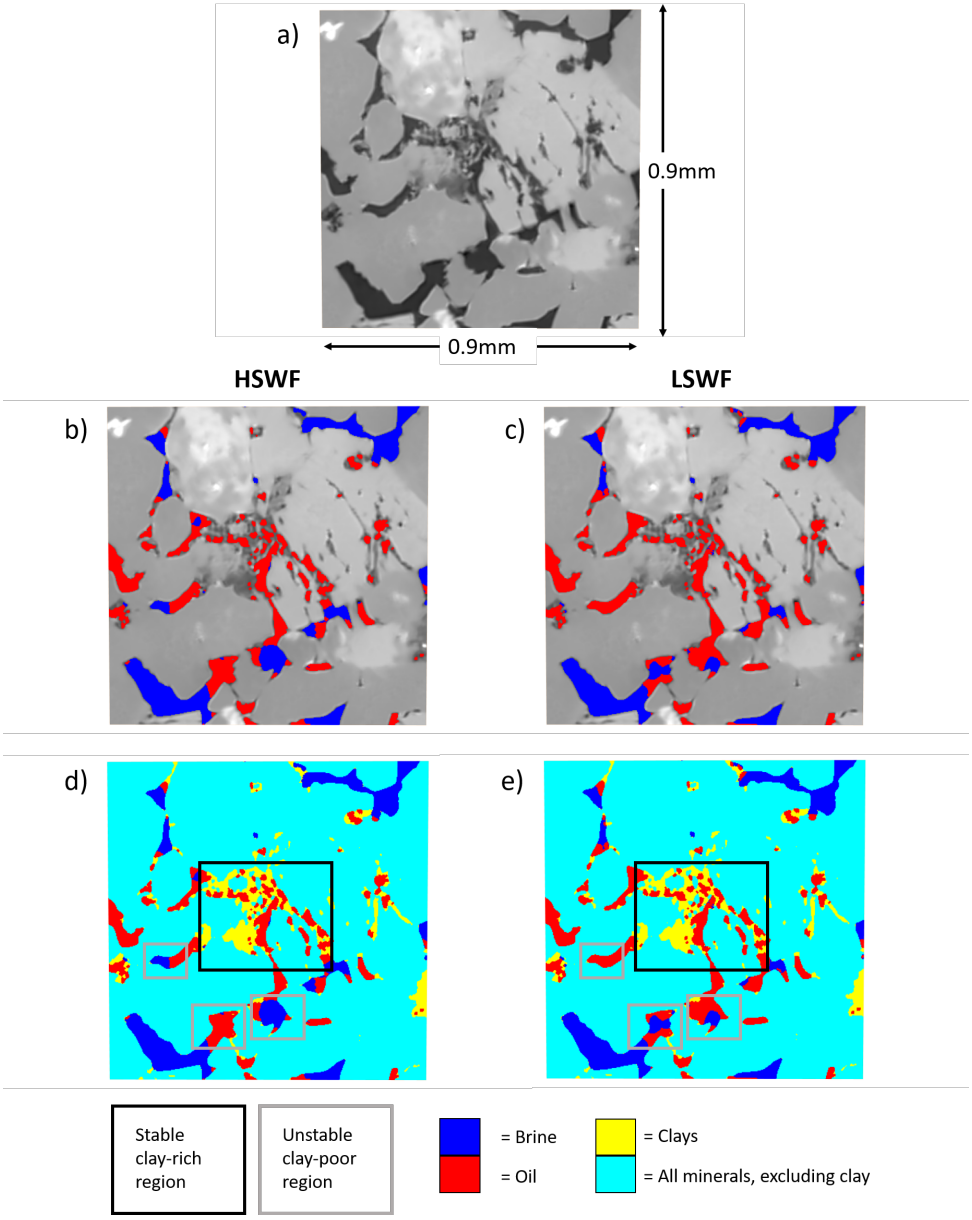


Figure 6.9: Direct observations of mineralogy and fluid distribution within a subvolume of the Bunter sample. a) Undoped scan of slice through subvolume b) raw scan of minerals presented with segmented fluid phases (blue = brine, red = oil) after high salinity water flooding c) raw scan of minerals presented with segmented fluid phases (blue = brine, red = oil) after low salinity water flooding d) Segmented minerals (turquoise = bulk minerals, yellow = clays) and segmented fluid phases (blue = brine, red = oil) after high salinity waterflooding e) Segmented minerals (turquoise = bulk minerals, yellow = clays) and segmented fluid phases (blue = brine, red = oil) after low salinity water flooding, stable clay-rich areas of the pore space are represented by solid black boxes, unstable clay-rich regions are represented by dashed black boxes, unstable clay-poor regions are represented by grey boxes.

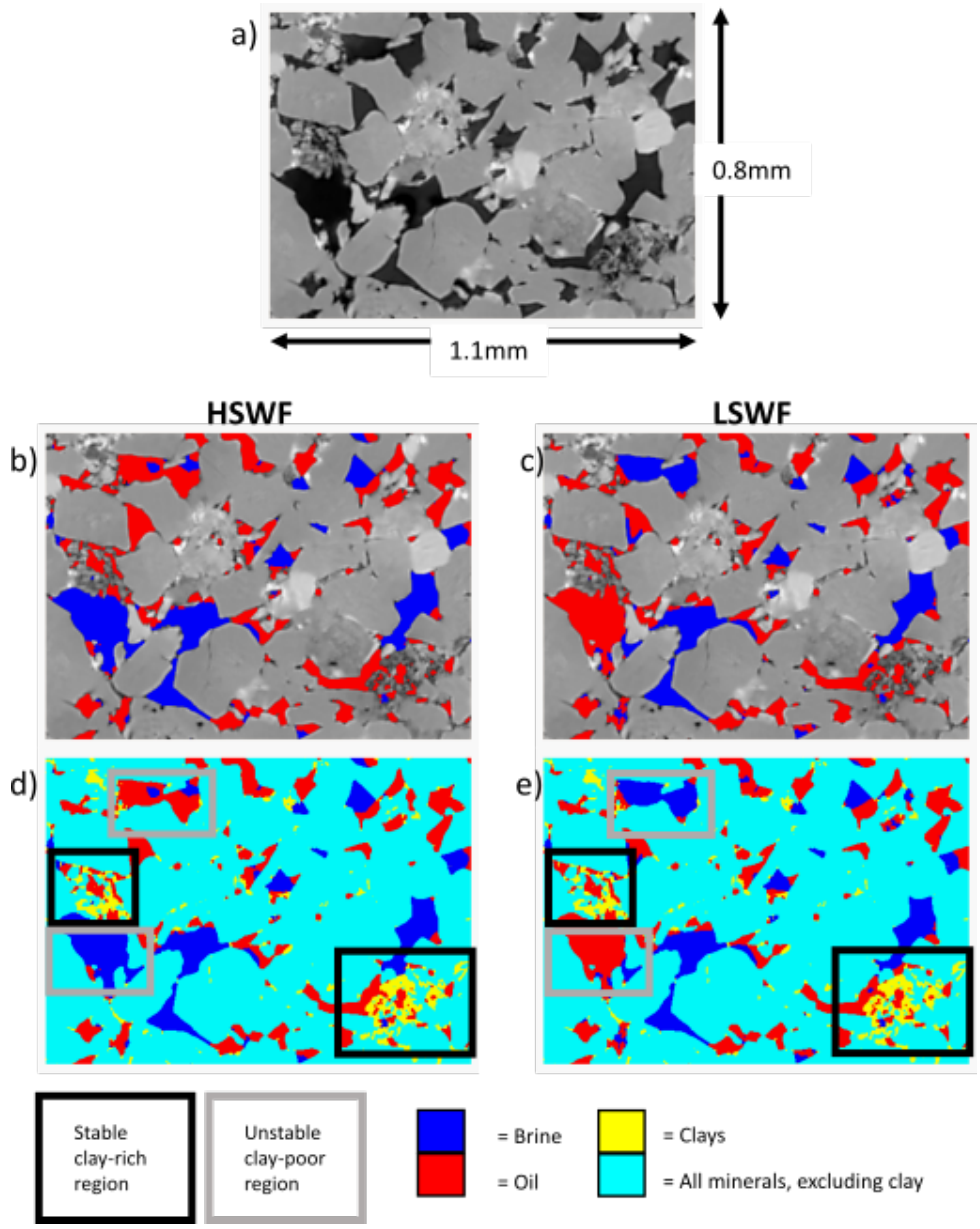


Figure 6.10: Direct observations of mineralogy and fluid distribution within a subvolume of the Castlegate sample. a) Undoped scan of slice through subvolume b) raw scan of minerals presented with segmented fluid phases (blue = brine, red = oil) after high salinity water flooding c) raw scan of minerals presented with segmented fluid phases (blue = brine, red = oil) after low salinity water flooding d) Segmented minerals (turquoise = bulk minerals, yellow = clays) and segmented fluid phases (blue = brine, red = oil) after high salinity waterflooding e) Segmented minerals (turquoise = bulk minerals, yellow = clays) and segmented fluid phases (blue = brine, red = oil) after low salinity water flooding, stable clay-rich areas of the pore space are represented by black boxes, unstable clay-poor regions are represented by grey boxes.

alteration on clay minerals during low salinity waterflooding, and clay-rich pores contributed 15% of total additional recovery during low salinity flooding, compared to just 5% and 3% for the Bunter and Castlegate sample, respectively. Below we will briefly describe two hypotheses to explain the differing clay response between the three samples.

The first potential factor effecting clay behaviour is pore structure and connectivity which is known to impact flow regimes and displacement mechanisms in a range of systems (*An et al.*, 2016; *Blunt*, 2017; *Holtzman*, 2016; *Singh et al.*, 2019, 2022; *Tanino and Blunt*, 2012; *Xu et al.*, 2014). In chapter 5, we hypothesised that in particular, the connectivity of the largest pores in each of the samples presented here impacted the low salinity response. We hypothesised that, in the Castlegate sample, a well connected network of large pores allowed for brine to flow easily through the pore space in a stable pathway during secondary high salinity flooding, so that during low salinity water, brine could easily flow over existing brine pathways, making oil displacement and mobilisation less favourable. We hypothesised that, in the Berea sample and Bunter samples a poorly connected network of large pores meant that the brine pathway created during high salinity flooding was broken up due to local and distal oil snap off events in small and medium pores. As a result, during low salinity flooding, brine had to displace oil from small and medium pores and throats to connect across the sample, making oil mobilisation more favourable. This effect is more complex when mineralogy is considered. In the Berea and Bunter samples, brine is forced to flow through small pores during low salinity water flooding, which are more likely to be clay-rich. As such, it is more likely that brine will come into contact with clays in the Berea sample, allowing for a more significant wettability alteration and oil displacement.

The second potential factor effecting clay behaviour is the initial wetting state of each sample. This may also have an impact on displacement of oil during low salinity flooding. In the Berea sample, both mineral groups are significantly less oil-wetting than for the Bunter and Castlegate samples, which are of comparable initial wetting states (Figure 6.3). The more oil-wetting nature of clays in Bunter and Castlegate samples makes brine invasion into clay-rich regions less favourable, therefore decreasing the likelihood of low salinity brine contacting clay-surfaces and invading clay-rich pores. This is because during waterflooding, the more oil-

wetting a pore is the higher its threshold capillary entry pressure. The more oil-wetting nature of the Bunter and Castlegate clay aggregates may be the determining factor in preventing brine invasion in clay-rich regions, and significant oil production from clay-rich pores.

Grouping the minerals in each sample into clay minerals and non-clay minerals is a simplistic approach intended to highlight the general behaviour of clays within each sample. However, this approach ignores the likely differences in clay mineralogy between each sample. There are many different clay minerals which are all thought to react differently to low salinity brine. Furthermore, as discussed in section 2.6.3, the orientation of clays can have a significant impact on their reactivity to low salinity brine (*Grim*, 1953; *Secor and Radke*, 1985; *Tombácz and Szekeres*, 2006; *Yesufu-Rufai et al.*, 2020). It is, therefore, possible that the different response of clay minerals to low salinity flooding in the three samples is a result of differences in clay mineralogy and orientation, and not the pore size distribution or initial wetting state of each sample.

The results presented here may appear to disagree with the extensive observations of oil detachment from clay minerals on planar surfaces and in micromodels during low salinity waterflooding (*Bartels et al.*, 2017b; *Berg et al.*, 2010; *Cense et al.*, 2011; *Mahani et al.*, 2015b; *Nasralla et al.*, 2013; *Song and Kovscek*, 2015). This is not necessarily the case. Rather, we observe that in most cases it is not favourable for low salinity brine to contact clay-minerals during low salinity flooding, which limits the potential for oil detachment from in situ clay surfaces and additional recovery from clay-rich pores. We have observed in the Berea sample that, where low salinity brine can come into contact with clays, it can cause a significant wettability alteration, oil-detachment and consequently additional oil recovery. However, an array of complex factors such as clay distribution, initial wetting state, and pore structure, determine the accessibility of clay aggregates to salinity brine and, therefore, the susceptibility to wettability alteration and oil detachment. This is not the case for quartz and feldspar grains, which typically make up the bulk of mineralogy in sandstones and are present across all pore radii. Whilst quartz and feldspar may be less susceptible to wettability alteration during low salinity waterflooding, a large body of research has found that significant ion exchange and wettability alteration, oil detachment, does still occur on these mineral surfaces (*Al-Saedi et al.*, 2019a,c; *Bartels et al.*,

2017b; *Hassenkam et al.*, 2011, 2012; *Liu et al.*, 2018; *Pu et al.*, 2010; *Suman*, 2014). Even if this effect is significantly lower than for clays, because quartz and feldspar rich pores are more abundant within typical sandstones and are more accessible to invading low salinity brine, it is likely that most oil production in sandstones occurs from quartz and feldspar rich pores, as observed here.

6.3 Conclusions

In this work, we presented results of tertiary low salinity flooding experiments in Berea, Bunter and Castlegate sandstone micro-cores of altered wetting state. The three samples had similar mineralogy but different pore topology and geometries. Our main findings are as follows:

- In all three samples, oil was trapped heterogeneously at relatively high saturations after high salinity water flooding, with S_o values of 0.62, 0.57 and 0.61 in the Berea, Bunter and Castlegate samples respectively. In all samples, a low salinity response was observed, with additional recovery of 3, 4 and 1 percentage points during low salinity water flooding in the Berea, Bunter and Castlegate samples, respectively.

- In all samples clay minerals were significantly more oil-wetting than non-clay minerals. In the Berea sample, we observed the largest wetting alteration on clays, with a significant shift to more water-wetting conditions for both clays and non-clay minerals. In the Bunter sandstone, there was a wettability alteration towards more water wetting conditions for both mineral groups, but this was largest for non-clay minerals. In the Castlegate sample, no systematic wettability alteration was observed for either mineral group.

- For all samples, there was an increase in brine saturation in small clay-poor pores during low salinity water flooding, consistent with a wettability alteration to more water-wet conditions. This was most significant in the Berea and Bunter sandstones. In all samples, the majority of oil displacement occurred in clay-poor pores, with very few oil displacement events in small clay-rich pores in the Bunter and Castlegate samples. Clay-rich pores

accounted for only 15%, 5% and 3% of total additional recovery in the Berea, Bunter, and Castlegate samples respectively.

- For very clay-rich pores (pores with $> 90\%$ clay coverage), after high salinity water flooding, S_o was > 0.95 for all samples. There was no significant change in S_o in these pores in the Bunter and Castlegate samples during low salinity water flooding, but we observed a 5 percentage point decrease in S_o in very clay-rich pores in the Berea sample. This behaviour is observed directly with clay aggregates remaining oil saturated throughout the experiment in Bunter and Castlegate samples, but with some low salinity brine invasion into clay aggregates in the Berea sample. It is likely that in the Bunter and Castlegate samples, clay-rich regions were so strongly oil-wet that low salinity brine did not contact significant volumes of clays, so that only small amounts of oil detachment could occur.

- The presence of clays does not appear to be a good indicator that low salinity waterflooding will improve recovery in sandstones. Clays can positively impact production in areas where they can be accessed by low salinity brine, as in the Berea sample. However, the presence of clays does not guarantee improved production, as brine may not be able to contact the majority of clay mineral surfaces. Further research should concentrate on quantifying the accessibility of clay-rich regions, considering pore structure and connectivity, initial wetting state and the distribution of clays within samples, and developing this as a measure to help predict low salinity response.

Chapter 7

Conclusions and Future Outlook

7.1 Conclusions

The overarching goal of this work was to gain further insight into low salinity water flooding through a systematic and controlled set of pore-network scale observations and analyses. In particular, we focused on how wetting state, pore structure and mineralogy impact fluid distribution and recovery during low salinity flooding.

We carried out tertiary low salinity waterflooding experiments on two Berea sandstone cores with different initial wetting states, an altered core and an unaltered core. We observed that fluid saturation profiles and the average saturation changes are distinct for water wet and altered rocks. In the unaltered rock, oil was trapped at a relatively high saturation ($S_o = 0.74$) that did not change significantly after subsequent flooding with low salinity brine. In the altered sample, oil was trapped at relatively low saturation (S_o= 0.62) after high salinity flooding, and subsequent low salinity flooding resulted in a 3% point enhancement to oil production. We used fluid coated area fraction to measure the wetting state of each sample, providing the most robust pore scale measurements of wetting state in low salinity water flooding research to date. We observed a wetting state shift in response to low salinity brine in the altered sample inferred from a shift in the solid surface area covered by the oil phase and changes in pore occupancy. No such wettability alteration was observed in the unaltered sample. In the altered sample, we

directly observe snap-off events after low salinity water flooding, behaviour indicative of a more water-wet system. We observe that in some areas, snap off events can lead to the trapping of oil ganglia at the centre of pores. This mechanism may help to explain the large amount of retrapping of mobilised oil that we observed in the altered sample. The combined impact of this was that a shift in the wetting state resulted in a large amount of oil redistributed, but only a small amount of oil produced. This implies that a wetting state shift is not sufficient to determine production. Low salinity flooding can cause a complex redistribution of fluids at the pore and pore-network scale, but may not lead to improved recovery.

In chapter 5, we presented the first systematic comparison of pore scale processes during low salinity waterflooding in sandstones. We compared the results of the altered Berea sandstone presented in chapter 4, with results from low salinity flooding of a Bunter and Castlegate sandstone cores of altered wetting state. We observed significant additional oil production of 3 and 4 percentage points in the Berea and Bunter samples respectively and a recovery of 1 percentage point in the Castlegate sample. We observed that in the Berea and Bunter samples, there was a significant wettability alteration towards more water wet conditions. This wettability alteration led to significant pore occupancy changes in the Berea and Bunter samples, with significant increase in S_w in smaller pores during low salinity waterflooding. There was no systematic wettability alteration observed in the Castlegate sample and consequently only a small shift in pore occupancy. We found that the topology of the largest pores had a significant impact on recovery in each of the samples. In the Castlegate sample the largest pores are well connected across the sample. This resulted in a stable, connected pathway of brine across the largest pores after high salinity waterflooding. However, in the Bunter and Berea samples no stable pathway of brine was presented after high salinity waterflooding, likely due to distal and local oil snap-off events because of poorly connected large pores. As such, during low salinity waterflooding there was no established path for the brine to follow, and so brine invaded oil filled pores and throats to connect across the sample, therefore mobilising larger quantities of oil.

In chapter 6 we investigated the role of clay minerals in recovery during low salinity flooding in the three experiments described in chapter 5. We used surface area fractional coverage analysis

to make the first pore scale in situ mineral specific wettability measurements during low salinity water flooding. In all samples we observed that clay minerals were significantly more oil-wetting than non-clay minerals. In the Berea sample, we observed the largest wetting alteration on clays, with a significant more to more water-wetting conditions for both clay minerals and non-clay minerals. In the Bunter sandstone, we also observed a wettability alteration towards more water wetting conditions for both mineral groups, but this was largest for non-clay minerals. In the Castlegate sample, no systematic wettability alteration was observed for either mineral group. For all samples, we observed an increase in brine saturation in small clay-poor pores during low salinity water flooding, consistent with a wettability alteration to more water-wet conditions. This was most significant in the Berea and Bunter sandstones. In all samples, the majority of oil displacement occurred in clay-poor pores, with very few oil displacement events in small clay-rich pores in the Bunter and Castlegate samples. Clay-rich pores accounted for only 15%, 5% and 3% of total additional recovery in the Berea, Bunter, and Castlegate samples respectively. This behaviour was also observed directly with clay aggregates remaining oil saturated throughout the experiment in Bunter and Castlegate samples, but with some low salinity brine invasion into clay aggregates observed in the Berea sample. This work showed that clay minerals were not the dominant factor in additional recovery in any of the samples, although their presence likely boosted production in the Berea sandstone. This work adds to the growing body of research that suggests that clays are not essential for a favourable response to low salinity flooding.

It is important to note that, due to some fundamental limitations to the experimental procedure, these observations cannot be assumed to exactly reflect subsurface conditions in real reservoirs. To mimic subsurface displacement as closely as possible, we used realistic reservoir fluids (with the exception of the iododecane which was added to the crude oil) and ensured a capillary dominated regime for all waterfloods. However, the drainage (oil-flooding) process carried out for these experiments does not closely simulate natural primary oil migration, which occurs at slow rates over millennia. As a result, the S_{wi} values for each sample (< 0.05 in each case) are not representative of real reservoirs, where typical S_{wi} values are significantly greater than 0.05. This difference is important to consider when interpreting pore occupancy changes and

additional recovery during low salinity flooding. As a result of the low S_{wi} values in each sample, the vast majority of the smallest pores are initially occupied by oil. We observed that the majority of additional recovery during low salinity waterflooding in the altered Berea and Bunter samples was from these initially oil occupied small pores. However, in real reservoirs, the majority of the smallest pores are typically occupied by water, and so the production of oil from small pores is limited. Therefore, the experiments presented in this thesis may overestimate pore occupancy changes and additional recovery during low salinity flooding. Another key uncertainty is how representative the results are of displacements over larger scales, and in particular how relevant results are when considering heterogeneity on the order of tens of metres. For example, in both Berea samples, we observed low porosity and permeability values. For the altered sample, we concluded that the pore structure, which partly influenced the low permeability values, was correlated with increased oil mobilisation and recovery during low salinity flooding. However, in real reservoirs with heterogeneity across different length scales, it is possible that localised low permeability and porosity areas would be bypassed by invading brine in favour of higher porosity and permeability regions, which may not produce the same response to low salinity flooding.

However, despite the limitations discussed above, some important conclusions can be drawn from this work. X-ray micro-CT imaging of flow experiments of micro-scale cores has a number of advantages. The most important of which is the ability to directly observe pore scale displacements and pore occupancy changes. Experiments over larger scales, e.g. core scale (10s of cms) experiments with medical-CT imaging, provide more representative S_{wi} values, but lack sufficient image resolution to observe pore scale displacement. This work uses X-ray micro-CT imaging to give the first systematic comparison of the pore sale response to low salinity flooding in different sandstone samples.

Above all, this work highlights the complex nature of the pore scale response to low salinity flooding, and the importance of pore-scale observations in building an exhaustive list of screening criteria. There remains a widely held belief that additional recovery during low salinity flooding is the inevitable consequence of a shift to more water-wetting conditions. This opinion largely originates from the interpretation of sub-pore scale observations of wettability

alteration on planar mineral surfaces exposed to low salinity brine. This work, Chapter 5 in particular, makes it very clear that the relationship between a wettability alteration and additional production is complex. A wettability alteration should be considered as necessary but not sufficient for additional recovery during low salinity flooding. A wettability alteration may lead to the mobilisation of oil, but the majority of this mobilised oil will likely be retrapped within the pore space. The amount of oil which is retrapped is determined by many factors including pore structure and initial wetting state. In chapter 6, we highlighted another important disconnect between sub-pore scale analysis and the displacement processes in real rocks. The majority of sub-pore scale analysis of clays is carried out using clay minerals deposited on flat surfaces where oil droplets are placed onto the clay before exposure to low salinity brine. In real sandstones, clays are distributed heterogeneously and with different orientations. Although the work presented in this thesis is simplistic in its grouping of all clays as one mineral group, it highlights the importance of observing the in-situ behaviour of clay minerals. The interpretation of the experiments on planar surfaces relies on the assumption that in real rocks brine can readily contact the clay minerals. In chapter 6, we showed that brine is unlikely to contact most clay minerals during low salinity flooding because of the unique distribution and initial wetting states of most clay minerals in typical sandstones.

As stated in chapter 1, there is no reliable reservoir characterisation criteria capable of predicting which systems will respond favourably to the technique. Whilst stopping short of offering an exhaustive list of characterisation criteria, the pore scale insights described in this work help to explain the current shortcomings and give an insight into the discoveries that are needed. We have shown that pore structure impacts oil mobilisation and recovery during low salinity waterflooding. However, no measure of pore structure is currently included as a screening criteria for low salinity water flooding. The findings presented here show that any exhaustive list of necessary conditions should include measures of pore structure, in particular the connectivity of the largest pores in a given rock sample. These findings represent initial insights, but more work is required to identify the full control of pore structure on recovery during low salinity waterflooding and to develop quantitative screening criteria. This work has also highlighted that clay minerals should be regarded as providing a potential boost to recovery (depending on

wetting state, pore structure and clay distribution) but should no longer be considered necessary for additional recovery during low salinity waterflooding. Therefore, if the presence of clays is to be included as a screening criteria, a more careful assessment is needed, and rocks with no, or a low, clay content should not be disregarded. However, more work is required to understand the in situ pore scale response of different clay minerals to low salinity flooding. Above all, this work shows that a fundamental understanding of pore scale behaviour is important within low salinity flooding research. However, more work, which builds upon the ideas presented in this thesis, is required to achieve the ultimate goal of developing a predictive model capable of identifying systems that will be responsive to low salinity water flooding.

7.2 Future Work

This work offers unique insights into pore scale displacement during low salinity flooding in sandstones. However, there is great scope for further work in the field

7.2.1 Pore Structure - Sensitivity Analysis

We have showed that pore structure has an important impact on displacement during low salinity waterflooding. Specifically, we have hypothesised that the topology of the large pores in a given sample can influence oil mobilisation and production. However, there are many properties and measures of pore structure (such as tortuosity, pore scale disorder, aspect ratio, coordination number) that may well also impact displacement and should be explored in future work. Potentially, advancements in modelling techniques could be implemented to do this, as a sensitivity analysis of these variables is difficult on experimental data due to the various restraints on experimental output and time consuming image analysis workflows. Modelling techniques such as Lattice Boltzmann, and volume of fluid, have already been implemented to investigate displacement mechanisms during low salinity waterflooding, but are yet to be used to investigate the impact of pore structure (*Akai et al.*, 2020b; *Aziz et al.*, 2019). A better understanding of how pore structure can impact the efficacy of low salinity flooding can then

introduce more conditions to the list of necessary conditions for successful low salinity water flooding. This would represent a big step forward in the pursuit of reliably predicting which COBR systems will respond favourably to low salinity flooding.

7.2.2 Clay Availability

Clearly, the presence of clays (typically measured as a volume fraction), is not a reliable indicator of either the clay coverage (i.e. the reactive surface available for oil detachment), or crucially, the accessibility of clays to low salinity brine. We have shown in the Berea sample that clays can positively impact production in areas where they can be accessed by low salinity brine. The accessibility of clays within a given sample is, therefore, the key measure - not clay volume. Further research should concentrate on quantifying the accessibility of clay-rich regions, considering pore structure, initial wetting state and the distribution of clays within samples, and developing this as a measure to help predict low salinity response. A significant limitation of this work is that we group all clay minerals together and, therefore, do not analyse the behaviour of different clay minerals. Different clay minerals are known to have a wide variety of properties and potentially responses to low salinity brine. Future work should also investigate the in-situ pore scale response of different clay minerals to low salinity flooding.

7.2.3 Synchrotron Imaging

Synchrotron CT imaging gives a temporal resolution on the order of seconds. This is far greater than typical laboratory micro-CT machines where temporal resolution is typically on the order of hours. The technology has been used to great effect in the field of multiphase flow in porous media, providing important insights into pore scale phenomena including, but not limited to, the dynamics of enhanced gas trapping (*Scanziani et al.*, 2020), Haines jumps (*Berg et al.*, 2013), droplet fragmentation (*Pak et al.*, 2015), and dynamic connectivity and intermittency (*Reynolds et al.*, 2017; *Spurin et al.*, 2019).

As previously stated, *Bartels et al.* (2017a) showed the merits of fast synchrotron imaging for the

observation of low salinity flooding. With high temporal resolution, they were able to accurately identify changes in pore occupancy during LSWF. However, the absence of multivalent cations in both the high and low salinity brines could have hindered any positive impact of low salinity water flooding. There is great scope for further synchrotron experiments using more realistic brine recipes, to observe real time pore scale displacement during low salinity flooding. This would provide important insights into displacement mechanisms, and in particular test the hypothesis presented in this work of distal and local snap off events during high salinity water flooding impacting the efficacy of subsequent low salinity flooding. The experiments would also provide insight into the full extent of oil mobilisation and redistribution during low salinity waterflooding, potentially providing the first real-time observations of oil bank formation during low salinity waterflooding.

7.2.4 Low Salinity Water Alternating Gas Injection

New studies suggest that the large scale roll out of Carbon Capture and Storage (CCS) is absolutely necessary if the world is to hit even the modest IPCC target of minimising global warming to below $2°C$ (*Edenhofer*, 2015; *Koelbl et al.*, 2014). Currently, however, CCS currently has little economic incentive. One of the few ways that CCS may be economically viable is its use as an EOR technique. CO_2-EOR, where liquid or supercritical CO_2 is injected into depleted reservoirs, typically as part of water alternating gas (WAG) cycles, has been widely used for decades to improve oil recovery. In fact, 140 CO_2-EOR projects, producing approximately 100,000,000 bbl of incremental oil per year, are currently in use (*Bui et al.*, 2018). However, in typical CO_2-EOR projects little thought is given to entrapment of CO_2. True CCS-EOR projects, where both oil recovery and CO_2 entrapment are maximised, are rarer. A detailed analysis of the viability of CCS-EOR carried out by the IEA found that a 'balanced' approach, where both CO_2 storage and incremental oil recovery are optimised, can yield an estimated net utilisation of 0.6 tCO_2 per bbl oil produced for an incremental oil recovery of 13% OOIP (*IEA*, 2015b). The technology has been shown to function in practice; as of 2018, 13 of the 17 operating commercial-scale CCS projects were examples of CCS-EOR (*Bui et al.*, 2018).

Preliminary work has investigated combining CCS-EOR with low salinity waterflooding (*AlQuraishi et al.*, 2017; *Naderi and Simjoo*, 2019; *Teklu et al.*, 2017). Early results suggest that CO_2 low salinity water alternating gas injection (LSWAG) combines the benefits of CO_2 injection and low salinity water floods, increasing recovery as well as entrapment of the injected CO_2 Recently three-phase flow experiments have been carried out and imaged within micro-CT scanners, showing promising signs for the success of LSWAG technologies. Firstly, *Iglauer et al.* (2016) found water-wet systems to be optimal (lower residual oil saturation and higher gas trapping) for gas injection. More recently, *Scanziani et al.* (2018) found significant trapping of injected gas and displacement of trapped oil in WAG flow experiments with water-wet samples. A wettability alteration towards more water-wet conditions during low salinity waterflooding may, therefore, improve WAG efficiency. It is also thought that CO_2-LSWAG may also improve CO_2 injectivity through minimising the precipitation of brine salts (*Sokama-Neuyam et al.*, 2019). There is, however, concern that LSWAG may result in increased permeability damage due to fines migration (*Othman et al.*, 2019). Early research into CO_2-LSWAG has been exclusively made up of modelling studies (*AlQuraishi et al.*, 2017; *Naderi and Simjoo*, 2019; *Teklu et al.*, 2017), however, there is great scope to validate the hypotheses experimentally. It is entirely possible to implement experimental and image analysis workflows similar to those presented in this work, to investigate pore scale response to CO_2-LSWAG. This would provide valuable insights into the EOR and CO_2 storage potential of the technology and potentially take it one step closer to deployment.

Bibliography

Abdulla, F., H. S. Hashem, B. Abdulraheem, M. Al-Naqi, A. Al-Qattan, H. John, P. Cunningham, P. Briggs, and R. Thawer (2013), First EOR trial using low salinity water injection in the greater Burgan field, Kuwait, in *SPE Middle East Oil and Gas Show and Conference*, OnePetro.

Agbalaka, C. C., A. Y. Dandekar, S. L. Patil, S. Khataniar, and J. R. Hemsath (2009), Coreflooding studies to evaluate the impact of salinity and wettability on oil recovery efficiency, *Transport in Porous Media*, *76*(1), 77–94.

Akai, T., Q. Lin, B. Bijeljic, and M. J. Blunt (2020a), Using energy balance to determine pore-scale wettability, *Journal of Colloid and Interface Science*, *576*, 486–495.

Akai, T., M. J. Blunt, and B. Bijeljic (2020b), Pore-scale numerical simulation of low salinity water flooding using the Lattice Boltzmann method, *Journal of Colloid and Interface Science*, *566*, 444–453.

Akbarabadi, M., and M. Piri (2013), Relative permeability hysteresis and capillary trapping characteristics of supercritical CO_2/brine systems: An experimental study at reservoir conditions, *Advances in Water Resources*, *52*, 190–206.

Al-Saedi, H. N., R. E. Flori, and S. K. Al-Jaberi (2019a), Eliminate the role of clay in sandstone: EOR low salinity water flooding, *Journal of Petroleum Exploration and Production Technology*, *9*(2), 1475–1483.

Al-Saedi, H. N., P. V. Brady, R. E. Flori, and P. Heidari (2019b), Insights into the role of clays

in low salinity water flooding in sand columns, *Journal of Petroleum Science and Engineering*, *174*, 291–305.

Al-Saedi, H. N., R. E. Flori, and P. V. Brady (2019c), Effect of divalent cations in formation water on wettability alteration during low salinity water flooding in sandstone reservoirs: Oil recovery analyses, surface reactivity tests, contact angle, and spontaneous imbibition experiments, *Journal of Molecular Liquids*, *275*, 163–172.

Aladasani, A., B. Bai, Y.-S. Wu, and S. Salehi (2014), Studying low-salinity waterflooding recovery effects in sandstone reservoirs, *Journal of Petroleum Science and Engineering*, *120*, 39–51.

Alagic, E., and A. Skauge (2010), Combined low salinity brine injection and surfactant flooding in mixed- wet sandstone cores, *Energy & Fuels*, *24*(6), 3551–3559.

Alhammadi, A. M., A. AlRatrout, K. Singh, B. Bijeljic, and M. J. Blunt (2017), In situ characterization of mixed-wettability in a reservoir rock at subsurface conditions, *Scientific Reports*, *7*(1), 10,753.

Alhosani, A., A. Scanziani, Q. Lin, S. Foroughi, A. M. Alhammadi, M. J. Blunt, and B. Bijeljic (2020), Dynamics of water injection in an oil-wet reservoir rock at subsurface conditions: invasion patterns and pore-filling events, *Physical Review E*, *102*(2), 023,110.

Alhuraishawy, A. K., B. Bai, M. Wei, J. Geng, and J. Pu (2018), Mineral dissolution and fine migration effect on oil recovery factor by low-salinity water flooding in low-permeability sandstone reservoir, *Fuel*, *220*, 898–907.

Alotaibi, M. B., R. A. Nasralla, H. A. Nasr-El-Din, et al. (2011), Wettability studies using low-salinity water in sandstone reservoirs, *SPE Reservoir Evaluation & Engineering*, *14*(06), 713–725.

AlQuraishi, A. A., A. M. Amao, N. I. Al-Zahrani, M. T. AlQarni, and S. A. AlShamrani (2017), Low salinity water and CO_2 miscible flooding in Berea and bentheimer sandstones, *Journal of King Saud University-Engineering Sciences*.

AlRatrout, A., A. Q. Raeini, B. Bijeljic, and M. J. Blunt (2017), Automatic measurement of contact angle in pore-space images, *Advances in Water Resources*, *109*, 158–169.

AlRatrout, A., M. J. Blunt, and B. Bijeljic (2018), Spatial correlation of contact angle and curvature in pore-space images, *Water Resources Research*, *54*(9), 6133–6152.

An, S., J. Yao, Y. Yang, L. Zhang, J. Zhao, and Y. Gao (2016), Influence of pore structure parameters on flow characteristics based on a digital rock and the pore network model, *Journal of Natural Gas Science and Engineering*, *31*, 156–163.

Andrews, E., A. Muggeridge, G. Garfi, A. Jones, and S. Krevor (2021), Pore-scale x-ray imaging of wetting alteration and oil redistribution during low-salinity flooding of Berea sandstone, *Energy & Fuels*, *35*, 1197–1207.

Aziz, R., V. Joekar-Niasar, and P. Martinez-Ferrer (2018), Pore-scale insights into transport and mixing in steady-state two-phase flow in porous media, *International Journal of Multiphase Flow*, *109*, 51–62.

Aziz, R., V. Joekar-Niasar, P. J. Martínez-Ferrer, O. E. Godinez-Brizuela, C. Theodoropoulos, and H. Mahani (2019), Novel insights into pore-scale dynamics of wettability alteration during low salinity waterflooding, *Scientific Reports*, *9*(1), 1–13.

Bartels, W.-B., M. Rücker, S. Berg, H. Mahani, A. Georgiadis, A. Fadili, N. Brussee, A. Coorn, H. van der Linde, C. Hinz, et al. (2017a), Fast X-ray micro-CT study of the impact of brine salinity on the pore-scale fluid distribution during waterflooding, *Petrophysics*, *58*(01), 36–47.

Bartels, W.-B., H. Mahani, S. Berg, R. Menezes, J. A. van der Hoeven, and A. Fadili (2017b), Oil configuration under high-salinity and low-salinity conditions at pore scale: a parametric investigation by use of a single-channel micromodel, *SPE Journal*, *22*(05), 1362–1373.

Bartels, W.-B., H. Mahani, S. Berg, and S. Hassanizadeh (2019), Literature review of low salinity waterflooding from a length and time scale perspective, *Fuel*, *236*, 338–353.

Bass Jr, D. M., P. B. Crawford, et al. (1956), Experimental waterflooding recoveries above and below the bubble point, *Journal of Petroleum Technology*, *8*(01), 45–47.

Basu, S., and M. M. Sharma (1996), Measurement of critical disjoining pressure for dewetting of solid surfaces, *Journal of Colloid and Interface Science*, *181*(2), 443–455.

Basu, S., and M. M. Sharma (1999), Investigating the role of crude-oil components on wettability alteration using atomic force microscopy, *SPE Journal*, *4*(03), 235–241.

Bennion, D., D. Bennion, F. Thomas, and R. Bietz (1998), Injection water quality-a key factor to successful waterflooding, *Journal of Canadian Petroleum Technology*, *37*(06).

Berg, S., A. Cense, E. Jansen, K. Bakker, et al. (2010), Direct experimental evidence of wettability modification by low salinity, *Petrophysics*, *51*(05).

Berg, S., H. Ott, S. A. Klapp, A. Schwing, R. Neiteler, N. Brussee, A. Makurat, L. Leu, F. Enzmann, and J.-O. Schwarz (2013), Real-time 3D imaging of haines jumps in porous media flow, *Proceedings of the National Academy of Sciences*, *110*(10), 3755–3759.

Bernard, G. G. (1967), Effect of floodwater salinity on recovery of oil from cores containing clays, in *SPE California Regional Meeting*, OnePetro.

Beucher, S., and F. Meyer (1993), The morphological approach to segmentation: the watershed transformation, *Mathematical Morphology in Image Processing*, *34*, 433–481.

Blume, T., N. Weisbrod, and J. S. Selker (2002), Permeability changes in layered sediments: Impact of particle release, *Groundwater*, *40*(5), 466–474.

Blunt, M., L. Kearney, A. Alhosani, Q. Lin, and B. Bijeljic (2021), Wettability characterization from pore-scale images using topology and energy balance with implications for recovery and storage, in *SPE Annual Technical Conference and Exhibition*, OnePetro.

Blunt, M. J. (2017), *Multiphase flow in permeable media: A pore-scale perspective*, Cambridge University Press.

Blunt, M. J., Q. Lin, T. Akai, and B. Bijeljic (2019), A thermodynamically consistent characterization of wettability in porous media using high-resolution imaging, *Journal of Colloid and Interface Science*, *552*, 59–65.

Blunt, M. J., et al. (1997), Pore level modeling of the effects of wettability, *SPE Journal*, *2*(04), 494–510.

Buades, A., B. Coll, and J.-M. Morel (2005), A non-local algorithm for image denoising, in *2005 IEEE Computer Society Conference on Computer Vision and Pattern Recognition (CVPR'05)*, vol. 2, pp. 60–65, IEEE.

Buckley, J. (1998), Wetting alteration of solid surfaces by crude oils and their asphaltenes, *Revue de l'Institut Français du Pétrole*, *53*(3), 303–312.

Buckley, J., and Y. Liu (1998), Some mechanisms of crude oil/brine/solid interactions, *Journal of Petroleum Science and Engineering*, *20*(3-4), 155–160.

Buckley, J., and N. R. Morrow (1990), Characterization of crude oil wetting behavior by adhesion tests, in *SPE/DOE Enhanced Oil Recovery Symposium*, OnePetro.

Buckley, J. S., and T. Fan (2007), Crude oil/brine interfacial tensions1, *Petrophysics-The SPWLA Journal of Formation Evaluation and Reservoir Description*, *48*(03).

Buckley, J. S., Y. Liu, X. Xie, N. R. Morrow, et al. (1997), Asphaltenes and crude oil wetting-the effect of oil composition, *SPE Journal*, *2*(02), 107–119.

Bui, M., C. S. Adjiman, A. Bardow, E. J. Anthony, A. Boston, S. Brown, P. S. Fennell, S. Fuss, A. Galindo, L. A. Hackett, et al. (2018), Carbon capture and storage (CCS): the way forward], *Energy & Environmental Science*, *11*(5), 1062–1176.

Bultreys, T., L. Van Hoorebeke, and V. Cnudde (2015), Multi-scale, micro-computed tomography-based pore network models to simulate drainage in heterogeneous rocks, *Advances in Water Resources*, *78*, 36–49.

Bultreys, T., L. Van Hoorebeke, and V. Cnudde (2016a), Simulating secondary waterflooding in heterogeneous rocks with variable wettability using an image-based, multiscale pore network model, *Water Resources Research*, *52*(9), 6833–6850.

Bultreys, T., W. De Boever, and V. Cnudde (2016b), Imaging and image-based fluid transport modeling at the pore scale in geological materials: A practical introduction to the current state-of-the-art, *Earth-Science Reviews*, *155*, 93–128.

Bultreys, T., Q. Lin, Y. Gao, A. Q. Raeini, A. AlRatrout, B. Bijeljic, and M. J. Blunt (2018), Validation of model predictions of pore-scale fluid distributions during two-phase flow, *Physical Review E*, *97*(5), 053,104.

Cense, A., S. Berg, K. Bakker, E. Jansen, et al. (2011), Direct visualization of designer water flooding in model experiments, in *SPE Enhanced Oil Recovery Conference*, Society of Petroleum Engineers.

Chavez-Miyauch, T. E., Y. Lu, and A. Firoozabadi (2020), Low salinity water injection in Berea sandstone: Effect of wettability, interface elasticity, and acid and base functionalities, *Fuel*, *263*, 116,572.

Chavez-Miyauchi, T. E., A. Firoozabadi, and G. G. Fuller (2016), Nonmonotonic elasticity of the crude oil–brine interface in relation to improved oil recovery, *Langmuir*, *32*(9), 2192–2198.

Chen, Q., D. Mercer, and K. Webb (2010), Nmr study on pore occupancy and wettability modification during low salinity waterflooding, in *Paper SCA 2010-27 presented at the 24th International Symposium of Core Analysts, Halifax, Canada*, pp. 4–7.

Chen, Y., Q. Xie, W. Pu, and A. Saeedi (2018), Drivers of ph increase and implications for low salinity effect in sandstone, *Fuel*, *218*, 112–117.

Chen, Y., N. K. Jha, D. Al-Bayati, M. Lebedev, M. Sarmadivaleh, S. Iglauer, A. Saeedi, and Q. Xie (2020), Geochemical controls on wettability alteration at pore-scale during low salinity water flooding in sandstone using x-ray micro computed tomography, *Fuel*, *271*, 117,675.

Chen, Y., N. K. Jha, M. Lebedev, S. An, Q. Xie, and V. J. Niasar (2021), Integral effects of initial fluids configuration and wettability alteration on remaining saturation: characterization with x-ray micro-computed tomography, *Fuel*, *306*, 121,717.

Churcher, P., P. French, J. Shaw, L. Schramm, et al. (1991), Rock properties of Berea sandstone, baker dolomite, and indiana limestone, in *SPE International Symposium on Oilfield Chemistry*, Society of Petroleum Engineers.

Cissokho, M., H. Bertin, S. Boussour, P. Cordier, G. Hamon, et al. (2010a), Low salinity oil recovery on clayey sandstone: experimental study, *Petrophysics*, *51*(05).

Cissokho, M., H. Bertin, S. Boussour, P. Cordier, G. Hamon, et al. (2010b), Low salinity oil recovery on clayey sandstone: Experimental study, *Petrophysics*, *51*(05).

Coles, M., E. Muegge, and E. Sprunt (1991), Applications of cat scanning for oil and gas production, *IEEE Transactions on Nuclear Science*, *38*(2), 510–515.

Dang, C., L. Nghiem, N. Nguyen, Z. Chen, and Q. Nguyen (2016), Evaluation of CO_2 low salinity water-alternating-gas for enhanced oil recovery, *Journal of Natural Gas Science and Engineering*, *35*, 237–258.

Donaldson, E. C., R. D. Thomas, and P. B. Lorenz (1969), Wettability determination and its effect on recovery efficiency, *Society of Petroleum Engineers Journal*, *9*(01), 13–20.

Dong, H., and M. J. Blunt (2009), Pore-network extraction from micro-computerized-tomography images, *Physical Review E*, *80*(3), 036,307.

Drummond, C., and J. Israelachvili (2004), Fundamental studies of crude oil–surface water interactions and its relationship to reservoir wettability, *Journal of Petroleum Science and Engineering*, *45*(1-2), 61–81.

Dykstra, H., and R. Parsons (1950), The prediction of oil recovery by waterflood, *Secondary Recovery of Oil in the United States*, *2*, 160–174.

Edenhofer, O. (2015), *Climate change 2014: mitigation of climate change*, vol. 3, Cambridge University Press.

El-Maghraby, R. M., and M. J. Blunt (2012), Residual CO_2 trapping in indiana limestone, *Environmental Science & Technology*, *47*(1), 227–233.

Fogden, A. (2011), Effect of water salinity and pH on the wettability of a model substrate, *Energy & Fuels*, *25*(11), 5113–5125.

Freer, E., T. Svitova, and C. Radke (2003), The role of interfacial rheology in reservoir mixed wettability, *Journal of Petroleum Science and Engineering*, *39*(1-2), 137–158.

Gandomkar, A., and M. R. Rahimpour (2015), Investigation of low-salinity waterflooding in secondary and tertiary enhanced oil recovery in limestone reservoirs, *Energy & Fuels*, *29*(12), 7781–7792.

Garfi, G. (2021), Wettability characterisation of sandstone and carbonate rocks using X-ray micro-CT imaging, Ph.D. thesis, Imperial College London.

Garfi, G., C. M. John, Q. Lin, S. Berg, and S. Krevor (2020a), Fluid surface coverage showing the controls of rock mineralogy on the wetting state, *Geophysical Research Letters*, *47*(8), e2019GL086,380.

Garfi, G., C. M. John, S. Berg, and S. Krevor (2020b), The sensitivity of estimates of multiphase fluid and solid properties of porous rocks to image processing, *Transport in Porous Media*, *131*(3), 985–1005.

Garfi, G., M. Rücker, Q. Lin, S. Berg, C. M. John, and S. C. Krevor (2020c), Pore-by-pore wettability characterization in sandstone and carbonate rocks, in *AGU Fall Meeting 2020*, AGU.

Garfi, G., C. M. John, M. Rücker, Q. Lin, C. Spurin, S. Berg, and S. Krevor (2022), Determination of the spatial distribution of wetting in the pore networks of rocks, *Journal of Colloid and Interface Science*, *613*, 786–795, doi:https://doi.org/10.1016/j.jcis.2021.12.183.

Gawler, J., M. Sanders, J. Bull, G. Du Boulay, and J. Marshall (1974), Computer assisted tomography in orbital disease., *The British Journal of Ophthalmology*, *58*(6), 571.

Grim, R. E. (1953), *Clay mineralogy*, vol. 76, LWW.

Guo, C., X. Wang, H. Wang, S. He, H. Liu, and P. Zhu (2018), Effect of pore structure on displacement efficiency and oil-cluster morphology by using micro computed tomography (μCT) technique, *Fuel*, *230*, 430–439.

Hassenkam, T., C. S. Pedersen, K. Dalby, T. Austad, and S. L. S. Stipp (2011), Pore scale observation of low salinity effects on outcrop and oil reservoir sandstone, *Colloids and Surfaces A: Physicochemical and Engineering Aspects*, *390*(1-3), 179–188.

Hassenkam, T., A. C. Mitchell, C. Pedersen, L. Skovbjerg, N. Bovet, and S. Stipp (2012), The low salinity effect observed on sandstone model surfaces, *Colloids and Surfaces A: Physicochemical and Engineering Aspects*, *403*, 79–86.

Hassenkam, T., M. P. Andersson, E. Hilner, J. Matthiesen, S. Dobberschütz, K. N. Dalby, N. Bovet, S. L. Stipp, P. Salino, and C. Reddick (2016), Could atomic-force microscopy force mapping be a fast alternative to core-plug tests for optimizing injection-water salinity for enhanced oil recovery in sandstone?, *SPE Journal*, *21*(03), 720–729.

Hilner, E., M. P. Andersson, T. Hassenkam, J. Matthiesen, P. Salino, and S. L. S. Stipp (2015), The effect of ionic strength on oil adhesion in sandstone–the search for the low salinity mechanism, *Scientific Reports*, *5*(1), 1–9.

Hjuler, M. L., and L. Kristensen (2017), Pre-drilling geothermal assessment of porosity and permeability of the bunter sandstone formation, onshore denmark, *GEUS Bulletin*, *38*, 33–36.

Holtzman, R. (2016), Effects of pore-scale disorder on fluid displacement in partially-wettable porous media, *Scientific Reports*, *6*, 36,221.

Hu, R., J. Wan, Y. Kim, and T. K. Tokunaga (2017), Wettability impact on supercritical CO_2 capillary trapping: Pore-scale visualization and quantification, *Water Resources Research*, *53*(8), 6377–6394.

Iassonov, P., T. Gebrenegus, and M. Tuller (2009), Segmentation of x-ray computed tomography images of porous materials: A crucial step for characterization and quantitative analysis of pore structures, *Water Resources Research*, *45*(9).

IEA (2015a), The oil and gas industry in energy transitions (2020).

IEA (2015b), Storing CO_2 through enhanced oil recovery, *International Energy Agency Insights Series*.

Iglauer, S., T. Rahman, M. Sarmadivaleh, A. Al-Hinai, M. A. Fernø, M. Lebedev, et al. (2016), Influence of wettability on residual gas trapping and enhanced oil recovery in three-phase flow: a pore-scale analysis by use of microcomputed tomography, *SPE Journal*, *21*(06), 1–916.

Jackson, M., J. Vinogradov, G. Hamon, and M. Chamerois (2016a), Evidence, mechanisms and improved understanding of controlled salinity waterflooding part 1: Sandstones, *Fuel*, *185*, 772–793.

Jackson, M. D., D. Al-Mahrouqi, and J. Vinogradov (2016b), Zeta potential in oil-water-carbonate systems and its impact on oil recovery during controlled salinity water-flooding, *Scientific Reports*, *6*(1), 1–13.

Jadhunandan, P., N. R. Morrow, et al. (1995), Effect of wettability on waterflood recovery for crude-oil/brine/rock systems, *SPE Reservoir Engineering*, *10*(01), 40–46.

Kaestner, A., E. Lehmann, and M. Stampanoni (2008), Imaging and image processing in porous media research, *Advances in Water Resources*, *31*(9), 1174–1187.

Kar, T., H. Cho, and A. Firoozabadi (2022), Assessment of low salinity waterflooding in carbonate cores: Interfacial viscoelasticity and tuning process efficiency by use of non-ionic surfactant, *Journal of Colloid and Interface Science*, *607*, 125–133.

Katende, A., and F. Sagala (2019), A critical review of low salinity water flooding: mechanism, laboratory and field application, *Journal of Molecular Liquids*, *278*, 627–649.

Khilar, K. C., H. S. Fogler, et al. (1983), Water sensitivity of sandstones, *Society of Petroleum Engineers Journal*, *23*(01), 55–64.

Khishvand, M., A. Alizadeh, I. O. Kohshour, M. Piri, and R. Prasad (2017), In situ characterization of wettability alteration and displacement mechanisms governing recovery enhancement due to low-salinity waterflooding, *Water Resources Research*, *53*(5), 4427–4443.

Koelbl, B. S., M. A. van den Broek, A. P. Faaij, and D. P. van Vuuren (2014), Uncertainty in carbon capture and storage (CCS) deployment projections: a cross-model comparison exercise], *Climatic change*, *123*(3-4), 461–476.

Krevor, S. C., R. Pini, B. Li, and S. M. Benson (2011), Capillary heterogeneity trapping of CO_2 in a sandstone rock at reservoir conditions, *Geophysical Research Letters*, *38*(15).

Lager, A., K. Webb, and C. Black (2007), Impact of brine chemistry on oil recovery, in *IOR 2007-14th European symposium on improved oil recovery*, pp. cp–24, European Association of Geoscientists & Engineers.

Lager, A., K. J. Webb, C. Black, M. Singleton, K. S. Sorbie, et al. (2008a), Low salinity oil recovery-an experimental investigation, *Petrophysics*, *49*(01).

Lager, A., K. J. Webb, I. R. Collins, D. M. Richmond, et al. (2008b), Losal enhanced oil recovery: Evidence of enhanced oil recovery at the reservoir scale, in *SPE Symposium on Improved Oil Recovery*, Society of Petroleum Engineers.

Lai, P., and S. Krevor (2014), Pore scale heterogeneity in the mineral distribution and surface area of Berea sandstone, *Energy Procedia*, *63*, 3582–3588.

Lai, P., K. Moulton, and S. Krevor (2015), Pore-scale heterogeneity in the mineral distribution and reactive surface area of porous rocks, *Chemical Geology*, *411*, 260–273.

Lake, L. W., R. Johns, B. Rossen, and G. A. Pope (2014), *Fundamentals of enhanced oil recovery*, vol. 1, Society of Petroleum Engineers Richardson, TX.

Lcdley, R., G. Di Chiro, A. Luessenhop, and H. Twigg (1974), Computerized transaxial x-ray tomography of the human body, *Science*, *186*(4160), 207–212.

Lebedeva, E. V., and A. Fogden (2010), Adhesion of oil to kaolinite in water, *Environmental Science & Technology*, *44*(24), 9470–9475.

Lebedeva, E. V., and A. Fogden (2011), Micro-ct and wettability analysis of oil recovery from sand packs and the effect of waterflood salinity and kaolinite, *Energy & Fuels*, *25*(12), 5683–5694.

Leu, L., S. Berg, F. Enzmann, R. T. Armstrong, and M. Kersten (2014), Fast X-ray micro-tomography of multiphase flow in Berea sandstone: A sensitivity study on image processing, *Transport in Porous Media*, *105*(2), 451–469.

Ligthelm, D. J., J. Gronsveld, J. Hofman, N. Brussee, F. Marcelis, H. van der Linde, et al. (2009), Novel waterflooding strategy by manipulation of injection brine composition., in *EUROPEC/EAGE Conference and Exhibition*, Society of Petroleum Engineers.

Lin, Q., B. Bijeljic, R. Pini, M. J. Blunt, and S. Krevor (2018), Imaging and measurement of pore-scale interfacial curvature to determine capillary pressure simultaneously with relative permeability, *Water Resources Research*.

Liu, F., H. Yang, J. Wang, M. Zhang, T. Chen, G. Hu, W. Zhang, J. Wu, S. Xu, and X. Wu (2018), Salinity-dependent adhesion of model molecules of crude oil at quartz surface with different wettability, *Fuel*, *223*, 401–407.

Loahardjo, N., X. Xie, P. Yin, and N. R. Morrow (2007), Low salinity waterflooding of a reservoir rock, in *International Symposium of the Society of Core Analysts*, vol. 29, p. 2007.

Loahardjo, N., X. Xie, and N. R. Morrow (2010), Oil recovery by sequential waterflooding of mixed-wet sandstone and limestone, *Energy & Fuels*, *24*(9), 5073–5080.

Mahani, H., A. L. Keya, S. Berg, W.-B. Bartels, R. Nasralla, and W. R. Rossen (2015a), Insights into the mechanism of wettability alteration by low-salinity flooding (LSF) in carbonates, *Energy & Fuels*, *29*(3), 1352–1367.

Mahani, H., S. Berg, D. Ilic, W.-B. Bartels, and V. Joekar-Niasar (2015b), Kinetics of low-salinity-flooding effect, *SPE Journal*, *20*(01), 8–20.

Mahmoudvand, M., A. Javadi, P. Pourafshary, H. Vatanparast, and A. Bahramian (2021),

Effects of cation salinity on the dynamic interfacial tension and viscoelasticity of a water-oil system, *Journal of Petroleum Science and Engineering*, *206*, 108,970.

Martin, J. C., et al. (1959), The effects of clay on the displacement of heavy oil by water, in *Venezuelan annual meeting*, Society of Petroleum Engineers.

Mehana, M., M. Fahes, Q. Kang, and H. Viswanathan (2020), Molecular simulation of double layer expansion mechanism during low-salinity waterflooding, *Journal of Molecular Liquids*, *318*, 114,079.

Moeini, F., A. Hemmati-Sarapardeh, M.-H. Ghazanfari, M. Masihi, and S. Ayatollahi (2014), Toward mechanistic understanding of heavy crude oil/brine interfacial tension: The roles of salinity, temperature and pressure, *Fluid phase equilibria*, *375*, 191–200.

Morin, B., Y. Liu, V. Alvarado, and J. Oakey (2016), A microfluidic flow focusing platform to screen the evolution of crude oil–brine interfacial elasticity, *Lab on a Chip*, *16*(16), 3074–3081.

Morrow, N., J. Buckley, et al. (2011), Improved oil recovery by low-salinity waterflooding, *Journal of Petroleum Technology*, *63*(05), 106–112.

Morrow, N. R., G.-q. Tang, M. Valat, and X. Xie (1998), Prospects of improved oil recovery related to wettability and brine composition, *Journal of Petroleum science and Engineering*, *20*(3-4), 267–276.

Muggeridge, A., A. Cockin, K. Webb, H. Frampton, I. Collins, T. Moulds, and P. Salino (2014), Recovery rates, enhanced oil recovery and technological limits, *Philosophical Transactions. Series A, Mathematical, Physical, and Engineering Sciences*, *372*(2006).

Naderi, S., and M. Simjoo (2019), Numerical study of low salinity water alternating CO_2 injection for enhancing oil recovery in a sandstone reservoir: Coupled geochemical and fluid flow modeling, *Journal of Petroleum Science and Engineering*, *173*, 279–286.

Nasralla, R. A., M. A. Bataweel, H. A. Nasr-El-Din, et al. (2013), Investigation of wettability alteration and oil-recovery improvement by low-salinity water in sandstone rock, *Journal of Canadian Petroleum Technology*, *52*(02), 144–154.

Nasralla, R. A., H. A. Nasr-El-Din, et al. (2014), Double-layer expansion: is it a primary mechanism of improved oil recovery by low-salinity waterflooding?, *SPE Reservoir Evaluation & Engineering*, *17*(01), 49–59.

Olivarius, M., R. Weibel, M. L. Hjuler, L. Kristensen, A. Mathiesen, L. H. Nielsen, and C. Kjøller (2015), Diagenetic effects on porosity–permeability relationships in red beds of the lower triassic bunter sandstone formation in the north german basin, *Sedimentary Geology*, *321*, 139–153.

Othman, F., M. A. Naufaliansyah, and F. Hussain (2019), Effect of water salinity on permeability alteration during CO_2 sequestration, *Advances in Water Resources*, *127*, 237–251.

Pak, T., I. B. Butler, S. Geiger, M. I. van Dijke, and K. S. Sorbie (2015), Droplet fragmentation: 3D imaging of a previously unidentified pore-scale process during multiphase flow in porous media, *Proceedings of the National Academy of Sciences*, *112*(7), 1947–1952.

Pan, Z., and J. M. Trusler (2022), Interfacial tensions of systems comprising n2, 7 mass% ki (aq), decane and iododecane at elevated pressures and temperatures, *Fluid Phase Equilibria*, *556*, 113,364.

Petrovic, A., J. Siebert, and P. Rieke (1982), Soil bulk density analysis in three dimensions by computed tomographic scanning 1, *Soil Science Society of America Journal*, *46*(3), 445–450.

Pinerez Torrijos, I. D., T. Puntervold, S. Strand, T. Austad, H. I. Abdullah, and K. Olsen (2016), Experimental study of the response time of the low-salinity enhanced oil recovery effect during secondary and tertiary low-salinity waterflooding, *Energy & Fuels*, *30*(6), 4733–4739.

Prempeh, K., L. Chequer, A. Badalyan, and P. Bedrikovetsky (2020), Effects of kaolinite on fines migration and formation damage, in *SPE International Conference and Exhibition on Formation Damage Control*, OnePetro.

Pu, H., X. Xie, P. Yin, and N. R. Morrow (2010), Low salinity waterflooding and mineral dissolution, in *SPE Annual Technical Conference and Exhibition*, OnePetro.

Qin, Z., M. Arshadi, and M. Piri (2019), Micro-scale experimental investigations of multiphase flow in oil-wet carbonates. i. in situ wettability and low-salinity waterflooding, *Fuel*, *257*, 116,014.

Rabbani, H. S., B. Zhao, R. Juanes, and N. Shokri (2018), Pore geometry control of apparent wetting in porous media, *Scientific Reports*, *8*(1), 15,729.

Raeini, A. Q., B. Bijeljic, and M. J. Blunt (2014), Numerical modelling of sub-pore scale events in two-phase flow through porous media, *Transport in porous media*, *101*(2), 191–213.

Raeini, A. Q., B. Bijeljic, and M. J. Blunt (2017), Generalized network modeling: Network extraction as a coarse-scale discretization of the void space of porous media, *Phys. Rev. E*, *96*, 013,312.

Raeini, A. Q., B. Bijeljic, and M. J. Blunt (2018), Generalized network modeling of capillary-dominated two-phase flow, *Physical Review E*, *97*(2), 023,308.

Raeini, A. Q., J. Yang, I. Bondino, T. Bultreys, M. J. Blunt, and B. Bijeljic (2019), Validating the generalized pore network model using micro-ct images of two-phase flow, *Transport in Porous Media*, *130*(2), 405–424.

Reynolds, C. A., H. Menke, M. Andrew, M. J. Blunt, and S. Krevor (2017), Dynamic fluid connectivity during steady-state multiphase flow in a sandstone, *Proceedings of the National Academy of Sciences*, *114*(31), 8187–8192.

RezaeiDoust, A., T. Puntervold, T. Austad, et al. (2010), A discussion of the low-salinity EOR potential for a north sea sandstone field, in *SPE Annual Technical Conference and Exhibition*, Society of Petroleum Engineers.

RezaeiDoust, A., T. Puntervold, and T. Austad (2011), Chemical verification of the EOR mechanism by using low saline/smart water in sandstone, *Energy & Fuels*, *25*(5), 2151–2162.

Rivet, S., L. W. Lake, G. A. Pope, et al. (2010), A coreflood investigation of low-salinity enhanced oil recovery, in *SPE Annual Technical Conference and Exhibition*, Society of Petroleum Engineers.

Romero, M. I., P. Gamage, H. Jiang, C. Chopping, and G. Thyne (2013), Study of low-salinity waterflooding for single-and two-phase experiments in Berea sandstone cores, *Journal of Petroleum Science and Engineering*, *110*, 149–154.

Roof, J. (1970), Snap-off of oil droplets in water-wet pores, *Society of Petroleum Engineers Journal*, *10*(01), 85–90.

Sandengen, K., A. Kristoffersen, K. Melhuus, L. O. Jøsang, et al. (2016), Osmosis as mechanism for low-salinity enhanced oil recovery, *SPE Journal*, *21*(04), 1–227.

Satter, A., and G. M. Iqbal (2015), *Reservoir engineering: the fundamentals, simulation, and management of conventional and unconventional recoveries*, Gulf Professional Publishing.

Scanziani, A., K. Singh, T. Bultreys, B. Bijeljic, and M. J. Blunt (2018), In situ characterization of immiscible three-phase flow at the pore scale for a water-wet carbonate rock, *Advances in Water Resources*, *121*, 446–455.

Scanziani, A., K. Singh, H. Menke, B. Bijeljic, and M. J. Blunt (2020), Dynamics of enhanced gas trapping applied to CO_2 storage in the presence of oil using synchrotron X-ray micro tomography, *Applied Energy*, *259*, 114,136.

Schlüter, S., A. Sheppard, K. Brown, and D. Wildenschild (2014), Image processing of multiphase images obtained via x-ray microtomography: a review, *Water Resources Research*, *50*(4), 3615–3639.

Schmatz, J., J. L. Urai, S. Berg, and H. Ott (2015), Nanoscale imaging of pore-scale fluid-fluid-solid contacts in sandstone, *Geophysical Research Letters*, *42*(7), 2189–2195.

Schmid, S., R. Worden, and Q. Fisher (2004), Diagenesis and reservoir quality of the sherwood sandstone (triassic), corrib field, slyne basin, west of ireland, *Marine and Petroleum Geology*, *21*(3), 299–315.

Seccombe, J., A. Lager, G. Jerauld, B. Jhaveri, T. Buikema, S. Bassler, J. Denis, K. Webb, A. Cockin, and E. Fueg (2010), Demonstration of low-salinity EOR at interwell scale, Endicott field, Alaska, in *SPE Improved Oil Recovery Symposium*, OnePetro.

Secor, R., and C. Radke (1985), Spillover of the diffuse double layer on montmorillonite particles, *Journal of Colloid and Interface Science*, *103*(1), 237–244.

Selem, A. M., N. Agenet, Y. Gao, A. Q. Raeini, M. J. Blunt, and B. Bijeljic (2021), Pore-scale imaging and analysis of low salinity waterflooding in a heterogeneous carbonate rock at reservoir conditions, *Scientific Reports*, *11*(1), 1–14.

Sen, P., C. Straley, W. Kenyon, and M. Whittingham (1990), Surface-to-volume ratio, charge density, nuclear magnetic relaxation, and permeability in clay-bearing sandstones, *Geophysics*, *55*(1), 61–69.

Shabaninejad, M., R. Marathe, J. Middleton, and A. Fogden (2015), Micro-ct pore-scale analysis of low salinity recovery from reservoir sandstones, in *77th EAGE Conference and Exhibition 2015*.

Shabaninejad, M., J. Middlelton, and A. Fogden (2018), Systematic pore-scale study of low salinity recovery from Berea sandstone analyzed by micro-ct, *Journal of Petroleum Science and Engineering*, *163*, 283–294.

Shaker Shiran, B., A. Skauge, et al. (2012), Wettability and oil recovery by low salinity injection, in *SPE EOR Conference at Oil and Gas West Asia*, Society of Petroleum Engineers.

Shams, M., K. Singh, B. Bijeljic, and M. J. Blunt (2021), Direct numerical simulation of pore-scale trapping events during capillary-dominated two-phase flow in porous media, *Transport in Porous Media*, pp. 1–16.

Shaw, J. C., P. L. Churcher, B. F. Hawkins, et al. (1991), The effect of firing on Berea sandstone, *SPE formation evaluation*, *6*(01), 72–78.

Sheng, J. (2014), Critical review of low-salinity waterflooding, *Journal of Petroleum Science and Engineering*, *120*, 216–224.

Singh, K., T. Bultreys, A. Q. Raeini, M. Shams, and M. J. Blunt (2019), Imbibition in porous media: correlations of displacement events with pore-throat geometry and the identification of a new type of pore snap-off.

Singh, K., T. Bultreys, A. Q. Raeini, M. Shams, and M. J. Blunt (2022), New type of pore-snap-off and displacement correlations in imbibition, *Journal of Colloid and Interface Science*, *609*, 384–392.

Sohrabi, M., P. Mahzari, S. A. Farzaneh, J. R. Mills, P. Tsolis, S. Ireland, et al. (2017), Novel insights into mechanisms of oil recovery by use of low-salinity-water injection, *SPE Journal*, *22*(02), 407–416.

Sokama-Neuyam, Y. A., J. R. Ursin, and P. Boakye (2019), Experimental investigation of the mechanisms of salt precipitation during CO_2 injection in sandstone, *C*, *5*(1), 4.

Song, W., and A. R. Kovscek (2015), Functionalization of micromodels with kaolinite for investigation of low salinity oil-recovery processes, *Lab on a Chip*, *15*(16), 3314–3325.

Soraya, B., C. Malick, C. Philippe, H. J. Bertin, G. Hamon, et al. (2009), Oil recovery by low-salinity brine injection: Laboratory results on outcrop and reservoir cores, in *SPE Annual Technical Conference and Exhibition*, Society of Petroleum Engineers.

Spiteri, E. J., R. Juanes, M. J. Blunt, and F. M. Orr (2008), A new model of trapping and relative permeability hysteresis for all wettability characteristics, *SPE Journal*, *13*(03), 277–288.

Spurin, C., T. Bultreys, B. Bijeljic, M. J. Blunt, and S. Krevor (2019), Mechanisms controlling fluid breakup and reconnection during two-phase flow in porous media, *Physical Review E*, *100*(4), 043,115.

Spurin, C., T. Bultreys, M. Rücker, G. Garfi, C. M. Schlepütz, V. Novak, S. Berg, M. J. Blunt, and S. Krevor (2021), The development of intermittent multiphase fluid flow pathways through a porous rock, *Advances in Water Resources*, *150*, 103,868.

Suijkerbuijk, B., J. Hofman, D. J. Ligthelm, J. Romanuka, N. Brussee, H. van derLinde, and A. Marcelis (2012), Fundamental investigations into wettability and low salinity flooding by parameter isolation, in *SPE Improved Oil Recovery Symposium*, OnePetro.

Suman, Y. K. (2014), *Evaluation of low saline "smart water" enhanced oil recovery in light oil reservoirs*, The University of Regina (Canada).

Sun, C., J. E. McClure, P. Mostaghimi, A. L. Herring, D. E. Meisenheimer, D. Wildenschild, S. Berg, and R. T. Armstrong (2020a), Characterization of wetting using topological principles, *arXiv preprint arXiv:2005.02873*.

Sun, C., J. E. McClure, P. Mostaghimi, A. L. Herring, M. Shabaninejad, S. Berg, and R. T. Armstrong (2020b), Linking continuum-scale state of wetting to pore-scale contact angles in porous media, *Journal of Colloid and Interface Science*, *561*, 173–180.

Sun, C., J. E. McClure, P. Mostaghimi, A. L. Herring, S. Berg, and R. T. Armstrong (2020c), Probing effective wetting in subsurface systems, *Geophysical Research Letters*, *47*(5), no–no.

Sun, C., J. McClure, S. Berg, P. Mostaghimi, and R. T. Armstrong (2021), Universal description of wetting on multiscale surfaces using integral geometry, *arXiv preprint arXiv:2108.09445*.

Tabrizy, V. A., R. Denoyel, and A. Hamouda (2011), Characterization of wettability alteration of calcite, quartz and kaolinite: Surface energy analysis, *Colloids and Surfaces A: Physicochemical and Engineering Aspects*, *384*(1-3), 98–108.

Tang, G., and N. R. Morrow (2002), Injection of dilute brine and crude oil/brine/rock interactions, *Washington DC American Geophysical Union Geophysical Monograph Series*, *129*, 171–179.

Tang, G., N. R. Morrow, et al. (1997), Salinity, temperature, oil composition, and oil recovery by waterflooding, *SPE Reservoir Engineering*, *12*(04), 269–276.

Tang, G.-Q., and N. R. Morrow (1999), Influence of brine composition and fines migration on crude oil/brine/rock interactions and oil recovery, *Journal of Petroleum Science and Engineering*, *24*(2-4), 99–111.

Tanino, Y., and M. J. Blunt (2012), Capillary trapping in sandstones and carbonates: Dependence on pore structure, *Water Resources Research*, *48*(8).

Teklu, T. W., W. Alameri, H. Kazemi, R. M. Graves, and A. M. AlSumaiti (2017), Low salinity water–surfactant–CO_2 EOR, *Petroleum*, *3*(3), 309–320.

Tombácz, E., and M. Szekeres (2006), Surface charge heterogeneity of kaolinite in aqueous suspension in comparison with montmorillonite, *Applied Clay Science*, *34*(1-4), 105–124.

Unsal, E., A. Ten Berge, and D. Wever (2018), Low salinity polymer flooding: Lower polymer retention and improved injectivity, *Journal of Petroleum Science and Engineering*, *163*, 671–682.

Uren, L. C., and E. Fahmy (1927), Factors influencing the recovery of petroleum from unconsolidated sands by waterflooding, *Transactions of the AIME*, *77*(01), 318–335.

Valvatne, P. H., and M. J. Blunt (2004), Predictive pore-scale modeling of two-phase flow in mixed wet media, *Water Resources Research*, *40*(7).

Vermolen, E., M. Pingo Almada, B. M. Wassing, D. J. Ligthelm, and S. K. Masalmeh (2014), Low-salinity polymer flooding: improving polymer flooding technical feasibility and economics by using low-salinity make-up brine, in *International petroleum technology conference*, OnePetro.

Vincent, L., and P. Soille (1991), Watersheds in digital spaces: an efficient algorithm based on immersion simulations, *IEEE Transactions on Pattern Analysis & Machine Intelligence*, *13*(06), 583–598.

Vlassenbroeck, J., M. Dierick, B. Masschaele, V. Cnudde, L. Van Hoorebeke, and P. Jacobs (2007), Software tools for quantification of x-ray microtomography at the ugct, *Nuclear Instruments and Methods in Physics Research Section A: Accelerators, Spectrometers, Detectors and Associated Equipment*, *580*(1), 442–445.

Vledder, P., I. E. Gonzalez, J. C. Carrera Fonseca, T. Wells, D. J. Ligthelm, et al. (2010), Low salinity water flooding: proof of wettability alteration on a field wide scale, in *SPE Improved Oil Recovery Symposium*, Society of Petroleum Engineers.

Wang, L., and X. Fu (2018), Data-driven analyses of low salinity water flooding in sandstones, *Fuel*, *234*, 674–686.

Wang, R., W. Shi, X. Xie, W. Zhang, S. Qin, K. Liu, and A. B. Busbey (2020), Clay mineral content, type, and their effects on pore throat structure and reservoir properties: Insight from the permian tight sandstones in the hangjinqi area, north ordos basin, china, *Marine and Petroleum Geology*, *115*, 104,281.

Wang, S., T. K. Tokunaga, J. Wan, W. Dong, and Y. Kim (2016), Capillary pressure-saturation relations in quartz and carbonate sands: Limitations for correlating capillary and wettability influences on air, oil, and supercritical CO_2 trapping, *Water Resources Research*, *52*(8), 6671–6690.

Wickramathilaka, S., N. R. Morrow, and J. Howard (2010), Effect of salinity on oil recovery by spontaneous imbibition, in *24th International Symposium of Core Analysts, Halifax, Canada*.

Wildenschild, D., and A. P. Sheppard (2013), X-ray imaging and analysis techniques for quantifying pore-scale structure and processes in subsurface porous medium systems, *Advances in Water Resources*, *51*, 217–246.

Wilmott, Z., C. Breward, and S. Chapman (2019), Modelling low-salinity oil recovery mechanisms using an ion dissociation model, *Transport in Porous Media*, *127*(3), 685–709.

Winoto, W., N. Loahardjo, X. S. Xie, P. Yin, and N. R. Morrow (2012), Secondary and tertiary recovery of crude oil from outcrop and reservoir rocks by low salinity waterflooding, in *SPE Improved Oil Recovery Symposium*, OnePetro.

Xiao, D., S. Jiang, D. Thul, S. Lu, L. Zhang, and B. Li (2018), Impacts of clay on pore structure, storage and percolation of tight sandstones from the songliao basin, china: implications for genetic classification of tight sandstone reservoirs, *Fuel*, *211*, 390–404.

Xie, Q., A. Saeedi, E. Pooryousefy, and Y. Liu (2016), Extended dlvo-based estimates of surface force in low salinity water flooding, *Journal of Molecular Liquids*, *221*, 658–665.

Xu, W., J. T. Ok, F. Xiao, K. B. Neeves, and X. Yin (2014), Effect of pore geometry and interfacial tension on water-oil displacement efficiency in oil-wet microfluidic porous media analogs, *Physics of fluids*, *26*(9), 093,102.

Yang, S.-Y., G. Hirasaki, S. Basu, and R. Vaidya (1999), Mechanisms for contact angle hysteresis and advancing contact angles, *Journal of Petroleum Science and Engineering*, *24*(2-4), 63–73.

Yesufu-Rufai, S., M. Rücker, S. Berg, S. F. Lowe, F. Marcelis, A. Georgiadis, and P. Luckham (2020), Assessing the wetting state of minerals in complex sandstone rock in-situ by Atomic Force Microscopy (AFM), *Fuel*, *273*, 117,807.

Yousef, A. A., S. Al-Saleh, A. U. Al-Kaabi, M. S. Al-Jawfi, et al. (2010), Laboratory investigation of novel oil recovery method for carbonate reservoirs, in *Canadian Unconventional Resources and International Petroleum Conference*, Society of Petroleum Engineers.

Yousef, A. A., S. H. Al-Saleh, A. Al-Kaabi, M. S. Al-Jawfi, et al. (2011), Laboratory investigation of the impact of injection-water salinity and ionic content on oil recovery from carbonate reservoirs, *SPE Reservoir Evaluation & Engineering*, *14*(05), 578–593.

Zeinijahromi, A., V. Ahmetgareev, R. Ibatullin, and P. Bedrikovetsky (2015), Sensitivity study of low salinity water injection in zichebashskoe oilfield, *Journal of Petroleum and Gas Engineering*, *6*(1), 10–21.

Zhang, Y., and N. R. Morrow (2006), Comparison of secondary and tertiary recovery with change in injection brine composition for crude-oil/sandstone combinations, in *SPE/DOE symposium on improved oil recovery*, OnePetro.

Zhang, Y., X. Xie, and N. R. Morrow (2007), Waterflood performance by injection of brine with different salinity for reservoir cores, in *SPE Annual Technical Conference and Exhibition*, OnePetro.

Zhao, Y., S. Yin, R. S. Seright, S. Ning, Y. Zhang, and B. Bai (2021), Enhancing heavy-oil-recovery efficiency by combining low-salinity-water and polymer flooding, *SPE Journal*, *26*(03), 1535–1551.